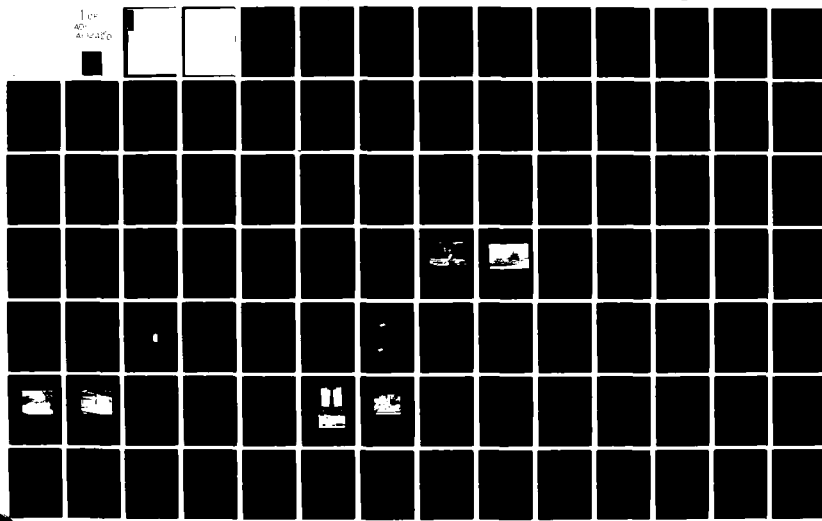


AD-A102 420 DAVID W TAYLOR NAVAL SHIP RESEARCH AND DEVELOPMENT CE--ETC F/G 13/10
STRUCTURAL RESPONSE METHODS AND EVALUATION RESULTS FOR HELICOPT--ETC(U)
JUL 81 M O CRITCHFIELD, J L RODD, W H HAY MIPR-Z-70099-6-65439
UNCLASSIFIED DTNSRDC-81/009 NL

1cc
40°
40' 40"



AD A102420

UNCLASSIFIED

SECURITY CLASSIFICATION OF THIS PAGE (When Data Entered)

REPORT DOCUMENTATION PAGE			READ INSTRUCTIONS BEFORE COMPLETING FORM
1. REPORT NUMBER 14 DTNSRDC-81/009	2. GOVT ACCESSION NO. AD-A102 430	3. RECIPIENT'S CATALOG NUMBER	
4. TITLE (and Subtitle) STRUCTURAL RESPONSE METHODS AND EVALUATION RESULTS FOR HELICOPTER LANDING DECKS ON 210- AND 270-FOOT USCG CUTTERS.		5. TYPE OF REPORT & PERIOD COVERED Final Sept. 1977 - 1980	
6. AUTHOR(s) M.O. Critchfield J.L. Rodd W.H. Hay		7. CONTRACT OR GRANT NUMBER(s) MIPR No. Z-70099-6-65439	
8. PERFORMING ORGANIZATION NAME AND ADDRESS David W. Taylor Naval Ship Research and Development Center Bethesda, Maryland 20084		10. PROGRAM ELEMENT, PROJECT, TASK AREA & WORK UNIT NUMBERS Govt Work Unit 1730-325	
11. CONTROLLING OFFICE NAME AND ADDRESS Commandant U.S. Coast Guard (G-ENE-5B/64) Washington, D.C. 20590		12. REPORT DATE July 1981	
14. MONITORING AGENCY NAME & ADDRESS (if different from Controlling Office) 15-1		13. NUMBER OF PAGES 127	
15. SECURITY CLASS. (of this report) UNCLASSIFIED			
15a. DECLASSIFICATION/DOWNGRADING SCHEDULE			
16. DISTRIBUTION STATEMENT (of this Report) APPROVED FOR PUBLIC RELEASE: DISTRIBUTION UNLIMITED			
17. DISTRIBUTION STATEMENT (of the abstract entered in Block 20, if different from Report) AUG 4 1981			
18. SUPPLEMENTARY NOTES A			
19. KEY WORDS (Continue on reverse side if necessary and identify by block number) Helicopter, helo deck, helo platform, landing deck, handling deck, U.S. Navy, U.S. Coast Guard, cutter, wheel load, plating, longitudinal, stiffener, structural analysis, design, analytical, evaluation, finite element, model, full scale, response, stress, deflection, strength, capacity, yielding, (Continued on reverse side)			
20. ABSTRACT (Continue on reverse side if necessary and identify by block number) Since 1976, the David W. Taylor Naval Ship Research and Development Center has been assisting the U.S. Coast Guard in evaluating the strength of several helicopter landing deck configurations for existing 210-foot long cutters and for the new 270-foot cutters. These evaluations were performed based on a combined program of (a) analytical, (b) one-fifth-scale rigid			
(Continued on reverse side)			

162

UNCLASSIFIED

SECURITY CLASSIFICATION OF THIS PAGE (When Data Entered)

(Block 19 continued)

bending, membrane, failure, nonlinear response, large deflection, validate, plate strength, NASTRAN

(Block 20 continued)

vinyl model, and (c) full-scale investigations for several landing gear load conditions, including the main and tail wheels on the U.S. Navy LAMPS Helicopter.

The analytical side of the program included: framing analyses using the finite-element method and other techniques; nonlinear, large-deflection analyses of the deck plating; and web bending analyses in the stiffeners. The web bending stresses referred to here are associated with local out-of-plane bending of the web due to a rotation of the joint between the stiffener web and the deck plating. These web stresses are distinct from those related to ordinary bending of the stiffener in the vertical plane. Web bending stresses in the stiffeners were first observed in full-scale tests on the 210-foot cutter STEADFAST and are not specifically addressed by current design procedures.

A one-fifth-scale rigid vinyl model was used to validate the analytical procedures and also to investigate such considerations as load placement, orientation, and tire print geometry.

Some observations made during the studies were: for single-wheel configurations, wheel loads over stiffeners can be more severe in terms of plating stresses than loads in panel centers; when straddling stiffeners, dual wheels can produce greater plating stresses than single wheels; web stresses in stiffeners, associated with web bending, may exceed flange stresses due to ordinary beam bending. The possibility of localized yielding is forecast in the helicopter deck plating and stiffener webs for two of the 270-foot helicopter deck configurations.

Overall, the evaluations pinpoint regions of high stress, provide the USCG with a technical basis for assessing the strength of existing 210-foot cutters and designing the new 270-foot cutters; provide validated analysis methods for future helicopter deck structures; and result in potential reductions in the 270-foot helicopter deck structural weight from the initial designs.

UNCLASSIFIED

SECURITY CLASSIFICATION OF THIS PAGE (When Data Entered)

TABLE OF CONTENTS

	Page
LIST OF FIGURES.	iv
LIST OF TABLES	vii
LIST OF ABBREVIATIONS.	ix
ABSTRACT	1
ADMINISTRATIVE INFORMATION	1
BACKGROUND	2
HELICOPTER DECK CONFIGURATIONS AND LOADS	5
DESCRIPTION OF EVALUATION METHODS.	6
FRAMING ANALYSES.	6
Finite-Element Model	7
AISC Equations	8
PLATING ANALYSES.	9
STIFFENER WEB BENDING ANALYSES.	10
Finite-Element Model	11
Design Equations	13
RIGID VINYL MODEL	13
FULL-SCALE TESTS.	16
RESULTS OF EVALUATION.	18
FRAMING RESPONSE.	18
Flange Stresses.	18
Deflections.	19
PLATING RESPONSE.	20
Stresses and Validation of Analysis Methods.	20
Influence of Tire Print Geometry and Load Placement.	22
STIFFENER WEB BENDING RESPONSE.	25
Validation of Web Bending Analyses	25
Maximum Web Bending Stresses	28
SUMMARY AND CONCLUSIONS.	29
270 DECK STRESSES	30
Framing.	30
Plating.	31

	Page
210 DECK STRESSES	31
GENERAL FINDINGS AND TRENDS	32
ANALYSIS METHODS FOR FUTURE APPLICATION	34
ACKNOWLEDGMENTS	35
APPENDIX A - DERIVATION OF WEB BENDING EQUATIONS	103
APPENDIX B - LISTING AND TYPICAL OUTPUT FOR TEKTRONIX 4051 COMPUTER PROGRAM "COMPUTATION OF VERTICAL WEB BENDING STRESS"	113
REFERENCES	115

LIST OF FIGURES

1 - Sketch of WMEC 270-Foot Cutter under Construction	37
2 - Starboard View of WMEC 210-Foot Cutter VIGOROUS at Sea	38
3 - 270 Foot, Basic Configuration I	39
4 - 270 Foot, Configuration II (Headers Added)	40
5 - 270 Foot, Configuration III (Plating Changed to 10.2# Plate)	41
6 - 210 Foot, Existing Configuration (STEADFAST)	42
7 - 270 Foot, Configuration IV (Number of Headers Reduced)	43
8 - 210 Foot, Existing Configuration (Basis for 210 Deck Modification)	44
9 - 210 Foot, Modified Configuration (Headers Added)	45
10 - Finite-Element Model for Overall Framing Analysis of 270-Class Configurations I-III	46
11 - Expanded View of Portion of Finite-Element Model in Figure 8	47
12 - Wheel Load Positions for Configuration I	48
13 - Wheel Load Positions for Configuration II	49
14 - Finite-Element Models for Large Deflection Plating Analyses (Configurations II and III)	50

Page

15 - Elastic Boundary Restraint for Plating Analyses (Configuration I, Central Panel Load)	51
16 - Elastic Boundary Restraint for Plating Analyses (Configurations II and III, Central Panel Load)	52
17 - Elastic Boundary Restraint for Plating Analyses (Configuration II, Load Straddling Panel Boundary)	53
18 - Illustration of Stiffener 'Web Bending' Along with Full-Scale Results for 210.	54
19 - Three Stiffener Configurations Requiring Web Bending Analyses.	55
20 - Finite-Element Model for Web Bending of Longitudinal (Without Headers)	56
21 - Finite-Element Model for Web Bending of Longitudinal (With Headers)	57
22 - View of Rigid Vinyl Model from Top	58
23 - View of Rigid Vinyl Model from Bottom.	59
24 - Strain Gage Locations on Stiffener Flange (Single Gages)	60
25 - Strain Gage Locations on Plating	61
26 - Helo Load Footprints Used in Model Evaluation.	62
27 - Top and Bottom Views of Helo Deck Panel on USCG Cutter STEADFAST Instrumented for Full-Scale Tests.	63
28 - View of Helo Deck Panel on STEADFAST under Simulated Tire Loading Using a Forklift	64
29 - Transducer Locations for USCG Cutter STEADFAST Static Tests.	65
30 - Flange Stress Profile for Center-Line Longitudinals in 270, Configuration I (for Load Case 1, Table 2)	66
31 - Flange Stress Profile for Center-Line Longitudinals in 270, Configuration II (for Load Case 1, Table 2).	67
32 - Flange Stress Profile for Headers in 270, Configuration II (for Load Case 1, Table 2).	68

Page

33 - Deflection Profile for Center-Line Longitudinal in 270, Configuration I (One and Two Wheels for Load Case 1, Table 2).	69
34 - Deflection Profile along Transverse Center-Line of 270, Configuration I (One and Two Wheels for Load Case 1, Table 2).	70
35 - Deflection Profiles Along Transverse Center-Line for 270, Configurations I and II (Wheel Load On and Between Stiffeners)	71
36 - Plating Stress Profiles in Transverse Direction for 270, Configuration I Stresses Plotted Include Bending and Membrane Components	72
37 - Plating Stress Profiles in Transverse Direction for 270, Configuration II Stresses Plotted Include Bending and Membrane Components	73
38 - Plating Stress Profiles in Transverse Direction for 210 Cutter STEADFAST.	74
39 - Plating Deflection Profile in Transverse Direction for 210 Cutter STEADFAST.	75
40 - Transverse Plating Stress at Center of Panel for Varying Load Type and Position on Configuration I.	76
41 - Transverse Plating Stress at Center of Panel for Varying Load Position on Configuration I Using 45 Degree Skew Load	77
42 - Transverse Plating Stress at Edge of Panel for Varying Load Type and Position on Configuration I.	78
43 - Transverse Plating Stress at Edge of Panel for Varying Load Position on Configuration I Using 45 Degree Skew Load	79
44 - Transverse Plating Stress at Center of Panel for Varying Load Type and Position for Configuration II.	80
45 - Transverse Plating Stress at Edge of Panel for Varying Load Type and Position for Configuration II.	81
46 - Longitudinal Plating Stress at Web Frame for Configuration I as a Function of Load Position Longitudinally	82
47 - Transverse Stress Directly Under Load for Configuration I	83

	Page
48 - Variation of Web Bending Stress with Web Depth for Longitudinal in 270, Configuration I.	84
49 - Variation of Web Bending Stress with Web Depth for Longitudinal in 270, Configuration II	85
50 - Variation of Web Bending Stress with Web Depth for Longitudinal in 210 H elo Deck (Unmodified).	86
51 - Local Vertical Bending Stress on Longitudinal Web--for No-Header Case	87
52 - Local Vertical Bending Stress on Longitudinal Web--for Header Case	88
53 - Variation of Panel Edge Moment and Web Bending Stress with Plating Thickness for Constant Longitudinal Stiffener Properties and Spacing from Configuration I.	89
54 - Typical Cross-Sectional Profile of Stiffener and Plating during Web Bending	111
55 - Decomposition of Web Bending Deflection into Force- and Moment-Induced Components.	112

LIST OF TABLES

1 - Evaluations Performed on Helicopter Landing Decks of 210- and 270-Foot-Long USCG Cutters	90
2 - Helicopter Landing Gear Load Data for 210- and 270-Class Evaluations.	91
3 - Sectional Properties of Longitudinals and Headers for 210- and 270-Class Evaluations.	92
4 - Comparison of Sectional Properties for Full-Scale Longitudinals and Headers Based on Rigid Vinyl Model	93
5 - Elastic Boundary Restraint Constants for Plating and Web Bending Analyses	94
6 - Comparison of Web Bending Predictions Using Design Equations and Finite Element	95
7 - Scaling Laws for 270-Class H elo Deck Model	96

	Page
8 - Maximum Framing Stresses for 210- and 270-Foot Heli Deck Configurations	97
9 - Plating Stresses for 270-Class Heli Deck Designs Due to Central Panel Loads	98
10 - Plating Stresses for 270-Class Heli Deck Designs Due to Wheel Loads Straddling Longitudinals and Transverse Stiffeners (Web Frames and Headers)	99
11 - Web Bending Stresses for 210- and 270-Class Heli Deck Designs	100
12 - Web Bending Stress Calculations for Longitudinals in Existing 210-Foot Decks	101
13 - Residual Stress Explanation for Web Bending in Heli Deck Longitudinals of 210-Foot Cutter STEADFAST.	102

LIST OF ABBREVIATIONS

AISC	American Institute of Steel Construction
DDS	Design Data Sheet
HELO	Helicopter
HTS	High Tensile Strength
I-T	By cutting off two sides of one flange of an I beam to within 1/8 in. of the web, one tee can be made having the same depth as the original beam (indicated as an I cut to a tee, or I-T)
LAMPS	Light Airborne Multipurpose System
MS	Mild Steel
PL	Plate
RAD	Radian
SRR	Search Rescue Recovery
USCG	United States Coast Guard

ABSTRACT

Since 1976, the David W. Taylor Naval Ship Research and Development Center has been assisting the U.S. Coast Guard in evaluating the strength of several helicopter landing deck configurations for existing 210-foot long cutters and for the new 270-foot cutters. These evaluations were performed based on a combined program of (a) analytical, (b) one-fifth-scale rigid vinyl model, and (c) full-scale investigations for several landing gear load conditions, including the main and tail wheels on the U.S. Navy LAMPS Helicopter.

The analytical side of the program included: framing analyses using the finite-element method and other techniques; nonlinear, large-deflection analyses of the deck plating; and web bending analyses in the stiffeners. The web bending stresses referred to here are associated with local out-of-plane bending of the web due to a rotation of the joint between the stiffener web and the deck plating. These web stresses are distinct from those related to ordinary bending of the stiffener in the vertical plane. Web bending stresses in the stiffeners were first observed in full-scale tests on the 210-foot cutter STEADFAST and are not specifically addressed by current design procedures.

A one-fifth-scale rigid vinyl model was used to validate the analytical procedures and also to investigate such considerations as load placement, orientation, and tire print geometry.

Some observations made during the studies were: for single-wheel configurations, wheel loads over stiffeners can be more severe in terms of plating stresses than loads in panel centers; when straddling stiffeners, dual wheels can produce greater plating stresses than single wheels; web stresses in stiffeners, associated with web bending, may exceed flange stresses due to ordinary beam bending. The possibility of localized yielding is forecast in the helicopter deck plating and stiffener webs for two of the 270-foot helicopter deck configurations.

Overall, the evaluations pinpoint regions of high stress, provide the USCG with a technical basis for assessing the strength of existing 210-foot cutters and designing the new 270-foot cutters; provide validated analysis methods for future helicopter deck structures; and result in potential reductions in the 270-foot helicopter deck structural weight from the initial designs.

ADMINISTRATIVE INFORMATION

The structural evaluations of the 210-ft and 270-ft helicopter decks were performed in the Surface Ship Structures Division of the Structures Department at the David W. Taylor Naval Ship Research and Development Center (DTNSRDC) (under Work Unit 1730-525) during Fiscal Years 1977-1980, sponsored by the U.S Coast Guard under Military Interdepartmental Purchase Requests Z-70099-6-65439. Additional efforts

involving the development of design equations for stiffener web bending and large-deflection plating responses were funded during Fiscal Years 1978-1980 under the NAVSEA Exploratory Development Program, Surface Ship Structures Block, Task Area SF 43 422 593, Work Units 1730-593 and 1730-610.

BACKGROUND

Helicopter landing decks are employed on nearly all large cutters operated by the U.S. Coast Guard (USCG).* In building new cutters, such as the 270-ft-long class recently under construction, the USCG strives to optimize helicopter deck scantlings and weight to the extent possible consistent with existing technology and constraints. Lighter landing decks are beneficial to the roll stability of cutters, but they must also provide a margin for potential growth in helicopter weight. Weight optimization of landing decks necessitates that reliable techniques for determining strength and deflections of decks be available to the structural designer.

In the last decade, DTNSRDC has developed considerable experience in applying finite-element and other analytical methods to the analysis of complex ship structure. Success has also been achieved with the use of the rigid vinyl model technique^{1**} for realistically modeling detailed ship structure. Using this technique, correlation has been obtained with analytical predictions and full-scale data² for cases investigated. In part because of this experience, DTNSRDC was requested in late 1976 to assist the USCG in evaluating the structural capacity of helicopter(helo) landing decks on the new 270-ft cutter (Figure 1), now under construction, and several existing 210-ft cutters in service (Figure 2). The scope of this work for the USCG, summarized in Table 1, included a series of structural analyses, rigid vinyl model evaluations, and full-scale measurements on the 210- and 270-ft cutters.

Initial structural evaluations were performed on preliminary design Configurations I, II, and III (Figures 3-5) for landing decks on the 270-class cutters. Since the requirement existed that the 270-class decks be certified for landing the U.S. Navy LAMPS (Light Airborne Multipurpose System) helicopter, these evaluations were conducted using the main and tail landing gear loads from the LAMPS

*A list of abbreviations used in this report is given on page ix.

**A complete listing of references is given on page 115.

(see Table 2). Analyses were performed using NASTRAN³ for the overall deck analyses and a special nonlinear finite-element program⁴ for the plating. These and other (see Appendix A) analytical techniques were validated on Configurations I and II by comparing analytical predictions with rigid vinyl model results¹ for these configurations.*,** Once validated, the analytical procedures were applied to Configuration III. Because of the approach taken here, it was necessary to build rigid vinyl models for only Configurations I and II. In addition to validating the various analytical methods for general helo deck analysis, the rigid vinyl model** was used to investigate the effect of such factors as helo tire placement, orientation, and bottoming on deck plating stresses.

During the 270-class evaluations mentioned above, the opportunity arose to gather full-scale stress and deflection data on two 210-class cutters (see Figure 6), the VIGOROUS and the STEADFAST.*** Instrumentation for the VIGOROUS was limited to dial gages for the measurement of deflections. A follow up opportunity on the STEADFAST allowed the use of strain gages for measuring plating strains and distributions to augment deflection data. In addition to these plating gages, strain gages were placed on the webs of the longitudinal stiffeners (on both sides at top) at the suggestion of the USCG. These gages produced the most significant result of the full-scale tests; vertical local stresses in the stiffener webs associated with web bending action had reached the yield point for the simulated helicopter tire loading.

The web bending stresses referred to here are associated with local out-of-plane bending of the web due to a rotation of the joint between the stiffener web and the deck plating. These web stresses, distinct from those related to ordinary bending of the stiffener in the vertical plane, are not directly addressed by current design

*M.O. Critchfield, J.L. Rodd, and W.H. Hay, "Structural Evaluation of Helicopter Landing Decks on 270 Foot and 210 Foot USCG Cutter," reported informally as enclosure (1) to DTNSRDC ltr 80-173-89 of 14 July 1980.

**J.L. Rodd, "Rigid Vinyl Model Evaluation of Helicopter Landing Deck on USCG 270 Foot Cutter," reported informally as enclosure (1) to DTNSRDC ltr 80-173-51 of 14 Apr 1980.

***W.H. Hay and M.O. Critchfield, "Full Scale Evaluation of Flight Deck Structural Responses for 210 Foot U.S. Coast Guard Cutters STEADFAST (WMEC 623) and VIGOROUS (WMEC 627) Under Simulated Helicopter Wheel Loads," reported informally as enclosure (1) to DTNSRDC ltr 77-173-75 of 26 Sep 1977.

procedure. As a result of this finding in June 1977, DTNSRDC initiated the development of design equations (see Appendix A) and a finite-element model for obtaining web bending stresses. These analytical techniques were validated against rigid vinyl model and full-scale results on the 270- (Configurations I and II) and 210-class cutters, respectively. Later, the techniques were applied to 270-class Configuration IV and the modified 210-class deck.

On the basis of the analytical and model results obtained for 270-class Configurations I through III, and other considerations, the USCG in early 1978 adopted revised deck Configuration IV (Figure 7). In going from Configurations III to IV, the plating thickness was kept at 10.2# (1/4 in.), but the material was changed from HY-80 to HY-100 (tempered up to a higher yield, approximately 118,000 psi). In addition, the three headers were reduced to one between transverse stiffeners. Here, the new longitudinals and headers were both 6x4x7 T's. The Center was requested to evaluate Configuration IV using the analytical techniques previously validated on the other 270- and 210-class deck configurations. These analyses were performed for the latest data available for the main gear loading on the LAMPS (Table 2). Additional analyses were also conducted for the load condition associated with the dual tail wheel on LAMPS. Stresses related to the dual wheel condition were investigated as a result of a suspicion that a dual wheel straddling deck stiffeners could potentially produce governing plating stresses. This in fact was confirmed by the rigid vinyl model tests* for a similar, but yet different, loading condition, i.e., a rim-type loading for the LAMPS main wheel associated with tire bottoming.

As a natural extension of the 270 and 210 work described thus far, DTNSRDC was requested by the USCG to perform a strength evaluation of the modified 210 helo deck.** Figure 8 shows the existing 210 deck configuration and Figure 9 shows the modified version. The evaluation was accomplished for wheel loadings corresponding to two SRR (SEARCH RESCUE RECOVERY) helicopter designs, French and Sikorsky (see Table 2 for loading data), under consideration for potential use on modified 210 decks. Results are included in this report for the framing portion of the evaluation.

*J.L. Rodd, "Rigid Vinyl Model Evaluation of Helicopter Landing Deck on USCG 270 Foot Cutter," reported informally as enclosure (1) to DTNSRDC ltr 80-173-51 of 14 Apr 1980.

**M.O. Critchfield, "Strength Analysis of Modified Helicopter Landing Decks on 210 Foot USCG Cutters for SRR Helicopter Wheel Loadings," reported informally as enclosure (1) to DTNSRDC ltr 79-173-80 of 14 May 1979.

In summary, the objectives of this work were: (a) to perform analytical, model, and full-scale evaluations of the various 270 and 210 helo deck configurations; (b) to provide the USCG with technical basis for assessing the strength and adequacy of the various deck designs for the new 270 cutters, as well as the decks in use on the existing 210 cutters, and for evolving design methods for configurations similar to the 270 and 210; and (c) to provide the USCG with methods applicable in the design process of their helo landing decks in general, either on future cutters or in modifications of existing cutters.

HELICOPTER DECK CONFIGURATIONS AND LOADS

The helo deck configurations included in this report are the four 270 designs, Figures 3-5 and 7, and the existing (Figures 6 and 8) and modified (Figure 9) 210 deck configurations as discussed previously. Configurations I and II for the 270 utilize 5/16-in. plating; however, the second one includes light transverse stiffeners or headers installed intercostally between longitudinals. Configuration III, the lightest of the three, is the same as Configuration II but with 1/4-in. plating instead of 5/16 in. In all three configurations, the plating is HY-80 and the framing is HTS steel. In going to Configuration IV the plating was held at 1/4 in., but the framing scantlings were revised to a common section (6x4x7 T) for both longitudinals and headers. In addition, the three headers used between transverse web frames in Configurations II and III was reduced to one header in Configuration IV. The plating material was revised from HY-80 to HY-100, tempered up approximately 118,000 psi yield. Various helo deck configurations associated with 210 cutters are included in Figures 6, 8, and 9. Figure 6 shows the scantlings for the portion of the helo deck instrumented during the full-scale tests on the STEADFAST.* Figure 8 shows the helo deck structure for the existing B class of 210-ft cutters as provided by the USCG. This particular deck configuration was used as a basis for arriving at the modified design in Figure 9 which was evaluated in support of the procurement of new SRR helicopters for the 210 cutters, as mentioned previously.

*W.H. Hay and M.O. Critchfield, "Full Scale Evaluation of Flight Deck Structural Responses for 210 Foot U.S. Coast Guard Cutters STEADFAST (WMEC-623) and VIGOROUS (WMEC-627) Under Simulated Helicopter Wheel Loads," reported informally as enclosure (1) to DTNSRDC ltr 77-173-75 of 26 Sep 1977.

Sectional properties for the longitudinals and headers, such as flange and width thickness, etc., employed in the various 270 and 210 configurations are given in Table 3. Table 4, the sectional properties from Table 3 are compared with those which resulted by scaling up the properties of the members in the rigid vinyl model by the scale factor of 4.6. It should be noted that the sectional dimensions are nearly identical for the headers but slightly different for the longitudinals. The main difference is the greater web thickness in the scaled-up (0.1886 in.) versus full-scale (0.17 in.) configurations.

The helo deck structures in Figures 3-9 were evaluated using the helo wheel load data in Table 2. This table lays out the specific tire contact data (load, pressure, footprint dimensions, area of contact) for each load case considered and identifies the deck configuration to which each was applied. Note in the table that a number of main gear landing load conditions for the Navy LAMPS helicopter were involved in the 270 evaluations. In each case, the analyses were performed using rectangular tire footprints which were equivalent to and simulated the actual tire footprints of elliptical shape. It was shown during the model tests that the rectangular footprint produced plating stresses very close to the elliptical one. The rectangular footprint was equivalent to the elliptical in that they had the same pressure and contact area. In addition, the ratio of long- to short-side dimensions on the rectangle was made equal to the ratio of the major to minor axis dimensions on the elliptical. For the finite-element and other analyses of the framing, where a wheel load was applied directly over a stiffener, it was sometimes necessary to simulate the actual footprint by one of equivalent total load, where the length and width dimensions were arrived at as discussed above.

All of the load data in Table 2 refers to tire contact data for fully inflated tires. The rigid vinyl model evaluation also investigated the stresses associated with an inflated tire which "bottoms out" on landing, or where the tire actually blows out and produces a rim load condition. These load conditions are discussed later in connection with the rigid vinyl model.

DESCRIPTION OF EVALUATION METHODS

FRAMING ANALYSES

The objectives of the framing analyses were twofold: first, to develop and validate state-of-the-art analysis methods suitable for helo deck structures of the

type favored by the USCG, and second, using these methods, to determine maximum stresses in the 270 and 210 cutter decks. The analyses dealt with stress evaluations for the longitudinals and headers. Stresses were not calculated for the transverses since they were expected to be of a relatively low magnitude.

Finite-Element Model

All of the analyses performed on the framing of the 270 Configurations I-IV utilized the NASTRAN³ finite-element model seen in Figure 10. This model consisted of approximately 1800 elements (1250 plate elements and 550 bar elements) and 1200 node points. Slight variations in the model were made to accommodate the various 270 configurations, such as the helo deck structure with or without headers. Note that due to symmetry about the transverse deck center line, it was only necessary to model half of the deck structure as indicated. The finite-element mesh for a portion of the model in Figure 10 is shown in Figure 11.

Boundary conditions for the finite-element model included the following: along the transverse center line boundary in Figure 10, the usual conditions of symmetry were imposed; along the opposite transverse boundary, the plating nodes were restrained for all six degrees of freedom, 3 perpendicular displacements and 3 rotations; stiffener nodes were fixed in all degrees of freedom except for rotations in the vertical plane which were elastically restrained as opposed to completely fixed; and the same kind of restraint conditions were used along the longitudinal boundary.

Load locations for the NASTRAN analyses appear on Figures 12 and 13 for the helo decks, with and without headers, respectively. The load cases investigated with the NASTRAN model were the loads applied directly to the longitudinal midspan and panel center in Figure 12 and to the longitudinal-header intersection, header midspan, and panel center in Figure 13. The other indicated load positions are discussed later in connection with the plating analyses and the rigid vinyl model investigations. In fact the outer boundary of the structure shown in Figures 12 and 13 corresponds to the boundary of the rigid vinyl model, as indicated by the dashed lines in Figures 3 through 5.

It should be noted here that the NASTRAN finite-element model of Figure 10 provides reliable and accurate stress and deflection results for the framing members, but not for the plating. For wheel loads placed on the plating, the

deflections were found to exceed one half the thickness of the plating and, therefore, introduce significant stresses. The inclusion of membrane stresses must be accomplished using a nonlinear finite-element or analytical model as discussed in the following section. The modified 210 helo deck of Figure 9 was evaluated using a beam-type NASTRAN finite-element model involving approximately 240 bar elements (no plate elements).

AISC Equations

In addition to the finite-element analyses, the framing members (longitudinals and headers) of all of the 270 and 210 helo deck configurations included in this report were also evaluated using a framing analysis procedure* based on equations published in the AISC design manual for orthotropic steel deck bridges.⁵

The AISC manual allows the determination of the effect of the flexibility of supporting members on the stresses in a loaded member, such as the effect of the flexibility of transverses on stresses in loaded longitudinals. As a part of a current review and updating of the design data sheets for helicopter and aircraft landing decks, the U.S. Navy is incorporating the effect of transverse flexibility and other features of the AISC design manual into the Navy DDS curves and charts.**

The framing analysis procedure referred to in the footnote on the previous page is restricted to the wheels, one or two (dual), of a single landing gear. The effect of a second landing gear was excluded from the study because the finite-element analyses of several USCG helo deck configurations showed that the effect of a second gear on modifying stresses under the first gear was only a few percent. However, more recent work*** has shown that a second gear can cause considerable increase in stress in a loaded longitudinal, especially when the span of the supporting transverse is large.

*D. Lay and M.O. Critchfield, "A Rapid Analysis Procedure for Determining Stresses in the Framing of Helicopter Landing Decks," reported informally as enclosure (1) to DTNSRDC ltr 79-173-180 of 30 Nov 1979.

**R. Chiu, J. Kuo and S. Arntson, "Design Guidelines for Helicopter Landing Deck Structures," reported informally as enclosure (1) to DTNSRDC ltr 80-173-135 of 9 Sep 1980.

***R. Chiu, J. Kuo, and J. Judy, "LSD-41 Helicopter Landing Deck Structural Analysis," reported informally as enclosure (1) to DTNSRDC ltr 79-173-110 of 20 June 1979.

PLATING ANALYSES

Plating analyses were performed for landing gear loads in two locations: in the center of a panel, and directly over a longitudinal header or transverse bulkhead at the panel boundary. It should be pointed out here that these load locations do not always correspond to maximum plating stresses. For typical panel and load geometry, somewhat larger plating stresses may result for a wheel load placed in the vicinity of one-quarter span. The nonlinear finite-element analyses were of a large deflection type, that is, they incorporated the membrane resistance of the plating in addition to the bending resistance. As a result of the full-scale measurements on the 210-ft cutter and preliminary calculations using handbook formulas, it was expected that the plating deflections would be of sufficient magnitude to warrant that the membrane stresses be considered. For example, in the case of the 210, the deflections (0.24 in.) were found to be equal to the thickness of the plating. The finite-element analyses were accomplished using a computer program developed at the University of California in 1971 under contract from the Naval Ship Systems Command.⁴ Figure 14 shows the type of finite-element model used for Configurations II and III. Models for Configurations I and IV used a similar approach. For the plating analyses with the wheel loading in the center of a panel, one quarter of the panel was modeled, as illustrated in Figure 14a. Conditions of symmetry were imposed along the boundaries BC and CD. External boundaries AB and AD were supported vertically and subjected to elastic rotational restraint or springs k_x and k_y , as illustrated in Figure 14a. The elastic restraint comes from two sources--the bending resistance of the plating outside of the loaded panel, and the lateral-torsional resistance of the boundary stiffeners due to rotation about their line of attachment to the plating.

For the plating analyses with the wheel loading over a header or bulkhead at the panel boundary, one half of a panel was modeled, as shown in Figure 14b. Symmetry constraints were imposed along panel boundaries AB and BC. Also along AB, elastic restraint or springs were utilized in the vertical direction in some of the analyses to represent the bending rigidity of the header or transverse bulkhead supporting the plating at that location.

The elastic boundary restraints k_x and k_y for the plating were calculated (see Table 5) using continuous beam theory, finite-element analyses, and design

equations. This is discussed in greater detail in the following section concerned with the stiffener web bending analyses. The elastic constants in Table 5 were in part taken from Figures 15-17, which show the manner of variation of elastic boundary restraint along longitudinal and transverse boundaries for Configurations I-III. The plating analyses were performed using k_x and k_y values which correspond to the horizontal dashed lines in Figures 15-17.

STIFFENER WEB BENDING ANALYSES

Full-scale measurements in 1977 on the helo deck structure of the 210-ft cutter VIGOROUS revealed the existence of a vertical bending deformation, of a local nature, in the webs of the deck longitudinals which produced stresses in excess of yield* (see Figure 18). This local mode of structural behavior will be referred to in the report as "web bending." Because web bending was only recently recognized as being of potential importance to the designer, it is not taken into consideration in the design procedures for helicopter landing decks in the USCG and U.S. Navy. A validated method of analysis was needed so that the importance of web bending in the design process of helo deck framing could be fully investigated and evaluated.

Analysis capabilities were pursued for determining web bending stresses in the following three design situations involving helo deck framing: (a) longitudinals--without headers; (b) longitudinals--with headers; and (c) headers alone (see Figure 19).

Structural problems (a) and (c) above, in Figures 19a and 19c are similar in that they both involve a lighter member subject to web bending (longitudinal or header) supported at its extremities by heavier intersecting members (transverses or longitudinals). Analyzing structural problem (b), Figure 19b, for web bending is more complex because the longitudinals are supported by lighter header members in addition to the heavier transverse members. The support provided by the headers is only of a partial nature in that it extends approximately half way down the web of the longitudinal. The lower half of the web and the flange of the longitudinal are free to deflect out of plane.

*W.H. Hay and M.O. Critchfield, "Full Scale Evaluation of Flight Deck Structural Responses for 210 Foot U.S. Coast Guard Cutters STEADFAST (WMEC 623) and VIGOROUS (WMEC 627) Under Simulated Helicopter Wheel Loads," reported informally as enclosure (1) to DTNSRDC ltr 77-173-75 of 26 Sep 1977.

Two types of analytical capabilities were pursued for addressing the above structural problems: design-oriented equations for rapidly predicting web bending stresses, and a finite-element model for correlating with and confirming the results of the design equations. These methods were to be validated by web stress results obtained from the rigid vinyl model evaluation of the 270 helo deck configurations and full scale tests on the 210 cutter. Development of both methods was pursued simultaneously with funding support for the web finite-element analysis, of immediate need for the Coast Guard work, being provided by the USCG. Development of the design equations was supported by the U.S. Navy since they have potential application to helo deck structures on Navy ships.

Finite-Element Model

A finite-element model for investigating web bending was first developed for a longitudinal without headers using the element capability present in a computer program available from the University of California.⁶ The web of the longitudinal was modeled with a fine mesh of elements, utilizing ten elements from the top to the bottom of the web to accurately model the bending of the web (see Figure 20). In the lengthwise direction of the stiffener, thirteen elements were used to represent the web from its intersection with the transverse member to midspan. Only one half of the stiffener was modeled due to symmetry. The web itself was therefore modeled with a total of 130 elements, 260 effectively for a full stiffener. The lateral bending rigidity of the flange of the stiffener strongly influences the degree to which web bending is allowed to occur (see Figure 18). This flange was modeled using thirteen beam-type elements (Figure 20) whose sectional inertia properties were calculated to represent those of the actual flange.

The last effect to be modeled is the plate bending rigidity. Referring to Figure 18, the applied moment M_1 at the edge of a loaded panel is resisted by a moment M_2 at the top of the web and the moment M_3 in the plating. The moment M_3 is equal to $k_p \gamma$ where γ is the angle of rotation of the stiffener web and plating at their point of intersection, and k_p is an elastic constant representing the rotational restraint or stiffness of the plating. The plating restraint k_p is converted to elastic springs which are attached to the nodes of the finite-element model along the

top of the web. Therefore, an important step in the development of the finite-element model was obtaining a method for providing a good approximation for the plating rotational restraint since it affects the way in which the applied moment M_1 in Figure 18 is distributed between the web and the plating. If the plating is represented by elastic constants which are too large, the calculated web bending moment M_2 and stress will be too low or unconservative, and vice versa. In determining approximate plating restraint constants, continuous beam theory was used to obtain k_p for panels with length-to-width ratios of three or greater where this approach may be shown to be valid. For panels with ratios less than three particularly the case of the helo deck configuration with headers, it was necessary to set up finite-element models for the panels of interest. In the later cases, the constant k_p was then determined by applying a moment distribution in the form of a half sine wave to one edge of the panel and then computing the rotation angle of the same edge. The approximate restraint constant is then obtained by dividing the moment (per unit length of panel edge) by the rotation angle. Table 5 gives the plating rotational constants which are calculated using the above methods for the helo deck configurations on the 270 and 210 cutters.

Besides the elastic springs which are attached to the nodes along the top of the web in Figure 20, the nodes at the left end were simply supported and the nodes at the right end or midspan were clamped to represent the desired symmetry condition.

The finite-element model for the longitudinal with headers is shown in Figure 21. It has ten less web elements and one less flange element than the model in Figure 20 for a longitudinal without headers. However, the main difference from the previous model is the fixing of the nodes against out-of-plane deflections where the headers intersect the web, as indicated in Figure 21.

The moment distribution applied to the top of the web is a quarter sine wave in Figure 20 and a full sine wave as illustrated in Figure 21. All calculations were performed for a maximum moment value of 100 in.-lb/in. The resulting web bending stresses were then scaled up to reflect the actual magnitude of the applied web moments as determined from the rigid vinyl model tests (270), full-scale tests (210), and plating large deflection calculations (210-modified deck).

Design Equations

Design equations have been derived for predicting web bending stresses in longitudinal (without headers) and headers alone, problems (a) and (c) described earlier. The derivation of these equations is given in Appendix A. In order to provide a rapid prediction capability for the designer, the solution procedure has been programmed on the 4051 Tektronix minicomputer. (See Appendix B for program listing.) It is important to note that the equations provide a rapid analysis capability for web bending stresses once the panel edge moment M_1 is known. This moment is determined either from available model or full-scale test data or large-deflection finite-element analyses of the loaded panel. Research, currently underway, is providing a design oriented method for rapidly calculating the moment M_1^7 .

As mentioned above, the design equations presently available are based on physical assumptions which closely model the web bending behavior of longitudinals (without headers) and of headers. In either situation, a lighter member is supported by heavier members at its ends. Table 6 shows the accuracy of the design equations when compared with calculations using the finite-element model in Figure 20. The two analysis methods are seen to be in excellent agreement. The validation of the finite-element procedure and design equations against the rigid vinyl model and full-scale results is discussed in a later section of the report.

RIGID VINYL MODEL

As stated earlier the 270 helo deck Configurations I and II (Figures 3 and 4) were chosen as the two cases to be evaluated using the rigid vinyl modeling technique.* This experimental analysis technique is described in detail in References 1 and 2. Both Configurations I and II are characterized by 5/16-in. plating and differ in framing arrangement only by the addition of transverse "headers" in Configuration II. By performing experiments on a rigid vinyl model of Configuration I and then modifying the structure to include headers, both configurations could be investigated using one model.

It was determined that a conveniently sized model would be one-fifth scale. Since deck plating stresses were of primary concern it was desired that the model plating thickness be exactly one fifth the prototype plating thickness. However,

*J.L. Rodd, "Rigid Vinyl Model Evaluation of Helicopter Landing Deck on USCG 270 Foot Cutter," reported informally as enclosure (1) to DTNSRDC ltr 80-173-51 of 14 Apr 1980.

the available thickness of large rigid vinyl sheets would have to govern the actual scale of the model. Using a model plating thickness of 0.068 in. resulted in a scale factor of 4.6, and sizes for stiffeners and overall dimensions were then determined accordingly. The scaling laws used to design the model and reduce the data are outlined in Table 7.

Figures 22 and 23 show the rigid vinyl model Configuration I mounted in the test foundation. The longitudinal stiffener arrangement as well as the heavy transverse web frames are visible in these photographs; the intercostal headers were not yet installed. Several boundary conditions were imposed on the structure to insure correct structural response to tire footprint loads. The extreme fore and aft edges of the model were attached to simulated transverse bulkheads using pinned joints (hinges at each longitudinal stiffener). A double hinge system was used at one edge to allow deck plating to deform longitudinally as well without restraint. The "transverse bulkheads" used were heavy steel channels rigidly fixed to the test foundation. These are visible in the figures as well as the stanchions located beneath the two transverse web frames. These boundary conditions allowed the vertical position of the deck to be fixed at the stanchions and at the transverse bulkheads without introducing unwanted resisting moments or membrane restraints in the deck plating. The design of the stanchions was governed by a number of considerations which are discussed in detail in the rigid vinyl evaluation report previously footnoted. A final set of boundary conditions imposed on the structure were the end moments applied to the transverse web frames at each stanchion location. Since no structure was used to simulate the restraining effects of the ship's hull, it was necessary to hang weights from the ends of each transverse web frame. The web frame end moment values at each stanchion location were taken from finite-element results for each load case. During the experimental process it was determined that the effects of these end moments on grillage and panel stresses were negligible.

For landing gear loads (Table 2, case 2) and locations (Figures 12 and 13), plating and stiffener stresses were measured with strain gages at various locations (Figures 24, 25) on the rigid vinyl model. In addition to these measurements, the vertical deflection of plating and grillage members was recorded using linear potentiometers at a limited number of locations for a few pertinent load cases.

The strain gage instrumentation included four types of installations:

(a) Single gages were mounted on the center of stiffener flanges to measure stiffener stresses. (b) To record plating stresses, biaxial gages were installed both on the top and bottom surfaces of the plating at panel centers and edges. Both transverse and longitudinal distributions of stresses were obtained. (c) On the webs of longitudinal stiffeners and headers, special biaxial gages were installed to measure vertical web bending stresses near the stiffener plating weld. (d) Finally, a pair of single axial gages was installed on each stanchion to compare stanchion loads.

Figure 24 illustrates the system of single gages used to measure stiffener stresses. Figure 25 shows the various installations used for measuring plating stresses.

The landing gear load chosen for the investigation of the 270 helo deck was the 18,500-lb LAMPS wheel load (Table 2, case 2). This load was simulated on the rigid vinyl model with 13.1 lb applied statically using several "footprints." The footprints of interest were the elliptical, rectangular, rim load, and combined rim and rectangular load, shown in Figure 26. The most appropriate footprint to use for model experiments was an elliptical shape since it represents the best approximation of the contact profile for an actual helo tire; however, it was desired to assess the use of a rectangular footprint of equal area. The corresponding finite-element analyses which were performed concurrently could be greatly simplified by the use of the rectangular footprint. Therefore, it was desired to establish early in the rigid vinyl model experiments if the rectangular footprint could be used in place of the elliptical for all subsequent tests. As will be shown in the discussion of the results, the rectangular load induced stresses very close to the elliptical load. Therefore the rectangular load footprint was utilized throughout the experimental evaluation.

It was suggested that tire bottoming effects be investigated during this program as well. The rim load defined in Figure 26 is a simplified representation of the footprint which occurs during complete bottoming or blowout of the helicopter wheel on impact (no tire pressure assumed). Finally, the combined load shown in Figure 26 is simply a superposition of the rectangular load and rim load footprints, each contributing half the total load. Loading devices for simulating the various footprints in Figure 26 are discussed in the previously footnoted rigid vinyl report.

An automatic data acquisition system was used to measure strains and deflections induced by the various wheel loads. An on-line computer was used to reduce the data and list equivalent stresses and deflections in prototype terms almost immediately for each experiment. An in-depth description of the experimental procedure is provided in Reference 1.

FULL-SCALE TESTS

In the course of the evaluation efforts on the 270 helo decks, an opportunity arose on relatively short notice to implement a limited effort to acquire full-scale data* on two 210-ft cutters, STEADFAST and VIGOROUS, (Figure 2) during their brief shipyard availability period. In each case, structural response measurements were obtained from a typical helo deck panel loaded by a simulated helicopter wheel. The objectives of these tests were (a) to provide data on the structural capacity of the helo flight deck for establishing design criteria for a new helicopter landing gear configuration; (b) to validate a general finite-element analysis procedure and other analytical methods for evaluating the 270 helo deck structure, as well as future helo deck configurations; and (c) to provide data for correlation with results from rigid vinyl model experiments on the 270 helo deck configurations.

The full-scale effort actually consisted of two phases. The first test was conducted on the USCG cutter VIGOROUS (WMEC 627) using the weight of a forklift truck as the applied load and measuring helo deck plating vertical deflections only. A second series of more comprehensive tests was conducted on the USCG cutter STEADFAST (WMEC 623) using varying loads while monitoring plate and longitudinal stringer deflections and stresses (Figures 27 and 28). A total of twenty-one strains and eight deflections were monitored during the STEADFAST static test. Scanlings for the instrumented panel on STEADFAST are given in Figure 6, and the location and orientation of each of the measurements made are shown in Figure 29.

Plate stresses were determined from strain measurements of eight biaxial strain gage rosettes that were installed at four exterior and corresponding interior locations on the selected helo flight deck panel. Individual gages for each plate rosette were oriented transversely and longitudinally (see Figure 29).

*W.H. Hay and M.O. Critchfield, "Full Scale Evaluation of Flight Deck Structural Responses for 210 Foot U.S. Coast Guard Cutters STEADFAST (WMEC 623) and VIGOROUS (WMEC 627) Under Simulated Helicopter Wheel Loads," reported informally as enclosure (1) to DTNSRDC ltr 77-173-75 of 26 Sep 1977.

Longitudinal stiffener strains were recorded using two biaxial gage rosettes (gages oriented vertically and longitudinally) located on either side of the stiffener web near the flight deck plating. A single longitudinal gage was also located on the center of the stiffener flange to measure longitudinal bending in the stringer.

To minimize the effect of thermal drift, all strain gages were temperature compensated, and frequent zero-load readings were taken.

Plating vertical deflections were measured at seven locations on the helicopter deck, three along the longitudinal centerline of the instrumented panel and four along the centerline of an adjacent panel (Figure 29). Longitudinal stiffener rotation was monitored with a dial gage (D8) placed between adjacent longitudinal stiffeners, as shown in Figure 29.

To apply the static load to the helo deck in such a manner as to simulate the weight and load pattern of a helicopter resting on the deck, a forklift truck of weight 11,930 lb was employed (Figure 28). One of the rear wheels of the forklift was used to apply a simulated helo wheel load while the tire pressure was adjusted to produce the desired tire contact dimensions and large rectangular weights were added to the rear of the forklift. The maximum load case was obtained by transmitting a load to the panel using a timber block under the rear end of the forklift. For both the "inflated tire" and "timber block" load conditions, a 1/2-in. rubber pad between the simulated wheel load and the plating having the desired tire-contact dimensions was used. In order to minimize the influence on the plating stresses of the forklift wheels not being used in the helo wheel simulation, wooden planks were used under those wheels to distribute their loading effect away from the instrumented region of the panel. Top and bottom views of the panel instrumented for the tests are shown in Figure 27 with specific transducer locations indicated in Figure 29. A total of seven loads cases , from 3260 to 8860 lb, were performed during the tests.

RESULTS OF EVALUATION

FRAMING RESPONSE

This section is concerned with the structural response of the framing members, i.e., stresses and deflections in the longitudinal and transverse stiffener members of the deck associated with the usual beam-type bending behavior. In obtaining these results, wheel loads were placed at those locations on deck stiffeners which would produce the greatest bending moment in the stiffeners. Maximum stresses occurred, at these locations, in the lower flange of the stiffeners since the lower flange is furthest from the section neutral axis. The corresponding stress in the upper "flange" of the stiffener occurs in the deck plating and acts in a direction parallel to the stiffener. This plating stress associated with overall stiffener bending is not governing for the plating since it is considerably exceeded by the local plating stress in the transverse or short-span direction. Framing stresses associated with web bending is treated in a later section.

Flange Stresses

Table 8 is a summary of maximum stresses for the framing of the four 270 helo deck and two 210 deck configurations investigated. Validation of the analytical methods (finite-element and AISC equations) was accomplished for Configurations I and II of the 270 and the existing 210 decks for which model and full-scale data were available, respectively. As indicated in the table, the analytical and experimental results for these configurations are in very close agreement. Because of this excellent correlation, the analytical methods were used to calculate framing stresses on Configuration IV of the 270 and on the modified deck on the 210 cutter, for which no experimental data was available.

All of the stresses in Table 8 are below yield, (33,000 psi) for mild steel. The addition of headers to Configuration I reduced the longitudinal flange stresses from 26,000 to 16,100 psi but resulted in a stress of 29,000 psi in the headers themselves. For Configuration IV, stresses in both the longitudinals and headers were found to be approximately 20,000 psi. Stresses in the 210 decks were found to be noticeably lower, in the range 9,000-15,000 psi, due to substantially lower wheel loadings.

In addition to the maximum stress data in Table 8, stress profiles showing the distribution of stress along the longitudinals and headers have been developed for Configurations I and II. Figure 30 illustrates the variation in flange stress in the center-line longitudinal of Configuration I from the stiffener midspan, where the load has been applied, to its intersection with the heavier transverse frame. Again, note the excellent agreement with the rigid vinyl model stress value at midspan. The flange stress profile for the center-line longitudinal in Configuration II (with headers case) is shown in Figure 31. This figure also shows that shifting the wheel load from the stiffener to the panel midspan resulted in a 16 percent reduction in the stiffener stress from 16,000 psi to 13,000 psi based on the finite-element analysis. This reduction figure, however, is only approximate because the deck plating is deflecting nonlinearly under the load and is therefore not validly modeled by the linear NASTRAN analysis. Lastly, Figure 32 gives the flange stress profile for the header in Configuration II when loaded at midspan. The agreement between the finite-element and model results are again seen to be very close.

Deflections

Stiffener deflection profiles are given in Figures 33-35 for 270 Configurations I and II. The deflection profile for one half of the center-line longitudinal (symmetry employed) for Configuration I is shown in Figure 33. This figure brings out the relatively small influence of the second helicopter wheel on the deflections produced under the first wheel. The small influence of the second wheel on the first wheel deflections is attributable to the fact that the second wheel is resting on a longitudinal adjacent to stanchions supporting the deck. The deflection profile along the transverse center line of the Configuration I deck is contained in Figure 34. Again, the small influence of the second wheel on deflections under the first wheel is evident. It should be noted that the plots in Figure 34 should only be viewed from the standpoint of providing a qualitative feel for the variation in plating deflection since the deflections particularly near the centerline wheel load are approaching the thickness of the plate where membrane stresses become important. NASTRAN does not account for such stresses. Lastly, Figure 35 provides some insight as to the effect on plating deflections along the transverse center line of the deck of adding headers, i.e., going from Configurations I to II. The headers were found

to take the oscillation out of the plating deflection between longitudinals L1 and L3; otherwise they did not affect the deflection of the longitudinal significantly.

PLATING RESPONSE

As mentioned previously, the structural response of the helo deck plating for various 210 and 270 deck configurations and wheel load conditions was evaluated using analytical, rigid vinyl model, and full-scale techniques. The three main objectives were (a) by obtaining maximum plating stresses, to provide the USCG with a basis for assessing the performance of the various designs; (b) on the basis of the rigid vinyl results, to validate the finite-element and other analytical procedures as general plating analysis tools; and (c) to investigate the influence of various load parameters such as tire print geometry, orientation, and load placement on plating responses. The maximum stresses and validation of analytical procedures are discussed first.

Stresses and Validation of Analysis Methods

The validation of analytical methods for plating response was accomplished and maximum stress results were obtained for two types of loading conditions: (a) wheel loads acting at the center of a panel where stresses at the panel center and edge in the short span or transverse direction were of interest, and (b) wheel loads straddling the stiffeners at transverse or longitudinal panel boundaries where the largest stress occurs directly under the load in a direction perpendicular to the panel boundary. Here it should be noted, that the above load locations do not necessarily correspond to the maximum plating stresses. Somewhat greater values may result, for typical panel and load geometry, when the wheel loading is in the vicinity of quarter span in the transverse direction.

Results for wheel loads at panel centers are summarized in Table 9. Stresses are presented for the 270-class Configurations I-IV and the 18,500- and 19,430-lb LAMPS main gear wheel loads. Plating stresses at the panel centers are seen to be consistently higher than at the panel edges. For the panel center locations, the finite element stresses are only 3 percent below the rigid vinyl model value for both Configurations I and II. The finite-element prediction for the panel edge is 15 percent below the model value. However, the panel edge is not the governing

location when the wheel load is in the center of a panel. In view of the excellent agreement in predicting governing stress magnitudes for the panel center, this suggests that the finite-element analyses may be considered suitable for application in preliminary design. Following validation, the finite-element procedure was used to calculate plating stresses for Configurations III and IV, as indicated in Table 9. Note that no rigid vinyl models existed for these configurations. Comparing stresses at the plate center based on the finite-element calculations, it is seen that they range from a low of 63,000 psi for the heaviest deck structure, Configuration II, to 77,800 psi for Configuration I. None of these exceed the yield point for HY-80 steel; the material of lowest yield under consideration for these configurations.

The correlation between the finite-element and model data discussed above is further illustrated in Figures 36 and 37 by the transverse stress profiles for the plating in Configurations I and III. These figures also demonstrate the excellent results obtained using a plate-strip finite-element model. These results motivated the development of nonlinear plate-strip equations⁷ for predicting stresses in long panels.

Recall that full-scale stress measurements were made on the 210 cutter STEADFAST using a forklift to simulate a helo tire loading. Stress and deflection results from these full-scale tests are shown in Figures 38 and 39, superimposed on transverse stress and deflection profiles obtained from nonlinear finite-element analyses of the plating. The agreement between full-scale and analytical results on the 210 is considered to be good, especially for the stress.

Table 10 presents the finite-element and rigid vinyl results for wheel loads straddling stiffeners at either transverse or longitudinal boundaries. Configuration II is the only one for which both finite-element and model data exists. Note that the finite-element prediction of 91,700 psi exceeds the model value (76,000 psi) by 21 percent. This is probably due to the assumptions of simply supported boundaries on three sides and a rigid nondeflecting stiffener on the fourth side where the wheel load is applied. Because of the conservative nature of the analytical prediction, the finite-element model and approach used appear to be valid for other panels of similar geometry. Results in Table 10 for Configuration I were obtained exclusively for the model tests. Comparing the 73,500-psi stress for a wheel load on

the transverse with 80,000 psi for a load in the center of a panel (Table 9), it is seen that the governing rectangular load condition for Configuration I is a central panel load. The stress entries of 100,000 psi for Configuration I and 86,500 psi for Configuration II indicate that an extreme rim load condition, associated with severe tire bottoming, can produce very large stresses when the loads exactly straddle stiffeners (longitudinals in this case). The stress value for Configuration I is 15 percent higher than the value for Configuration II. The results for Configuration II, when compared with stresses in Table 9 for central panel loads, indicate that the governing rectangular load condition for Configuration II is a wheel load straddling the header. (Recall that the opposite occurred for Configuration I.) The stresses determined for Configurations III and IV using the non-linear finite element analysis are considerably greater than those for Configurations I and II. The increased stresses are attributed to two factors: the lighter plating (1/4 in.) in III and IV compared to that (5/16 in.) in I and II; and the dual wheel effect (for the 20,000-lb tail wheel) where the spacing between the two tire prints increases the moment arm of the resultant force acting on each tire patch. In Table 10, the second entry of stress for Configuration IV (136,000 psi) shows that the plating stress is only alleviated slightly by going from the assumption of a rigid to a flexible longitudinal under the dual tail wheel. Since the longitudinal was modeled to be a little more flexible than in reality, the final plating stress should be within the range 136,000-141,500 psi.

Influence of Tire Print Geometry and Load Placement

In addition to forming a basis for validating the analytical procedures for helo deck evaluation, the rigid vinyl model evaluations were used to investigate the effect on plating stresses of various tire print geometries, load locations, and orientations on helo deck panels. Figure 26 illustrates the four tire footprints considered in the investigation: elliptical, rectangular, rim load, and combined rim and rectangular. The elliptical footprint representation is closest to the actual one. The rectangular footprint was computed from the elliptical one by maintaining the same contact area and ratio of major to minor axis dimensions. The rim condition represents an extreme and somewhat idealized condition associated with a

tire bottoming situation where the tire has blown out or collapsed. Finally, the combined footprint characterizes a bottoming condition where half of the load is carried by the rim and half by the inflated tire.

Along with various contact geometries, the model evaluation also looked into the influence on plating stress of shifting loads transversely and longitudinally on panels to locations indicated in Figures 12 and 13.

Before summarizing the results of the model evaluation, it should be pointed out that it was discovered near the end of the model evaluation program that a potentiometer positioned at the panel center and used to record panel deflections was "binding up" as the panel deflected. Since it was believed that this binding action of the potentiometer was likely to affect the measured values for panel stresses and deflections, a retesting effort was undertaken. The scope of the retest was limited to those stresses and locations which were found to be the governing ones during the original tests using a rectangular tire footprint. Since the retest effort did not encompass load and stress locations away from the panel center, the data points in Figures 40-47 for other than a central stress due to a central load represent results from the original tests with the uncertain potentiometer effect involved. It is for this reason that it is recommended that the results at other than the panel center in Figures 40-47 be viewed with that consideration in mind. This suggests that these curves are of more value for indicating the influence or trends associated with shifting loads on a panel than for the determination of stress, in an absolute sense, resulting from the load placement. Again, however, the retest values of the midspan stresses associated with midspan loads are included and these magnitudes are accurate representations.

Since the results of the rigid vinyl evaluation are discussed in detail elsewhere,* this report will only summarize the main points of the model effort. These are next presented below under the headings Tire Print Geometries and Load Location and Orientation.

Tire Print Geometries. The highest plating stresses at the panel edge (100 and 87 ksi, Configurations I and II) were obtained for the rim load straddling a longitudinal stiffener at stiffener midspan (see Figures 42 and 45).

*J.L. Rodd, "Rigid Vinyl Model Evaluation of Helicopter Landing Deck on USCG 270 Foot Cutter," reported informally as enclosure (1) to DTNSRDC ltr 80-173-51 of 14 Apr 1980.

The next highest stresses (80 and 65 kis, Configurations I and II) occurred at the panel center for a rectangular footprint in that location (see Figures 40 and 44).

For Configuration I, the elliptical tireprint at the panel center caused a transverse stress at the panel center which exceeded the rectangular tireprint value by less than 1 percent (Figure 40). The elliptical tire print at quarter span caused a stress at the panel edge (of adjacently loaded panel (see Figure 42) which was 11 percent greater than the rectangular tire print value.

For Configuration II, the elliptical tire print at the panel center caused a transverse stress at the panel center which exceeded the retangular tire print value by 16 percent (Figure 44).

The combined rim and rectangular print (Figures 40 and 42) did not produce a governing stress condition for any of the load locations. In general, the influence curves for the combined load followed the trend of the rim load curves, but with substantially lower stresses.

Load Location and Orientation. The influence of wheel load location and orientation on plating stresses for Configurations I and II is demonstrated in Figures 40-47. It should be noted that plating center and edge stresses have been measured for wheel loads in three locations: midspan, quarter span, and edge. For our panel configurations, the maximum plating stress probably occurs for a wheel load in the vicinity of quarter span and probably somewhat exceeds the value for an actual quarter-span load. Since these figures are discussed in detail in the report footnoted on the previous page, only the main points of the discussion are listed below.

1. For both Configurations I and II, rim loads straddling a longitudinal member result in the highest plating stresses (Figures 42 and 45), and rectangular loads in the panel center result in the next highest stresses (Figures 40 and 44). In each case, these stresses occur in the transverse direction under the load.
2. The effect on panel edge stress of moving a load from midspan to quarter span to edge is to cause an increase in stress for both the rim and combined footprints on Configurations I and II (Figures 42 and 45). The increase is particularly dramatic for a rim load between the quarter span and edge locations.

3. For both the rectangular and elliptical tire prints, loads positioned on a panel at quarter span between longitudinals produced a greater stress at the panel edge than either a load at the panel center or edge locations (Figures 42 and 45). This result is important because it necessitates that web bending stresses in longitudinals be calculated on the basis of a quarter-span rather than a midspan panel load.

4. The effect on plating response of rotating the rectangular load patch by 45 deg was explored using Configuration I. It was found that the 45 deg orientation reduced the maximum or governing plating stresses in all instances (Figures 41, 46, 47) except one (Figure 43). The plating stress at midspan under a central load was reduced from 80 ksi to 68 (Figure 41). A greater reduction in stress, from 74 ksi to 52 ksi, occurred in longitudinal direction under a load on the transverse panel boundary (Figure 46).

5. Rim and combined loads at quarter span produced greater stresses at panel centers than for loads at other locations (Figures 40 and 44).

6. It was found on Configuration I that moving the load longitudinally on the panel did not produce a significant reduction in transverse stress under the load until the load approached the far transverse boundary (Figure 47).

STIFFENER WEB BENDING RESPONSE

An earlier section of this report provided a description of stiffener web bending and the analytical and experimental methods used to evaluate web bending stresses. Therefore, this section will go immediately into a discussion of web bending results for the various configurations investigated.

A summary of web bending stresses obtained for the 270 and 210 helo deck configurations is provided in Table 11. These results are of particular interest for serving as the bases for the validation of the analytical methods for web bending and for providing maximum expected values of web bending stresses for the configurations of interest.

Validation of Web Bending Analyses

Using the finite-element method and design equations, web bending stresses in the longitudinals of Configuration I were determined to be 25,600 and 24,400 psi, respectively, as indicated in Table 11. The agreement between the two analytical

approaches is seen to be excellent and is further supported by the more detailed comparison of these two solution methods in Table 6.

The analytical predictions of 25,600 and 24,400 psi for the longitudinals in Configuration I are 11.9 percent and 15.3 percent under the corresponding model value of 28,800 psi. Similar correlation in results, in Table 11, was achieved for a load at quarter span. For the longitudinals in Configuration II, the finite-element prediction of 28,800 psi exceeded the test value of 24,500 psi by 17.3 percent. While the correlation between analytical and model results for Configuration I is a little better than for Configuration II, the key point is that the analytical results for Configuration II are on the conservative side. The best correlation was obtained for the headers in Configuration II. The header stress of 44,630 psi, based on the design equations, is seen to exceed the model value of 42,900 psi by only 4.0 percent.

A more graphic picture of the relationship between web bending stresses based on analyses and tests for longitudinals in Configurations I and II is given in Figures 48 and 49. In these figures, the model values are shown superimposed on plots of the variation in web bending stress from the top to the bottom of the web. The stress is seen to vary from a maximum value at slightly above the gage location to essentially zero at the bottom of the web. Although this suggests that web bending stresses may exceed those given for the gage elevation in the web, it is believed that the presence of weld fillets extending down into the web up to 1/4 in. may reduce the higher stresses indicated above the gage locations.

Finally, two points should be made concerning the model results for Configuration I. First, values of panel edge stress (used to arrive at the moment loading for the web bending analysis) and the web bending stress of 28,800 psi had to be taken from different gage sites and tests due to a gage failure. Secondly, as mentioned earlier, it was recognized that the deflection potentiometer under the panel load was binding.

The last entries in Table 11 are the web bending results for the longitudinal stiffeners on the existing 210 helo deck structures. Full-scale measurements on the 210 (see report cited by earlier footnote), for a simulated wheel load of 3260 lb produced a web bending stress of 22,800 psi, which is approximately five times the calculated values of 4500 and 4000 psi using the finite-element model and design

equations (see Appendices A and B). Plots of plate and web bending stress for the 210 are given in Figures 38 and 50. An explanation was sought to try to explain the large discrepancy between test and analysis above. The results just given indicate that the web of the longitudinal in the full-scale test saw considerably more moment than found in the analysis. This finding is supported by the results at the bottom of Table 12 where it is seen that the analytical models distributed the panel edge moment M_1 (177.1 in.-lb/in.) differently between the web M_2 and plating M_3 than occurred in the actual full-scale stiffener. One explanation for this behavior is that the bending stiffness of the plating in the full-scale structure is drastically less than the stiffness assumed in the finite-element model or present in the plastic model since the latter two correlated reasonably well for the 270-class cutter. Further study of this problem suggests that this explanation is a reasonable one. Table 13 indicates that the design equations, derived in Appendix A, produce a web stress essentially equal to the measured value of 22,750 psi if the plating stiffness constant k_p^* is reduced from 6700 (the nominal value used in computing the web stress) down to 200. Moreover, it is hypothesized in Table 13 that the presence of residual plating stresses associated with welding the stiffeners to the plating could be responsible for this drastic reduction in plating stiffness if they approached the buckling stress for the unstiffened plating. Measurements have indicated that plating residual stresses may be as much as 0.2 times the yield stress.⁸ Applying this line of reasoning to the HY-80 plating in the 210 deck, the residual stresses could potentially reach the vicinity of the computed panel buckling stress (approximately 15,000 psi). It must be cautioned here that no measurements of welding-induced residual stresses on helo deck plating have been made in the U.S. Coast Guard or U.S. Navy to support the discussion above.

The above hypothesis was presented in a meeting with the USCG and it was pointed out that an upper bound on web bending stress could be obtained by assuming the stiffness k_p of the plating equal to zero (to account for potential residual stresses). However, after some discussion, it was decided to retain the assumption of fully effective plating in performing the web bending stress calculations for all the helo deck configurations.

*It should be noted here that in the derivation of the web bending equations in Appendix A, the parameter c is used in place of k_p .

Maximum Web Bending Stresses

Maximum web bending stresses for the 270-class Configurations I through IV are readily identified from Table 11. For Configurations I and II, the greatest web bending stresses are 43,000 psi in the longitudinal (of Configuration I) and 60,000 psi in the headers in Configuration II.* Observe that the 43,000-psi value in the longitudinals is approaching a yield of 47,000 psi for HTS steel, and 60,000-psi stress is in excess of yield. Also, note that these maximum stresses are occurring for wheel loads at one-quarter span locations with respect to either transverse or longitudinal directions as illustrated in Table 11.

For Configuration IV, the maximum web bending stress in the longitudinals was calculated to be 59,000 psi for a wheel load at one-quarter span with respect to the transverse direction. Web bending stresses in the headers should not exceed this value and, in fact, should be less than yield as indicated in Table 11. The latter conclusion is based on the 21,000-psi stress calculation for a longitudinally oriented tire print at midspan in conjunction with the effect of shifting wheel loads from midspan to quarter-span locations. It was determined from the analyses that shifting the wheel load from panel midspan to quarter span, for either longitudinally or transversely oriented tire prints, resulted in an increase in web bending stresses in almost all instances. Increases based on rigid vinyl model results were 35 percent for longitudinals in Configuration I, 51 percent for the longitudinals in Configuration II, and 48 percent for the headers in Configuration II. This dependency of web bending stress on panel load locations is further illustrated in Figures 51 and 52.

The web bending stresses for the longitudinals in Configuration IV were found to be greater than the values for either Configurations I or II. A significant factor in accounting for the increase in web bending stress between Configurations II and IV appears to be the reduction in plating thickness from 5/16 to 1/4 in. between the two configurations. In order to develop more insight into the effect of plating thickness on web bending stress, the relationship between plating thickness and web bending stress was investigated for Configuration I. In this study, the stiffener scantlings and spacing of Configuration I were maintained while the plating thickness was varied from a maximum of 0.5 in. down to 0.15 in. The

*These stresses include a direct-compression stress component which has been added to the web bending component.

results of this study in Figure 53 showed that as the plating thickness decreases, the web bending stress increases, supporting the earlier observation regarding Configurations II and IV.

Some further observations on web bending in Configuration IV of the 270 deck may be made in light of the web bending results just given for the full-scale 210 deck. First note that the existing 210 deck (Figure 6) becomes essentially the same as Configuration IV (Figure 7) of the 270 if a 6x4x7 header is added between transverse web frames in the 210. Since the full-scale tests showed the web bending stresses in the 210 to be approaching yield for a wheel load of 8950 lb, it can be expected that doubling the wheel load to 18,500 lb (used on Configuration IV of the 270) while only adding a single header is unlikely to reduce the web bending stress from the vicinity of yield. In fact, the rigid vinyl model evaluation on the 270 resulted in the web bending stress dropping by only 14.0 percent when the headers were added. It is clear that this small reduction is out-weighed by the 100 percent increase in wheel load. So, if the web bending stresses in the 210 full-scale deck were really at yield, as measured, the possibility exists that the longitudinals of Configuration IV would experience some local yielding as well. This possibility hinges on whether the plating in the 270 turns out to be as ineffective as the plating in the 210 due to residual stresses or to some other unknown effect, as discussed previously.

SUMMARY AND CONCLUSIONS

This report presents the results of structural evaluations performed on four helo deck designs for the new 270 cutter and two designs for the 210 cutter (Table 1). Scantlings for these configurations are illustrated in Figures 3-9, and wheel load conditions are given in Table 2. The structural evaluation program included the validation, based on rigid vinyl model and full-scale tests, and performance of three types of analyses on the helo deck structures: (a) framing analyses using conventional finite element analyses³ and AISC published equations;^{*,5} (b) nonlinear large-deflection analyses⁴ of the plating for wheel loads in governing panel locations; and (c) analyses of web bending in the framing using finite-element models⁶ and design equations (Appendices A and B). These evaluations:

1. provide the USCG with a technical basis for evolving a design for the new

270 helo deck, for assessing the strength of existing and modified 210 helo decks, and for developing design methods for helo deck structures similar to those on the 270 and 210 cutters;

2. identify regions of relatively high stress in helo deck structures which are not addressed by current design procedure and tools;

3. validate a series of analytical methods for general application to the analysis of helo deck structure of similar configuration to those evaluated; and

4. result in reduction in helicopter deck structural weight for the 270 class of 6 percent in the framing and a possible reduction of 20 percent in the plating if 10.2# plating is used.

Specific results of the program are outlined below. Maximum stress results for the framing and plating of the various helo deck configurations are summarized first.

270 DECK STRESSES

Framing

Flange stresses in the longitudinals of the four 270 decks evaluated are 26,000 psi or less, below the yield strength for mild or HTS steel (Table 8). Header flange stresses are 29,000 psi for 270 Configurations II and III (Figures 4 and 5), approaching the yield for mild steel. For Configuration IV (Figure 7), the header flange stress is 20,000 psi, below yield.

Stresses were also evaluated associated with web bending in the longitudinals and headers. With one exception, stresses for longitudinals and headers of Configurations I and II were found to be within the range 25,000-40,000 psi (Table 11), all below yield for HTS steel. The one exception is that the web bending stress in the headers of Configuration II was determined to reach 60,000 psi (including direct compressive stress) for a transversely oriented tire print in the quarter-span location. Maximum web bending stress for Configuration IV were determined to be 59,000 psi for the longitudinals. The web bending stress in the headers for a mid-span wheel load was calculated to be 21,000 psi. If this stress is increased by an average factor of 50 percent to account for the effect discussed earlier of shifting panel loads from midspan to quarter span, the resulting web stresses for longitudinally and transversely oriented quarter-span loads would be about 32,000 psi, or

*D. Lay and M.O. Critchfield, "A Rapid Analysis Procedure for Determining Stresses in the Framing of Helicopter Landing Decks," reported informally as enclosure (1) to DTNSRDC ltr 79-173-18, 30 Nov 1979.

less than yield for HTS. It was noted that some of the web bending stresses given in Table 11 exceed the yield of 47,000 psi for HTS steel. Without further analyses of the plastic type, the calculated stresses above yield only indicate that some localized yielding is probable at stiffener midspan for the headers and longitudinals of Configurations II and IV, respectively.

Plating

Stresses in the plating were determined analytically and experimentally for two types of panel load conditions--loads in the center of a panel, and loads directly over a stiffener at a panel boundary. For typical deck and tire print geometries, wheel loads in the vicinity of quarter span may produce somewhat higher stresses at the panel edge (about 15 percent for Configuration I based on model evaluation--see Figure 42) than the maximum stress due to a central or boundary load. For central panel loads, plating stresses were found to be at 80,000 psi or below for 270 Configurations I-IV (Table 9). For panel boundary loads, plating stresses were determined to be approximately 149,000 psi at the panel edge for Configuration III and approximately 140,000 psi (136,000-141,000 psi) for Configuration IV (Table 10). (Since the three panel boundaries away from the loaded fourth edge for Configuration III were simply supported, not elastically restrained as in Configuration IV, it is believed that the 149,000-psi stress for Configuration III is on the conservative side.) Finally, it should be pointed out that the actual plating stresses would never reach 140,000 psi since yielding would occur at a lower stress level. Therefore, the 140,000-psi value indicates that some degree of yielding at the edge of a panel could possibly occur, the degree being dependent on the material used, such as HY-80, HY-100, or HY-130. Current design procedures for helo deck structures are to allow some local plasticity in plating at the panel edges. Based on these procedures,⁹ HY-130 plating would be acceptable for the 270 decks. However, a detailed plasticity analysis of the plating would be necessary to say whether either HY-100 or HY-80, or both, would be acceptable using these procedures.

210 DECK STRESSES

The maximum flange stress in the longitudinals of the existing 210 decks for a simulated wheel load of 8860 lb was determined to be 12,500 psi during the full-scale

evaluation of the STEADFAST.* For the modified 210 deck configuration, the flange stresses in the longitudinals and headers were 9300 and 15,500 psi, respectively. The maximum web bending stress for the longitudinals in the 210 STEADFAST deck was found during the full-scale evaluation to be 33,000 psi for a forklift inflated tire load of 5500 lb, which was used to simulate the helo wheel load. When a different loading arrangement was used with a timber lock positioned under the rear end of the forklift, a wheel load of 8860 lb was needed to produce the same 33,000 psi stress. In any event, it is clear that yielding was apparently imminent based on these tests results at realistic wheel loads. Recall that the full-scale web bending stress value for the 210 was approximately five times the corresponding analytical value (see Table 11). This was puzzling since the analytical tools produced web bending stresses which agreed with rigid vinyl model results. For square panels the difference could become important. The percent differences should be taken as trends only, as discussed previously.

The maximum plating stress for the 210 STEADFAST deck was 52,000 psi for a simulated wheel load of 8860 lb (timber block condition). This value is well under yield for the HY-80 deck. The maximum plating stress for the modified 210 decks under the Sikorsky wheel load of 7700 lb was calculated to be 77,100 psi.**

GENERAL FINDINGS AND TRENDS

In addition to providing maximum plating stresses, the structural evaluation program identified regions of the helo deck structures of relatively high stress and produced other more general findings. This is of interest for general application to helo decks which are similar in configuration to the 270 and 210 decks. The following observations and conclusions are reached relevant to these highly stressed regions.

*W.H. Hay and M.O. Critchfield, "Full Scale Evaluation of Flight Deck Structural Responses for 210 Foot U.S. Coast Guard Cutters STEADFAST (WMEC 623) and VIGOROUS (WMEC 627) Under Simulated Helicopter Wheel Loads," reported informally as enclosure (1) to DTNSRDC ltr 77-173-75 of Sep 1977.

**M.O. Critchfield, "Strength Analysis of Modified Helicopter Landing Decks on 210 Foot USCG Cutters for SRR Helicopter Wheel Loadings," reported informally as enclosure (1) to DTNSRDC ltr 79-173-80, 14 May 1979.

1. For helo deck Configuration I, involving long plate panels of aspect ratio 4, the governing wheel location in terms of plating stress was found to be a wheel in the center of a panel. For Configurations II-IV, having panel aspect ratios of 2 or less, the governing load location was found to be wheel loads straddling stiffeners which induced high stresses at panel edges. The dual wheel on the LAMPS helicopter, when straddling stiffeners, was found to produce greater plating stresses than the single main wheels. These observations should be valid for other helo deck structures and wheel loads similar to those involved in the 270 and 210 evaluations.

2. Based on the rigid vinyl model results, elliptically shaped tire prints were found to produce plating stresses which were 1-16 percent greater (1 percent for Configuration I, 16 percent for Configuration II) than the equivalent rectangular tire prints. Therefore, for long panels similar to Configurations I, the difference is negligible. For square panels the differences should be taken as trends only, as discussed previously.

3. The 45 degree orientation of the tire print reduced the maximum plating stresses in all cases except one (Figure 43) over the longitudinal orientation.

4. Maximum web bending stresses in the longitudinals occurred for wheel loads with the long axis of their tire prints in the direction of the longitudinals and the centroid of their tire print positioned on the panels at quarter span transversely and midspan longitudinally (Table 11).

5. Maximum web bending stresses in headers occurred for wheel loads with the long axis of their tire prints in the direction of the headers and the centroid of their tire print situated on the panel at quarter span longitudinally and midspan transversely.

6. In general, web bending stresses appear to increase as plating thickness decreases if the stiffener scantlings and other deck parameters are held fixed (Figure 53).

7. Reduced plating stiffness, due to fabrication-induced effects (such as residual stresses), can potentially occur in helo decks. The effect could be to transfer additional load into the stiffener web, thereby driving up the web bending stresses.

ANALYSIS METHODS FOR FUTURE APPLICATION

Another objective of the program was the validation of analytical techniques for general application to helo deck structures having scantlings and wheel load conditions similar to those evaluated in this study. This objective was accomplished with varying degrees of success in the course of the evaluations on Configurations I and II of the 270 and the helo deck on the existing 210 cutters.

1. Excellent correlation, within a few percent, was achieved among analyses (finite-element and AISC equations), rigid vinyl model, and full-scale (longitudinals only) results for flange stress in the longitudinals and headers.

2. The degree of correlation between analytical and model results for the plating was dependent upon the load condition and stress location. For central panel loads, the correlation ranged from 3 percent at the panel center to 15 percent at the edge. For wheel loads straddling a panel boundary, the analytical value exceeded the model value by 21 percent due to the conservative assumption of three simply supported boundaries on the panel, excluding the loaded boundary. Later analyses for Configuration IV introduced elastically supported boundaries. Along with the assumptions on vertical and rotational support at the panel edges just mentioned, the large-deflection analysis assumed that the plate edges were completely restrained with respect to in-plane displacement. Since the amount of in-plane restraint in actual helo deck is less than complete, and also the plating stress in large deflection analyses are sensitive to this fact, it is important that methods be developed in the future for accurately determining the degree of edge restraint and incorporating it into the analyses. The nonlinear finite-element computer program⁴ used in the above analyses allows one to introduce in-plane elastic restraint; however, the program was not found to perform reliably when the in-plane restraint was reduced from complete to partial.

3. Excellent agreement was obtained between the two analytical techniques, finite-element analyses, and design equations (see Appendices A and B) in predicting web bending stresses for the longitudinals of Configuration I and headers of Configuration II (Table 11). Based on the rigid vinyl model results, these analytical techniques were found to be 15 percent low for the longitudinals in Configuration I, 17 percent high for the longitudinals in Configuration II, and 4 percent high for the headers in Configuration II. However, the design equations and finite-element model were found to substantially underpredict the web bending stresses measured

during the full-scale tests on the 210 cutter STEADFAST. This result was discussed earlier and was attributed to a possible reduction in plating stiffness due to fabrication-induced residual stresses. Future full-scale tests are needed by the marine community if this question is to be explored and resolved in a definitive manner. These tests should be accompanied by a residual stress survey of helo deck structure, particularly those with lighter plating. In the meantime, the option available to the designer and analyst in a given situation is to compute an upper bound on web bending stress by assuming the stiffness of the deck plating to be zero ($k_p = 0$ in Appendix A). This approach, however, was not adopted in this work. Rather, as discussed earlier, the decision was made in a meeting with the USCG to assume the helo deck plating to be fully effective when computing web bending stresses.

ACKNOWLEDGMENTS

The authors wish to express their appreciation to a number of individuals at DTNSRDC and at the U.S. Coast Guard who made significant contributions in the course of this program.

At DTNSRDC, the authors are grateful to Mr. P. Meyer and Ms. J. Figula for their assistance in generating finite-element models; and assisting in the model tests; Mr. D. Ricks and Mr. J. Hardison for strain gage installation; Mr. S. Glahn for his participation in the experimental set up and Mr. F. Palmer for aid in data reduction and other aspects of the experimental program; and finally, Mr. A. Dinsenbacher for his expertise and guidance in all aspects of the experimental process and for reviewing the report draft. In the analytical area, the authors wish to thank Dr. J.C. Adamchak for many technical discussions and suggestions during this work, particularly for his assistance at several points in the development of the web bending equations.

The authors also wish to express their gratitude to CDR W. Simpson and Messrs. L. Baez, W. Dietz,* E. Haciski, G. North* and R. Williams of the Engineering Division at the USCG for their excellent cooperation during the course of the 270 and 210 programs. Messrs. L. Baez, and G. North are to be specifically thanked for their insightful suggestions and assistance throughout the program.

*Formerly of the Naval Engineering Division, USCG.

Finally, the authors would like to thank all members of the committee who reviewed this document for publication as a formal report: Dr. J. Adamchak, Mr. R. Chiu, Mr. A. Dinsenbacher, and Mr. R. Walz.



Figure 1 - Sketch of WMEC 270-Foot Cutter Under Construction



Figure 2 - Starboard View of WMEC 210-Foot Cutter VIGOROUS at Sea
(Official U.S. Coast Guard Photograph)

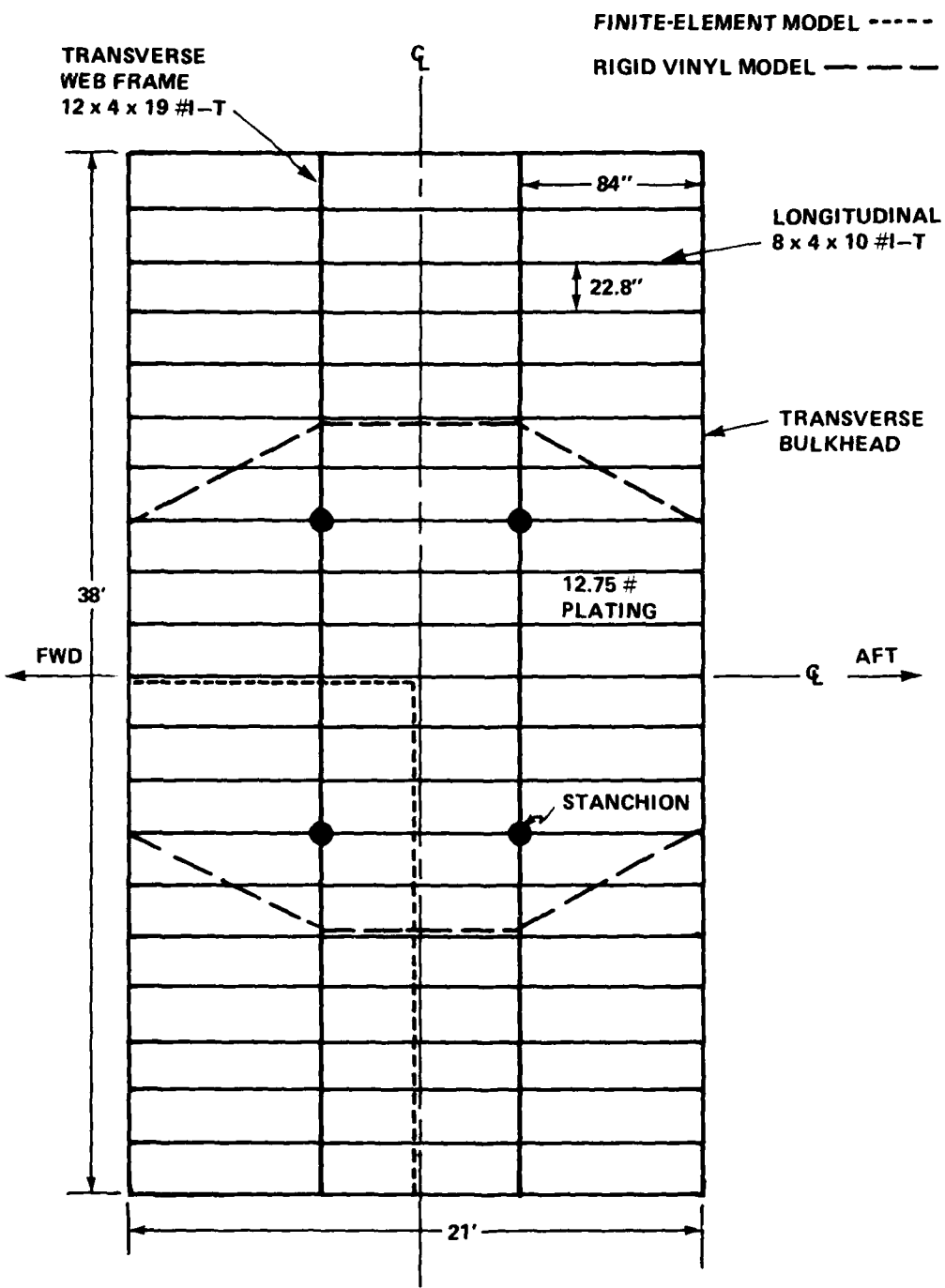


Figure 3 - 270 Foot, Basic Configuration I

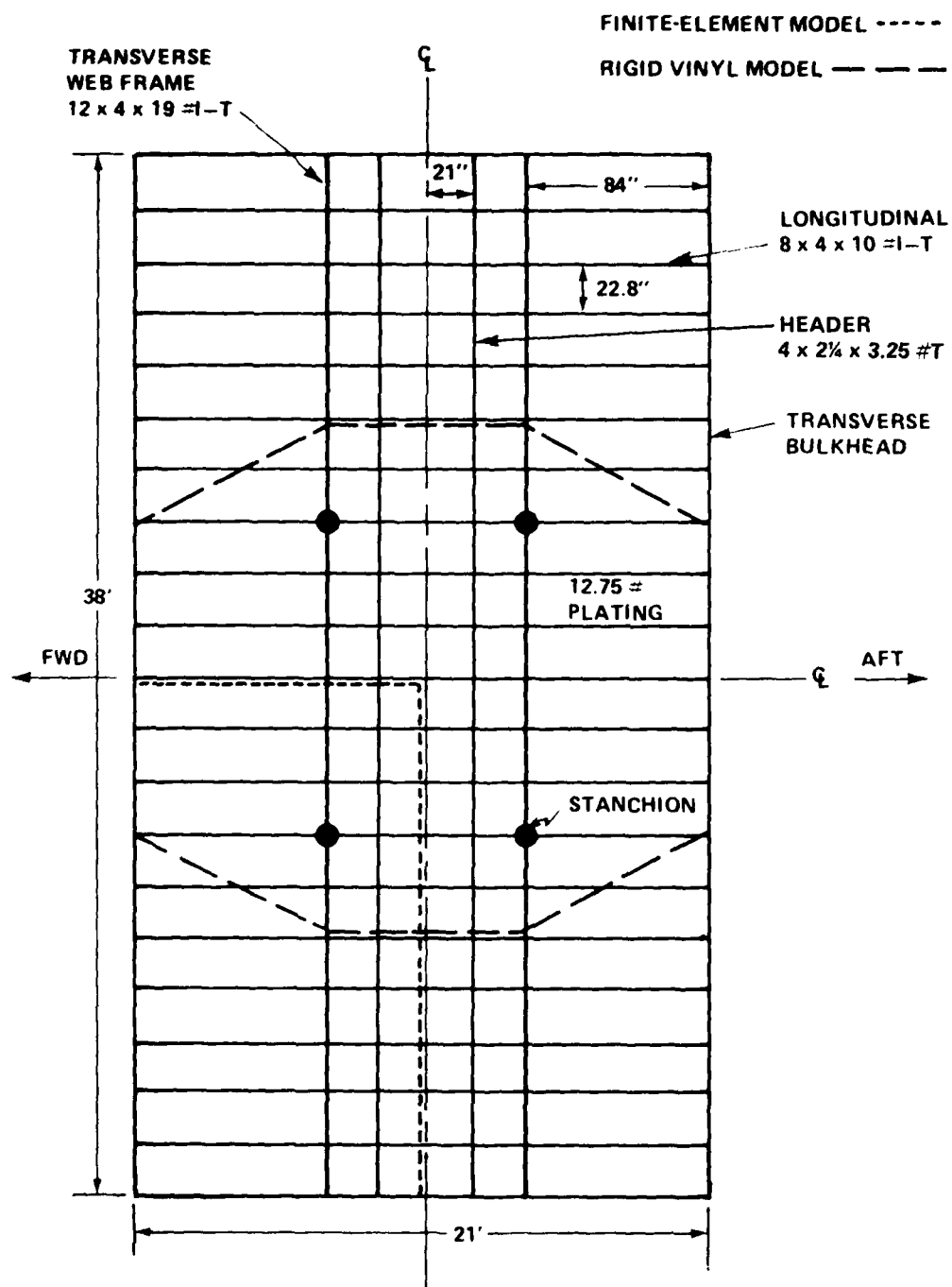


Figure 4 - 270 Foot, Configuration II (Headers Added)

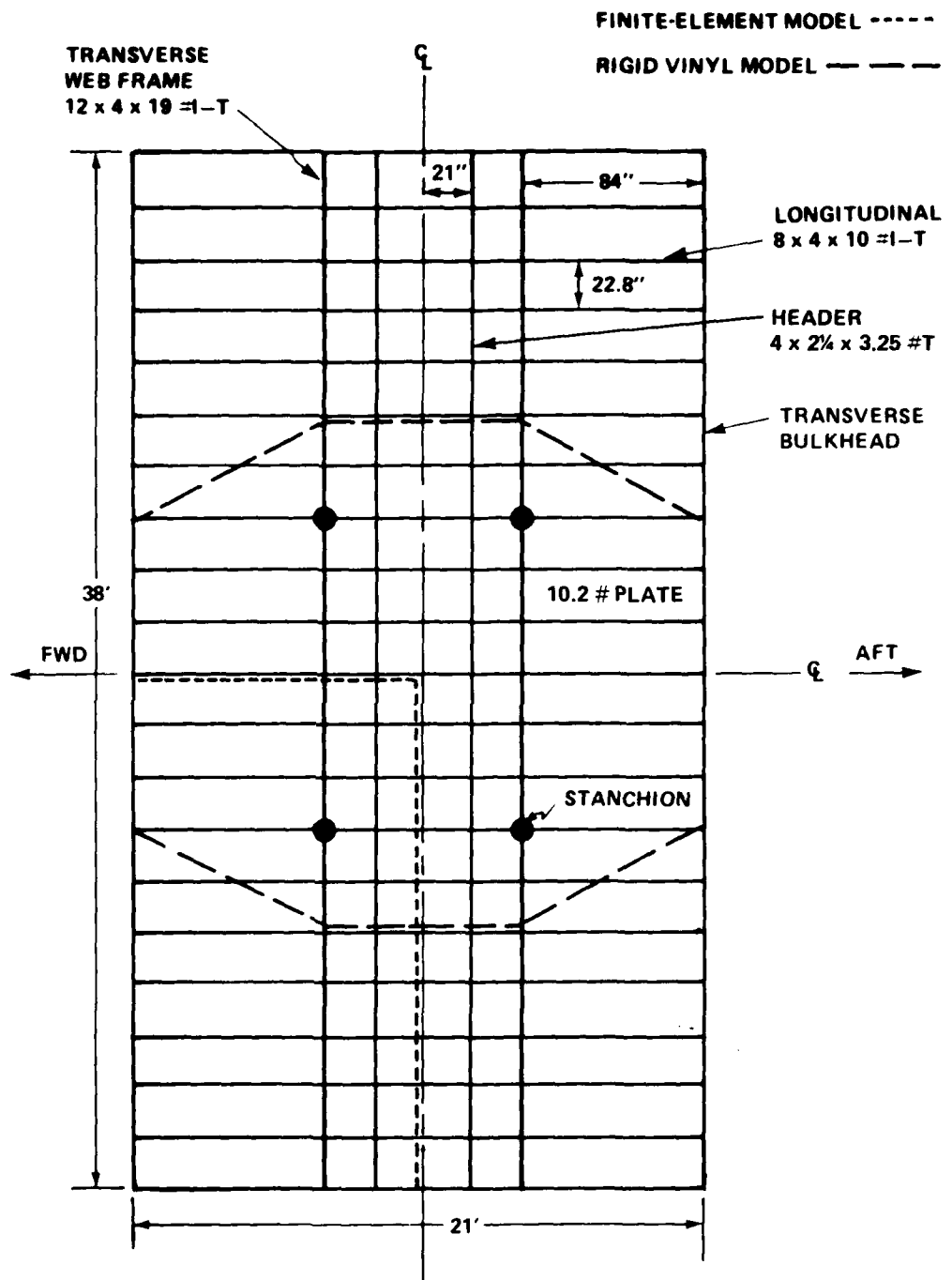


Figure 5 - 270 Foot, Configuration III (Plating Changed to 10.2# Plate)

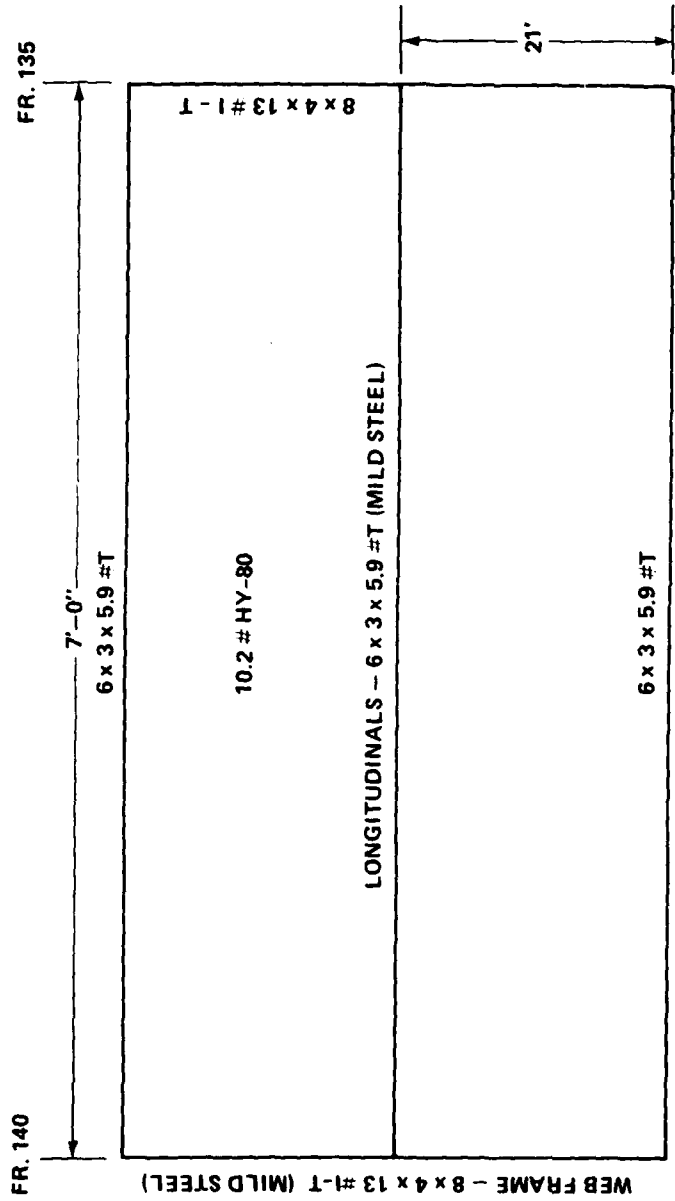


Figure 6 - 210 Foot, Existing Configuration (STEADFAST)

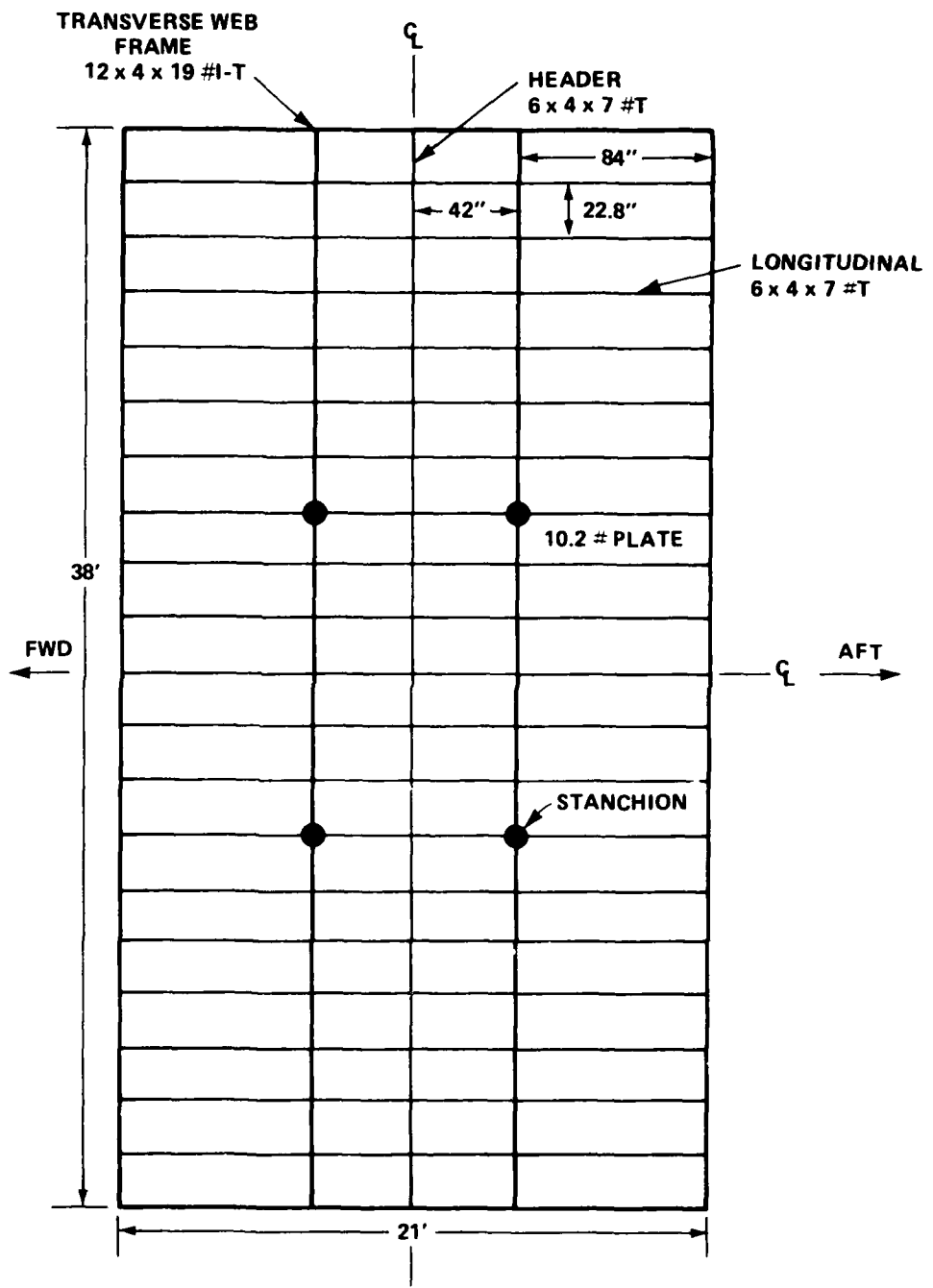
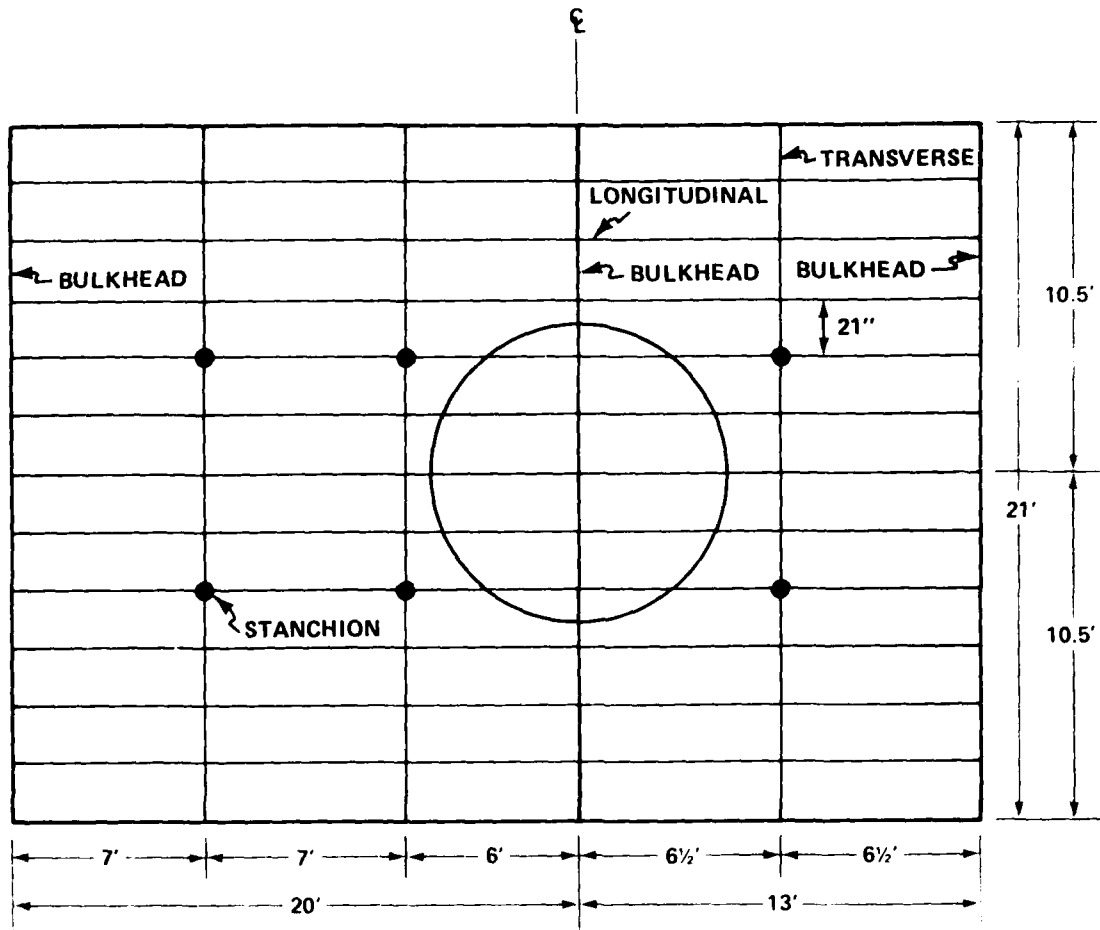
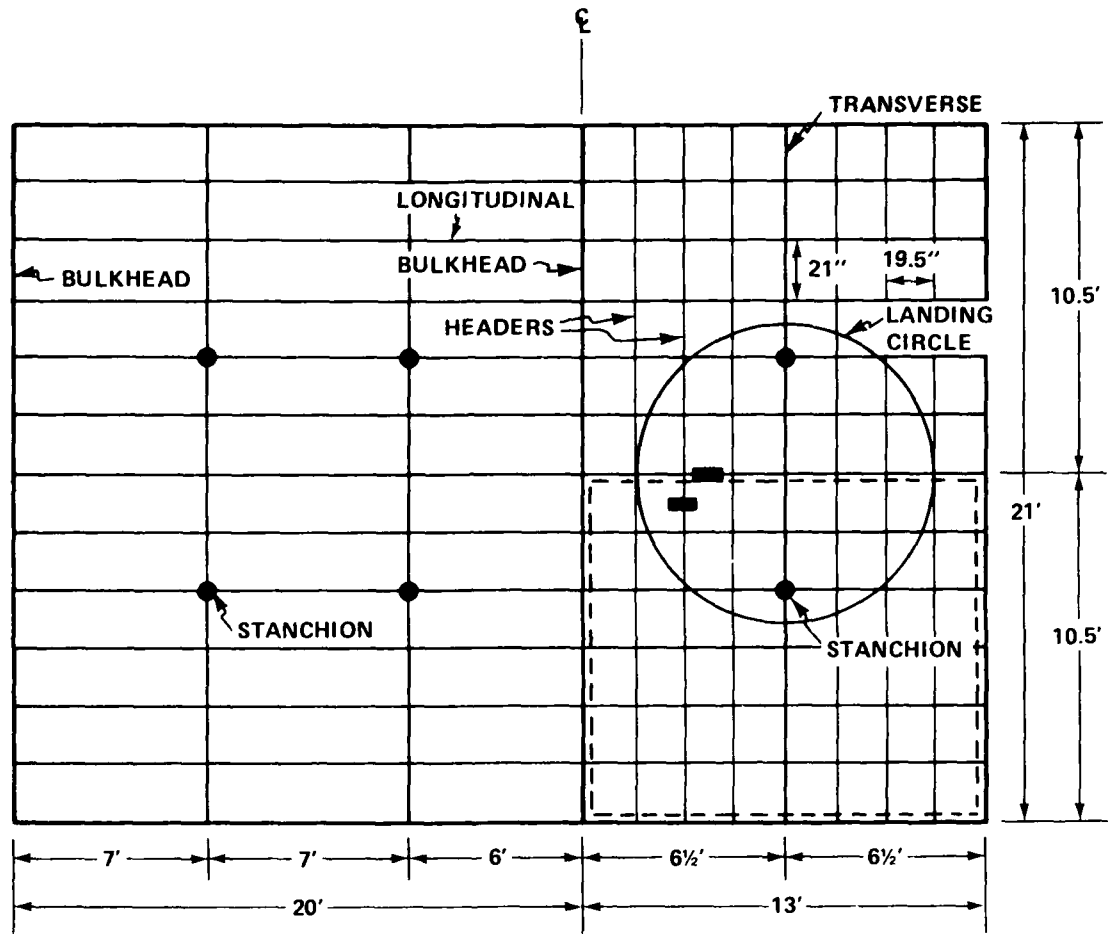


Figure 7 - 270 Foot, Configuration IV (Number of Headers Reduced)



LONGITUDINALS $6 \times 3 \times 5.9 \text{ #T (MS)}$
TRANSVERSES $8 \times 5\frac{1}{2} \times 13 \text{ #T (MS)}$
PLATING 10.2 #(HY-80)

Figure 8 - 210 Foot, Existing Configuration
(Basis for 210 Deck Modification)



HEADERS $4 \times 2\frac{1}{4} \times 3.25 \text{ #T (*)}$ FINITE-ELEMENT MODEL
 LONGITUDINAL $6 \times 3 \times 5.9 \text{ #T (MS) (WITHIN ----)}$
 TRANSVERSES $8 \times 5\frac{1}{2} \times 13 \text{ #T (MS) WHEEL LOADS INDICATED}$
 PLATING BY █
 PLATING 10.2 # (HY-80)

Figure 9 - 210 Foot, Modified Configuration (Headers Added)

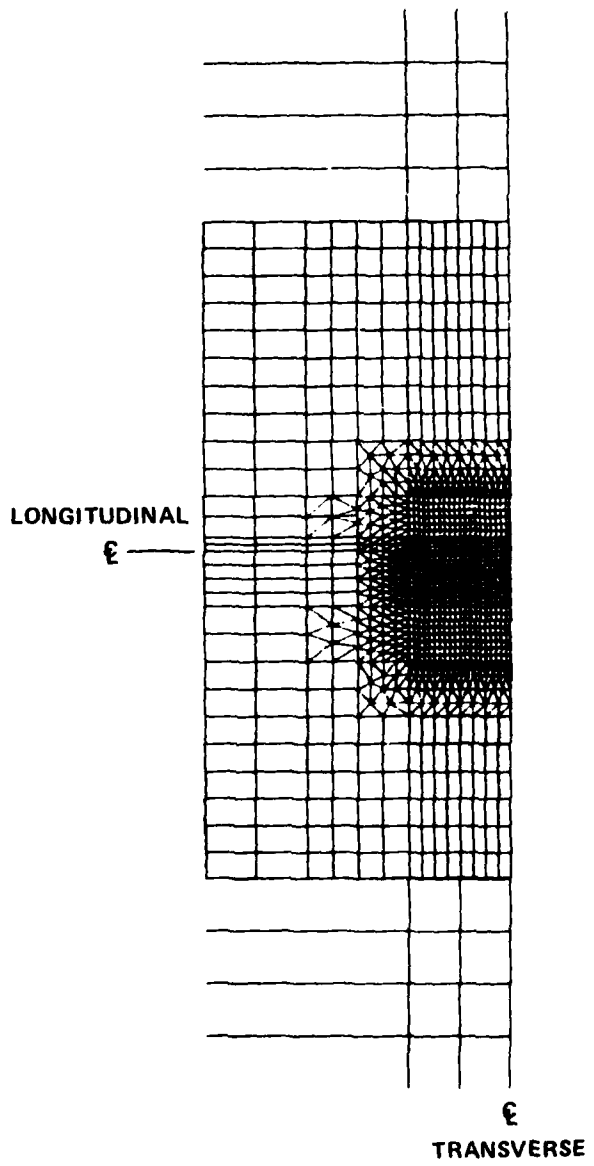


Figure 10 - Finite-Element Model for Overall Framing Analysis of 270-Class Configurations I-III

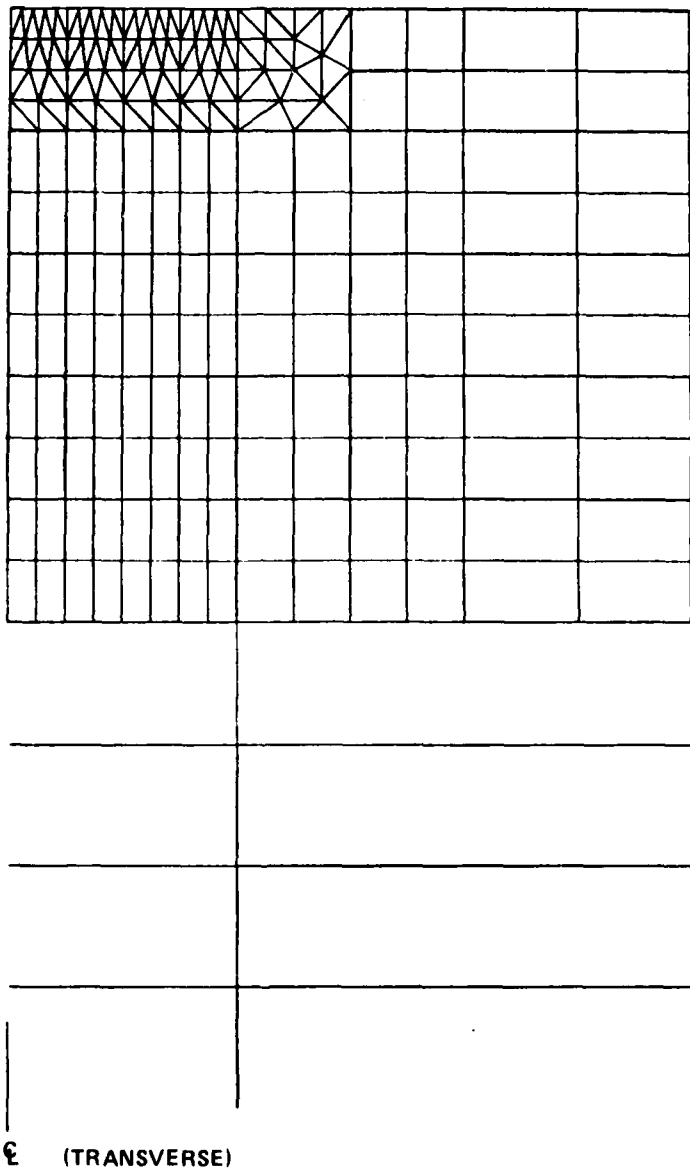
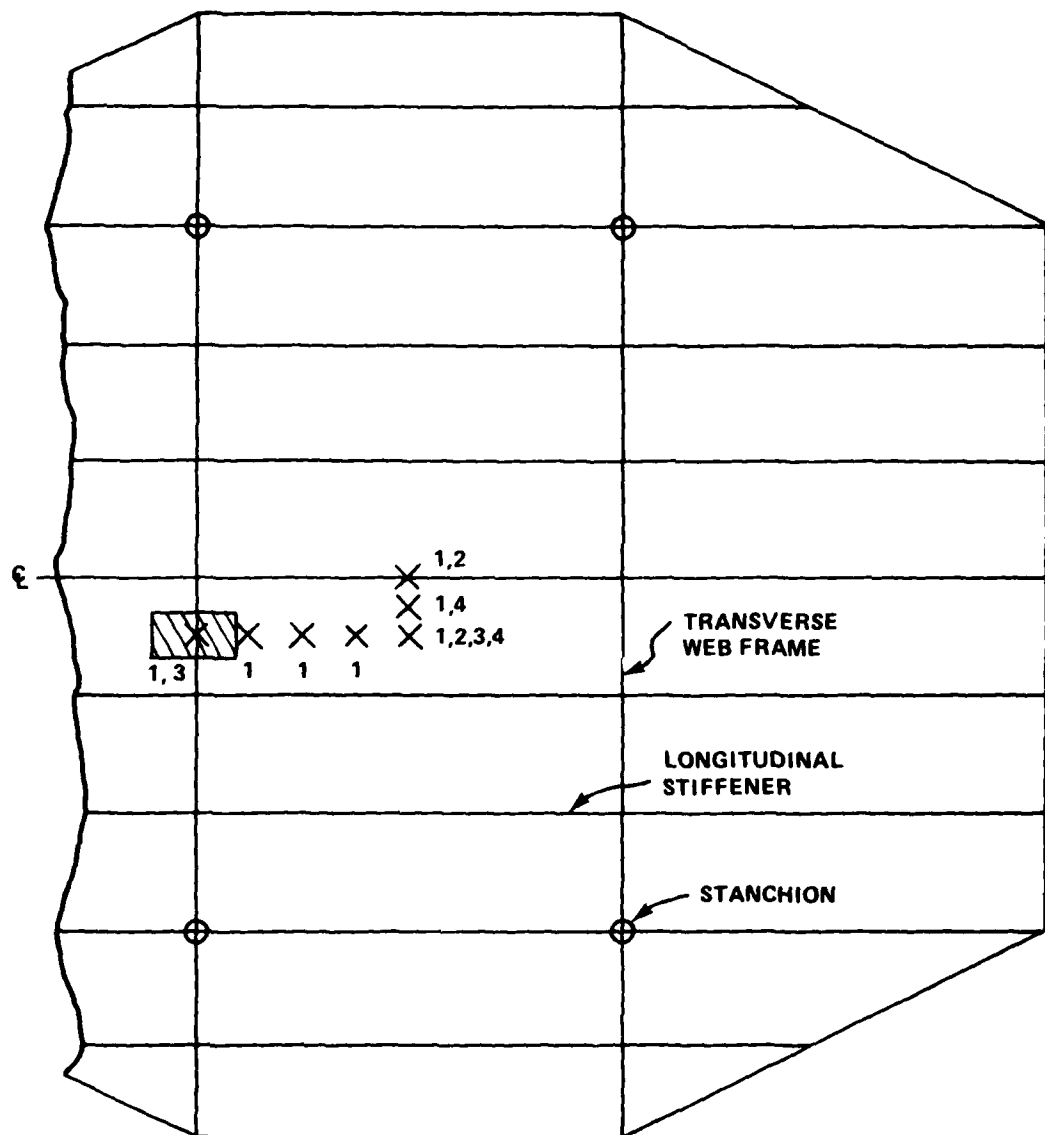
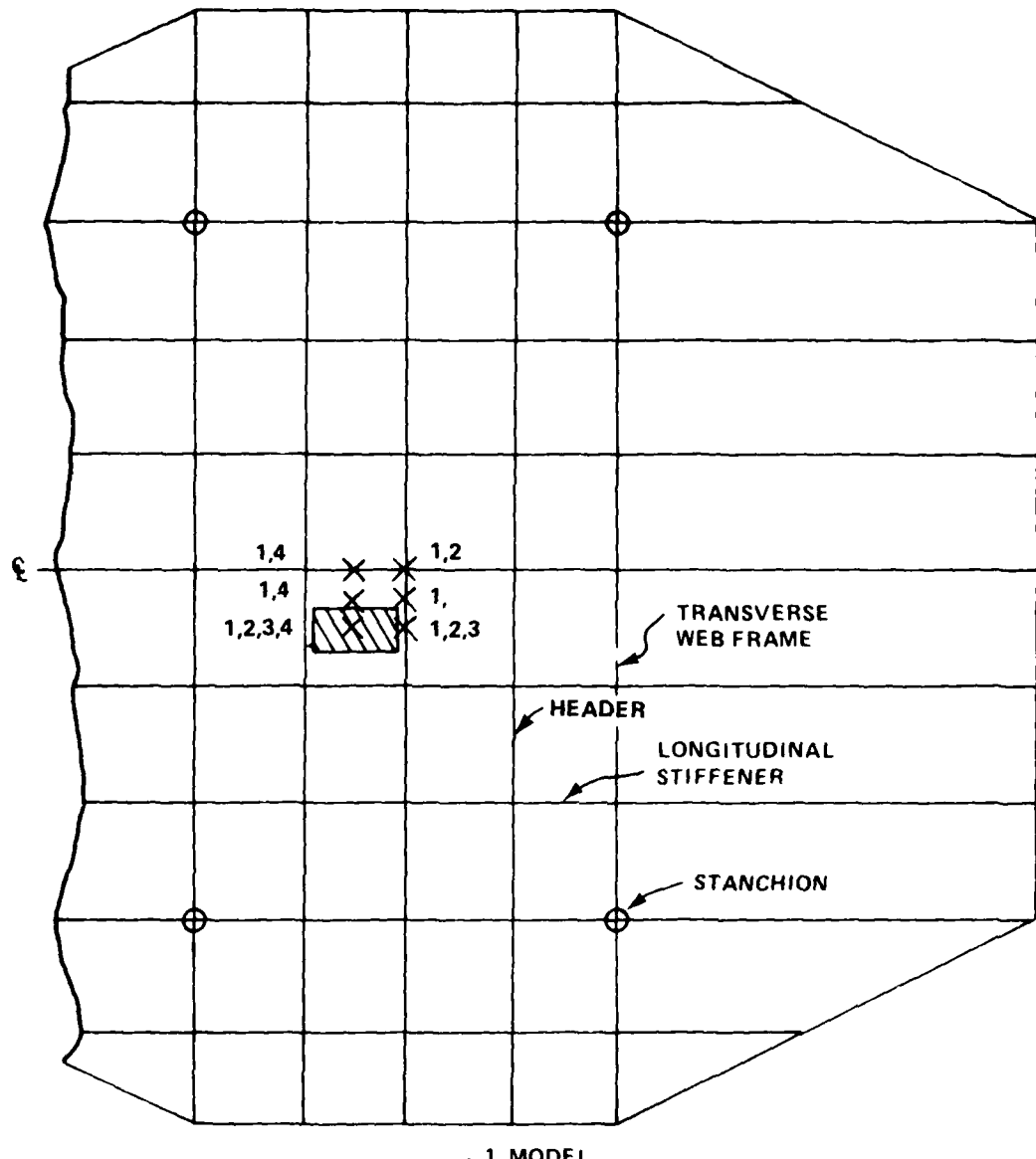


Figure 11 - Expanded View of Portion of Finite-Element Model in Figure 8



× LOAD POSITION CENTERS:
  RECTANGULAR FOOTPRINT SIZE

Figure 12 - Wheel Load Positions for Configuration I



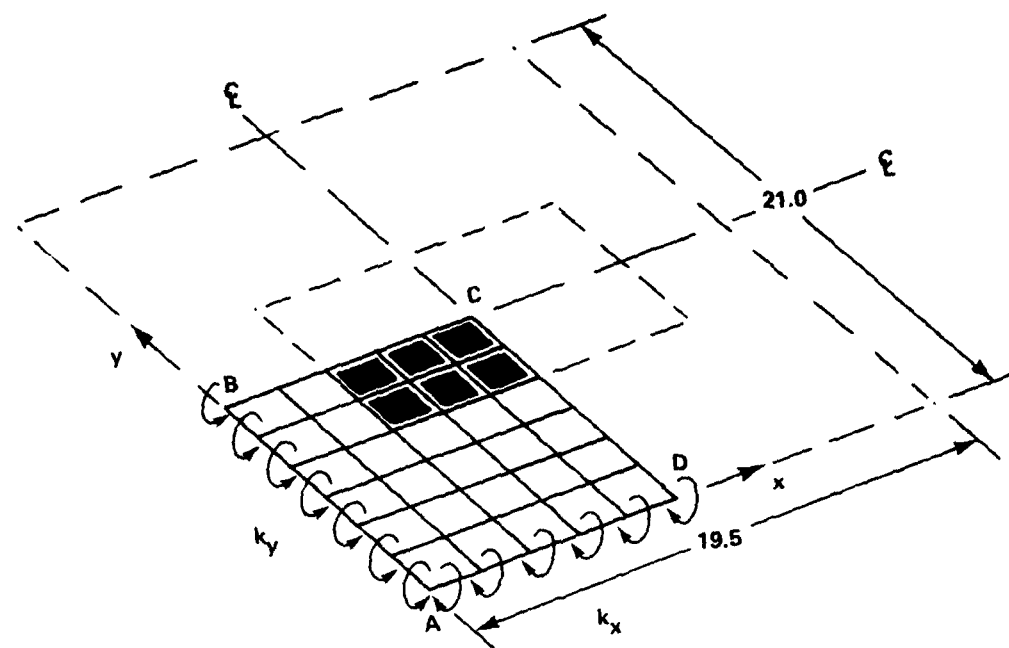
X LOAD POSITION CENTERS:

- 1. MODEL
- 2. NASTRAN (FRAMING) ANALYSIS
- 3. NONLINEAR PLATING ANALYSES
- 4. WEB BENDING ANALYSIS

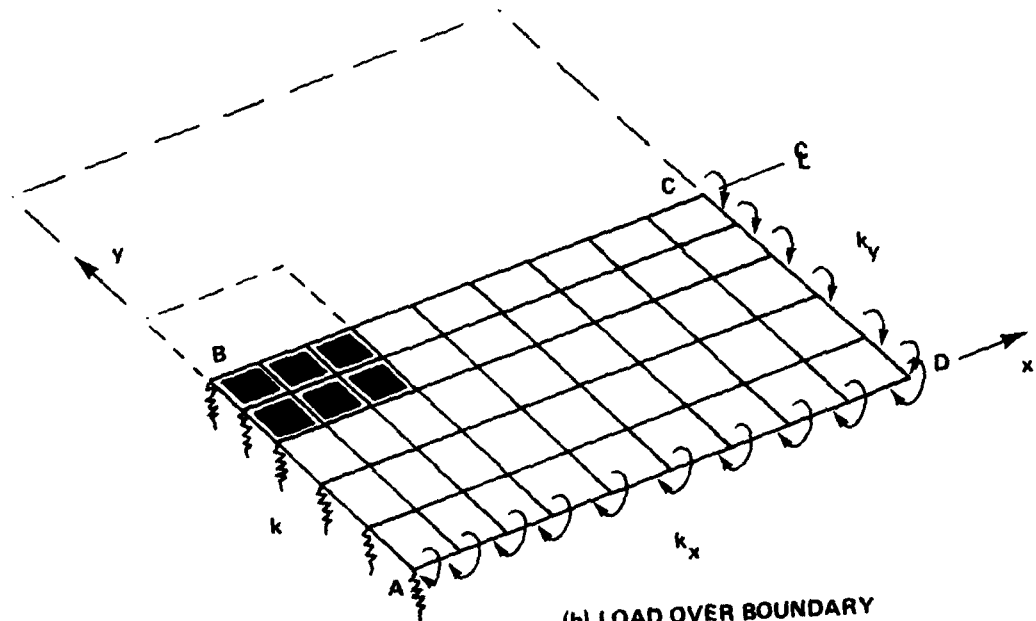


RECTANGULAR FOOTPRINT SIZE

Figure 13 - Wheel Load Positions for Configuration II



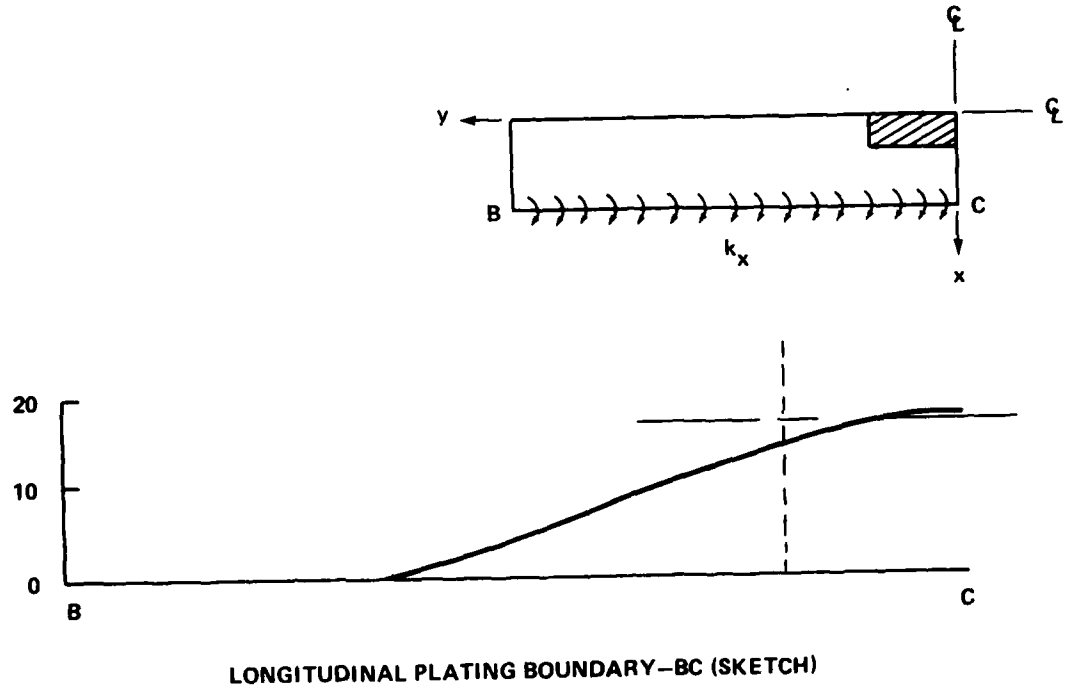
(a) LOAD IN CENTER



(b) LOAD OVER BOUNDARY

Figure 14 - Finite-Element Models for Large Deflection
Plating Analyses (Configurations II and III)

BOUNDARY SPRING CONSTANT k_x (10^3 in.-lb/in./rad)



LONGITUDINAL PLATING BOUNDARY-BC (SKETCH)

Figure 15 - Elastic Boundary Restraint for Plating Analyses
(Configuration I, Central Panel Load)

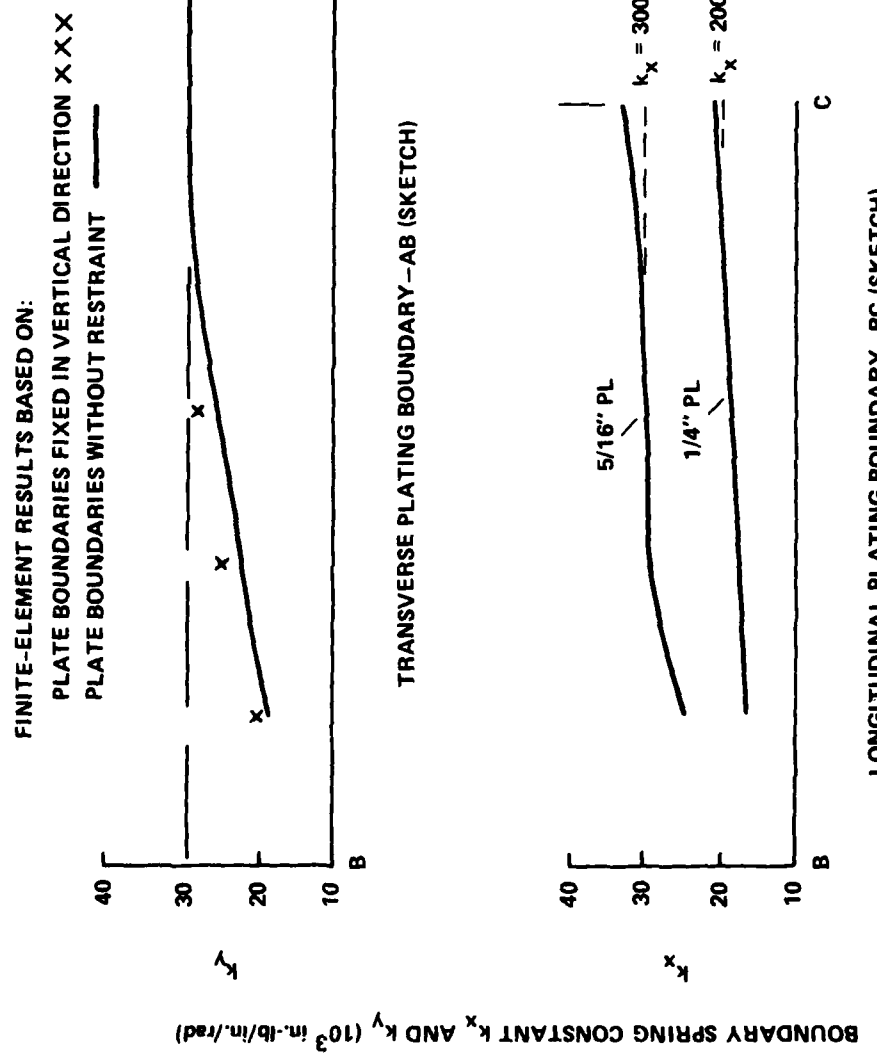


Figure 16 - Elastic Boundary Restraint for Plating Analyses
 (Configurations II and III, Central Panel Load)

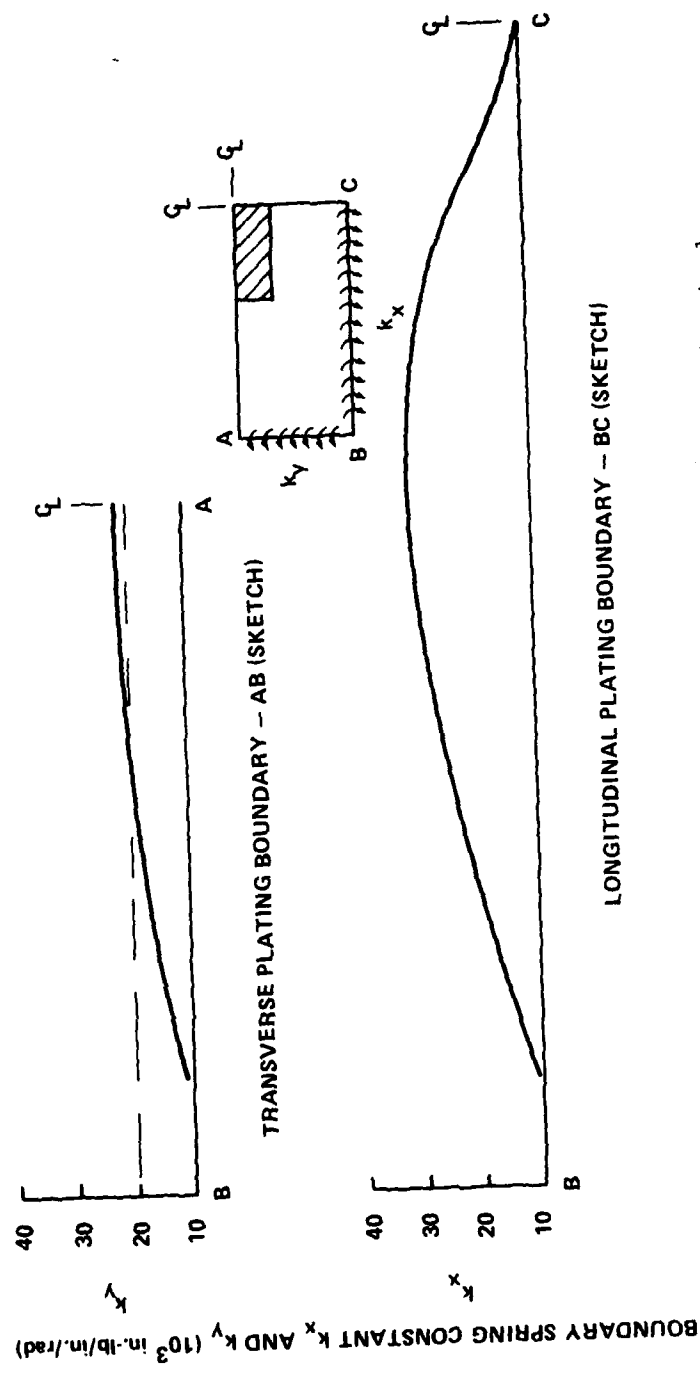


Figure 17 - Elastic Boundary Restraint for Plating Analyses
(Configuration II, Load Straddling Panel Boundary)

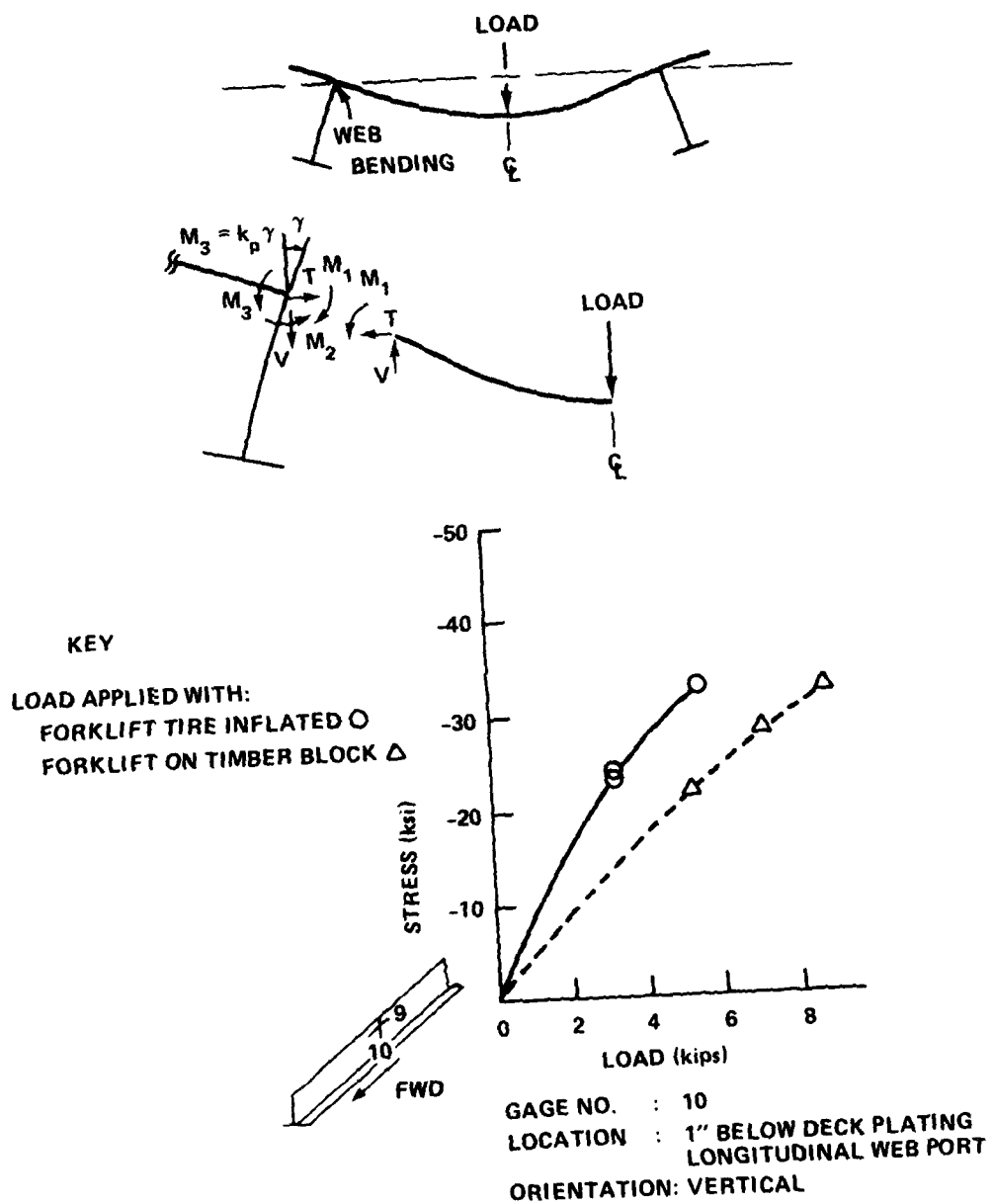
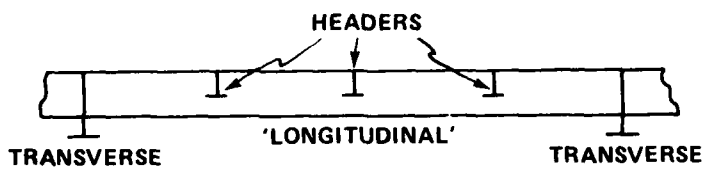


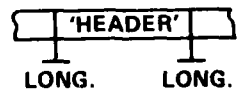
Figure 18 - Illustration of Stiffener 'Web Bending' Along with Full-Scale Results for 210



(a) LONGITUDINALS (WITHOUT HEADERS)



(b) LONGITUDINALS (WITH HEADERS)



(c) HEADERS ALONE

Figure 19 - Three Stiffener Configurations Requiring Web Bending Analyses

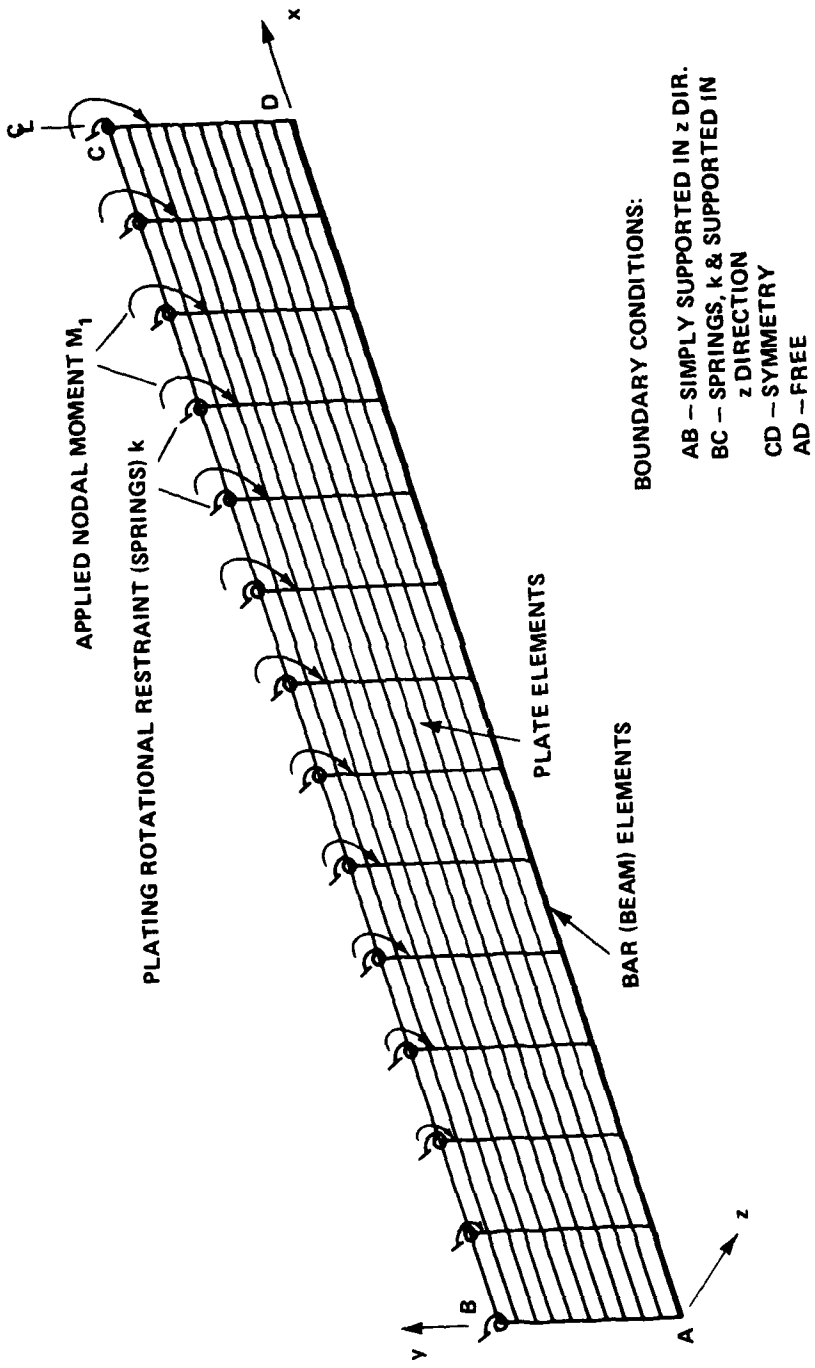


Figure 20 - Finite-Element Model for Web Bending of Longitudinal (Without Headers)

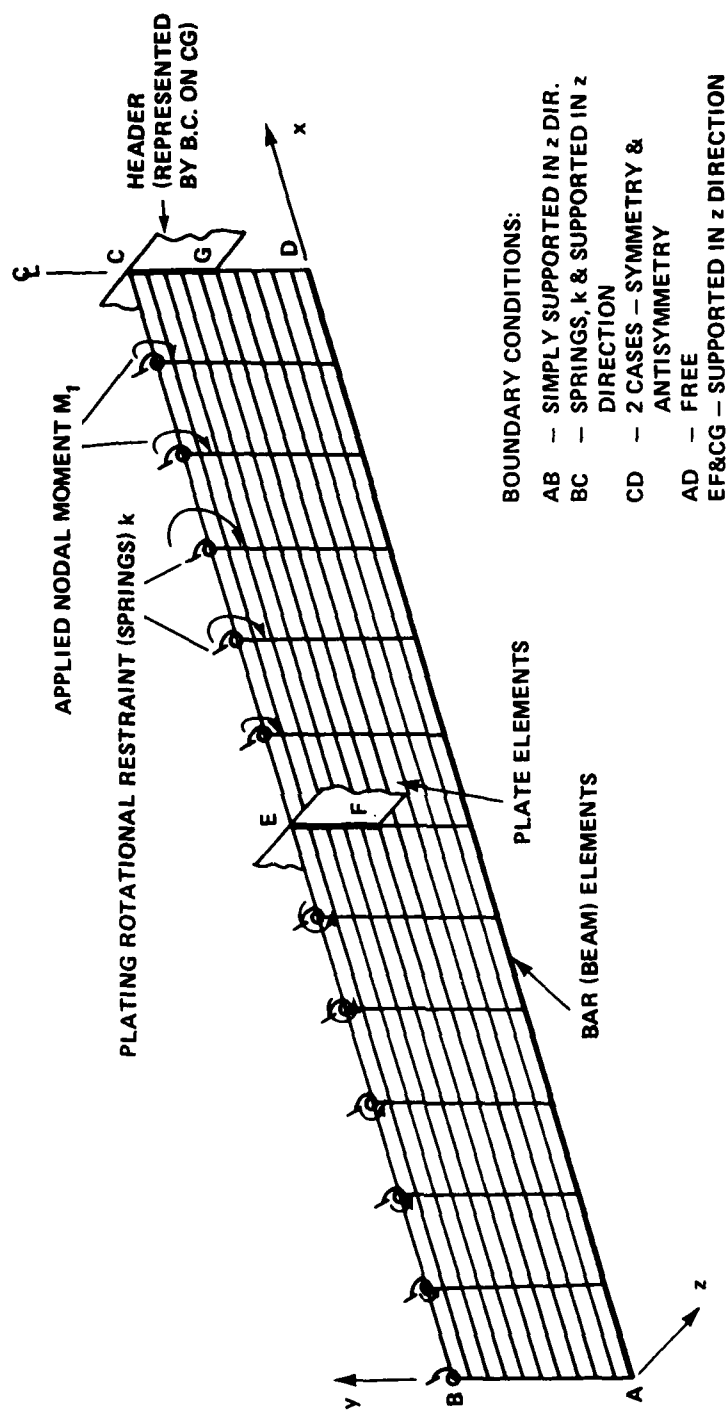


Figure 21 – Finite-Element Model for Web Bending of
Longitudinal Headers

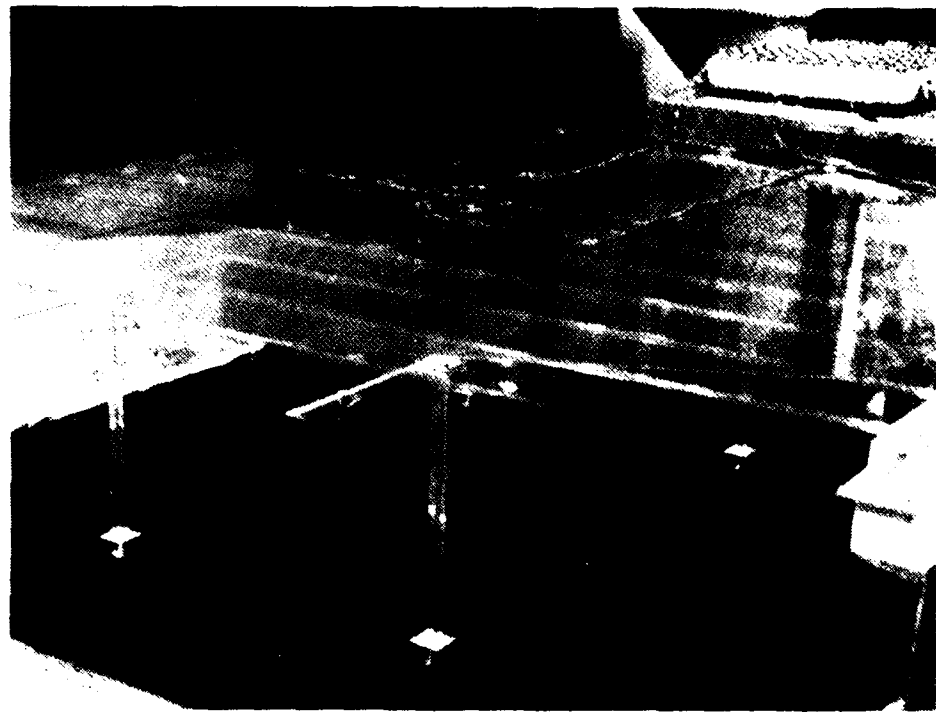


Figure 22 - View of Rigid Vinyl Model from Top

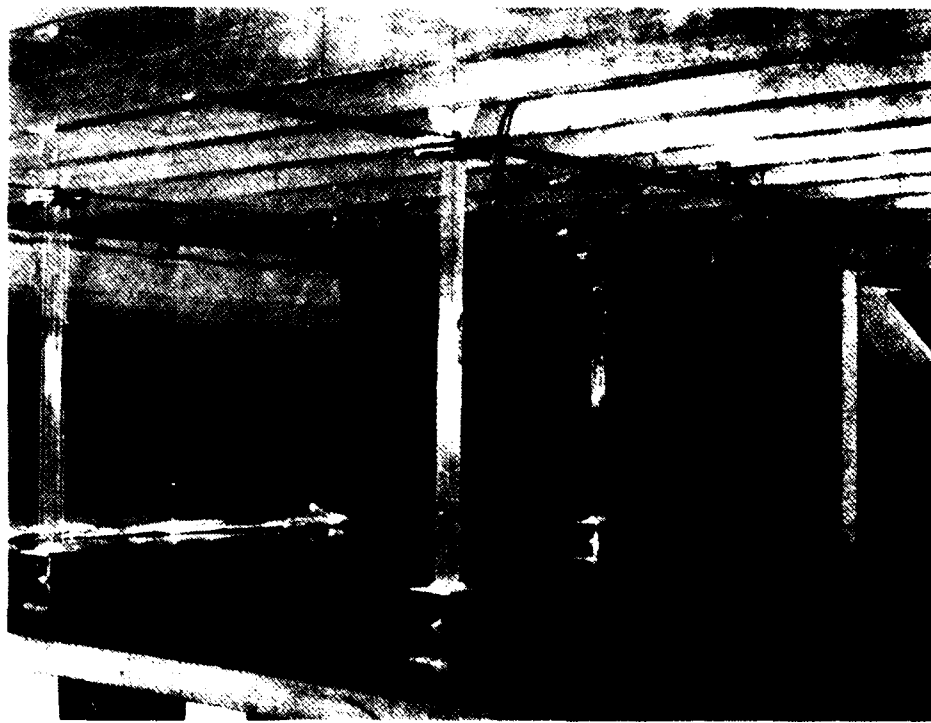
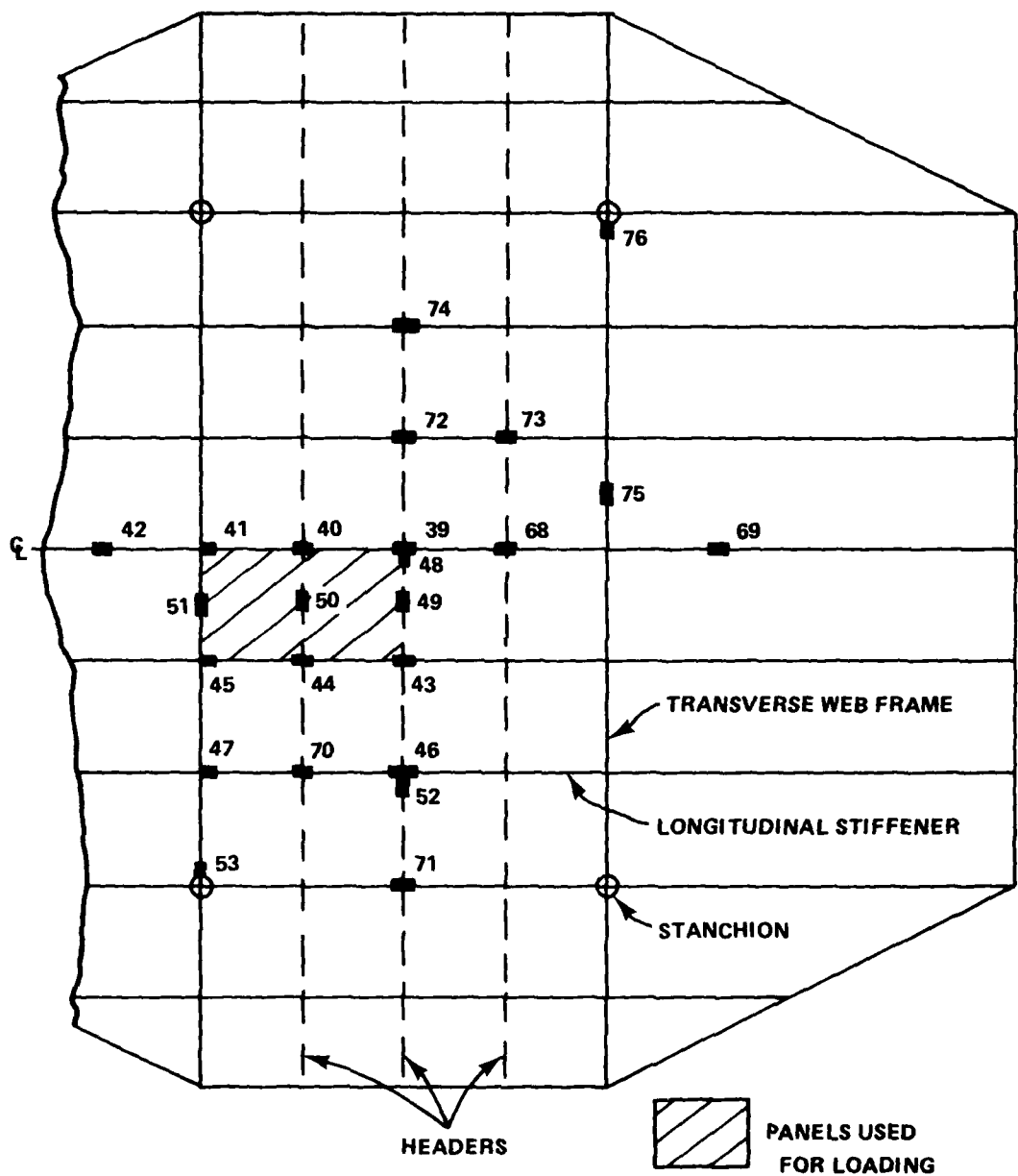
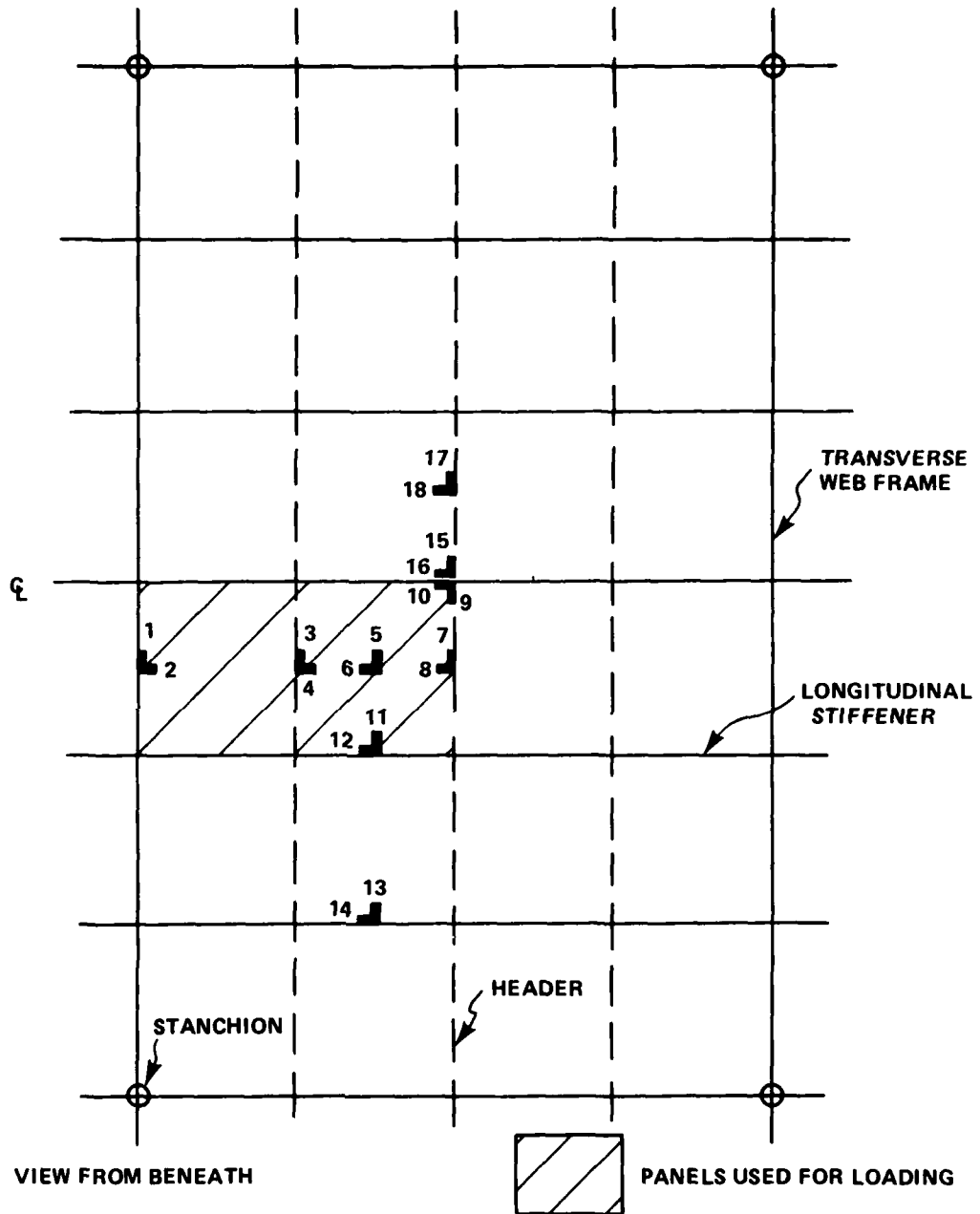


Figure 23 - View of Rigid Vinyl Model from Bottom



VIEW FROM BENEATH

Figure 24 - Strain Gage Locations on Stiffener Flange (Single Gages)



GAGES 1-18 ON TOP SURFACE, CORRESPONDING
GAGES 21-38 ON BOTTOM SURFACE (NO GAGES 19 & 20)

Figure 25 - Strain Gage Locations on Plating

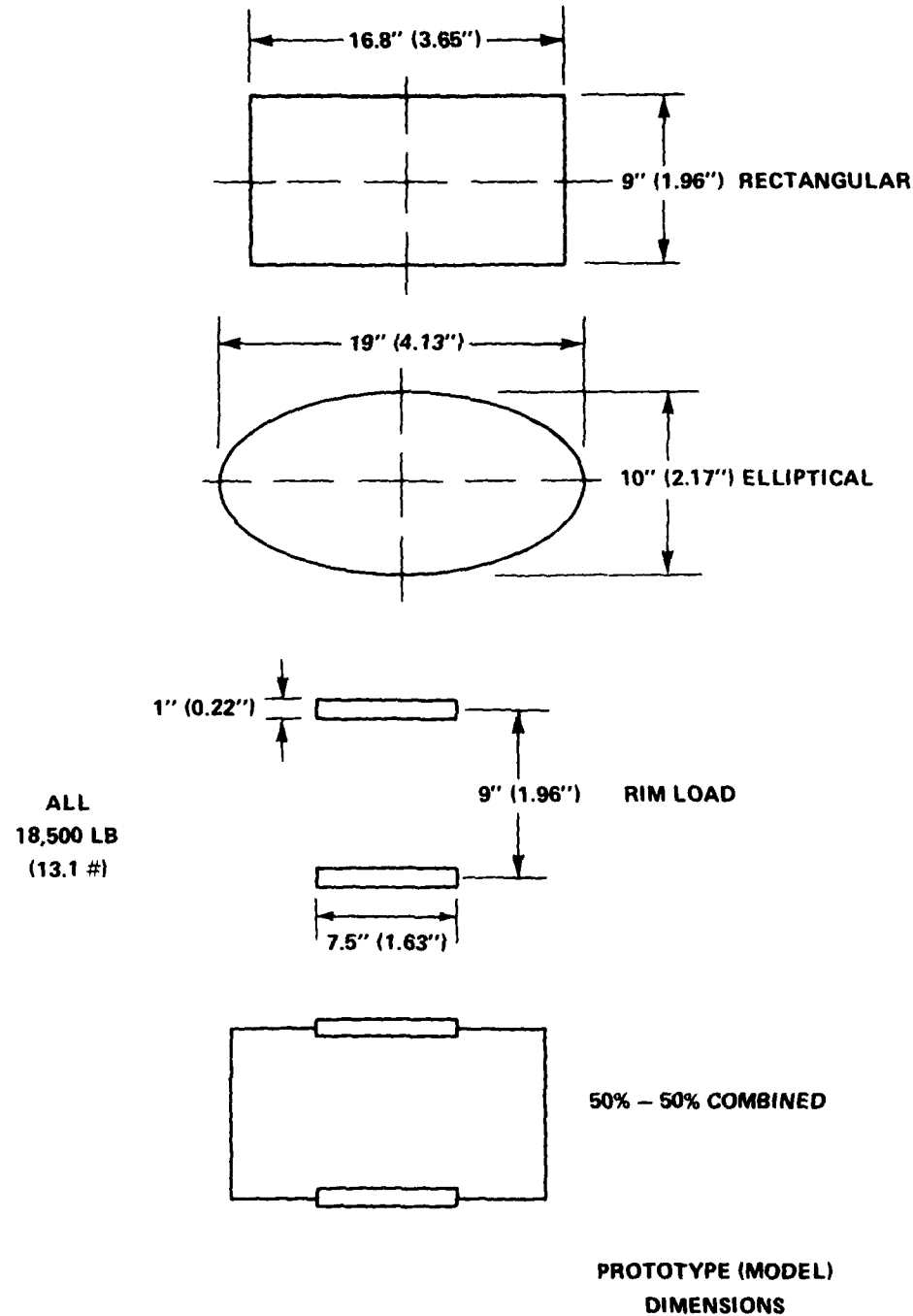


Figure 26 - Helo Load Footprints Used in Model Evaluation

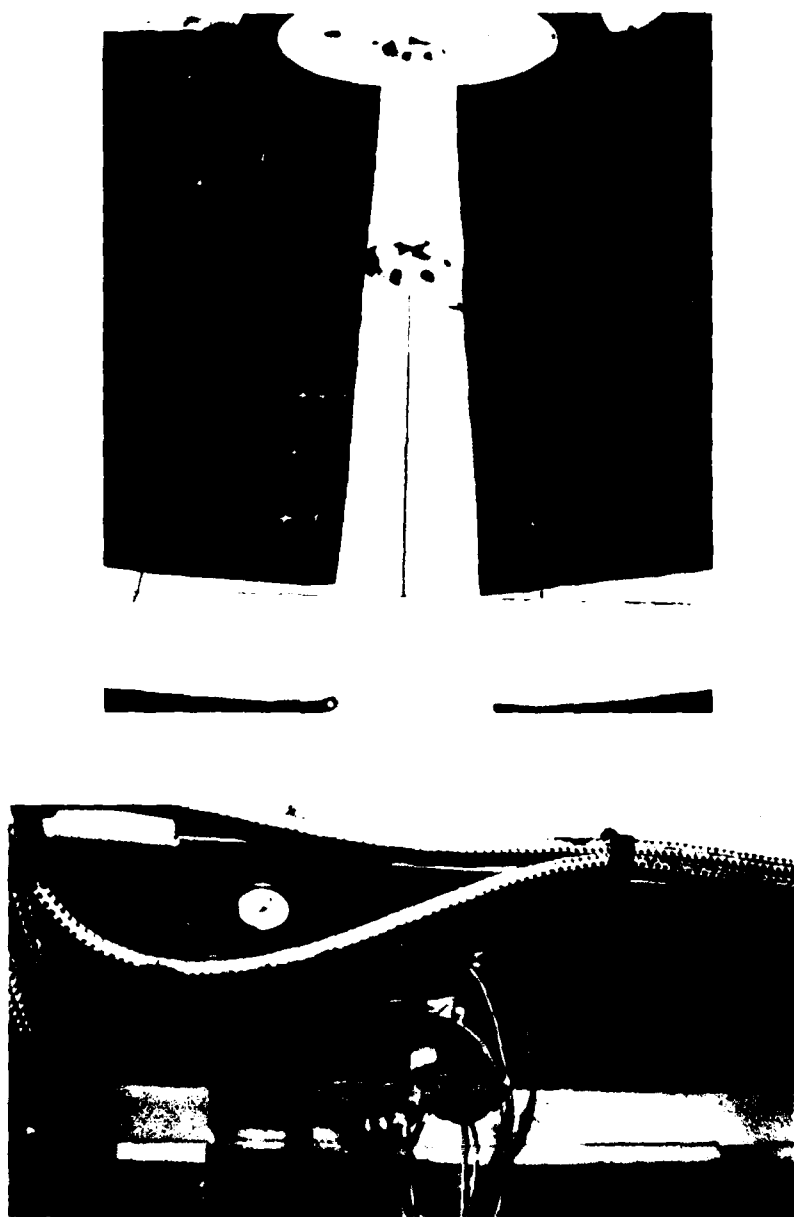


Figure 27 - Top and Bottom Views of Helo Deck Panel on USCG Cutter
STEADFAST Instrumented for Full-Scale Tests



Figure 28 - View of Helo Deck Panel on STEADFAST under Simulated Tire Loading Using a ForkLift

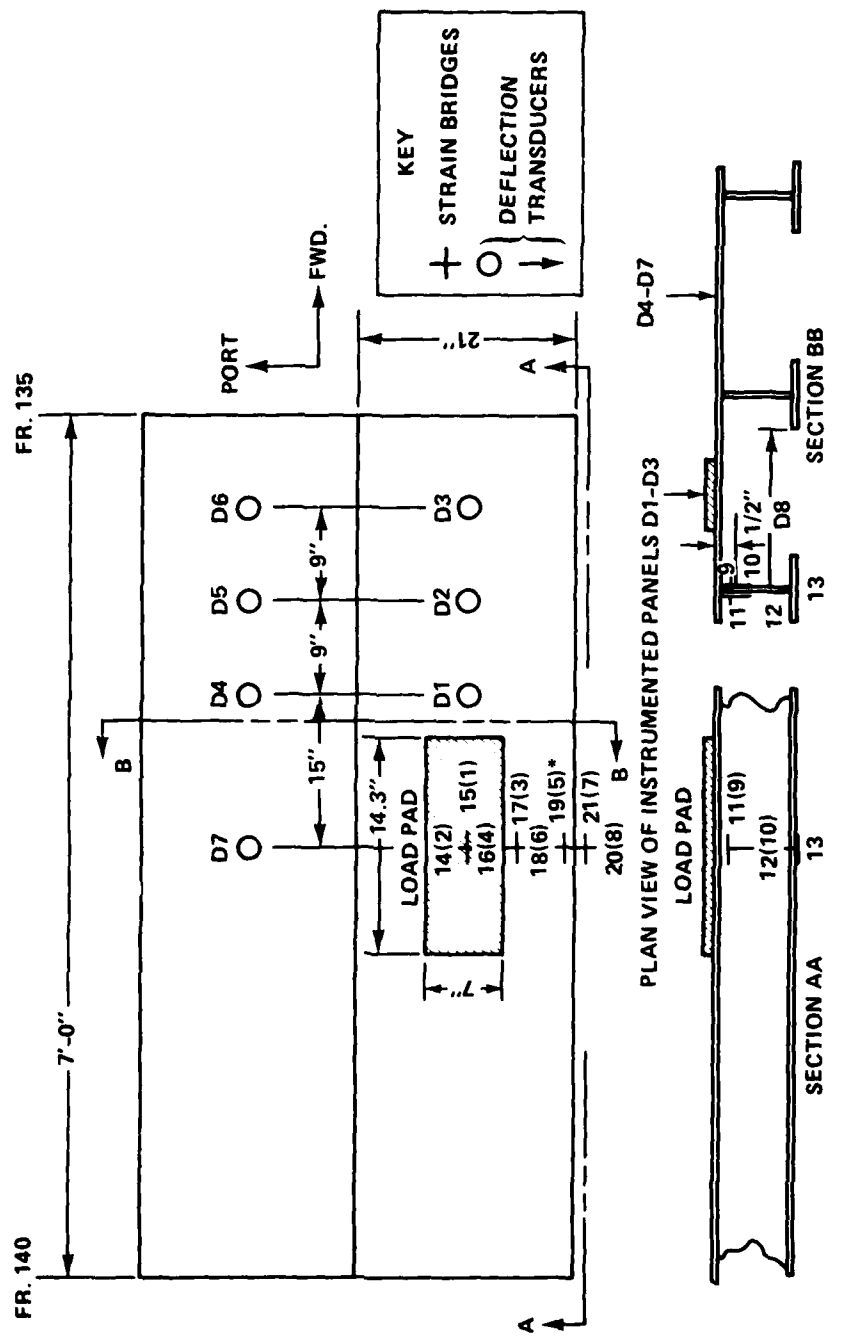


Figure 29 - Transducer Locations for USC; Cutter STEADFAST Static Tests

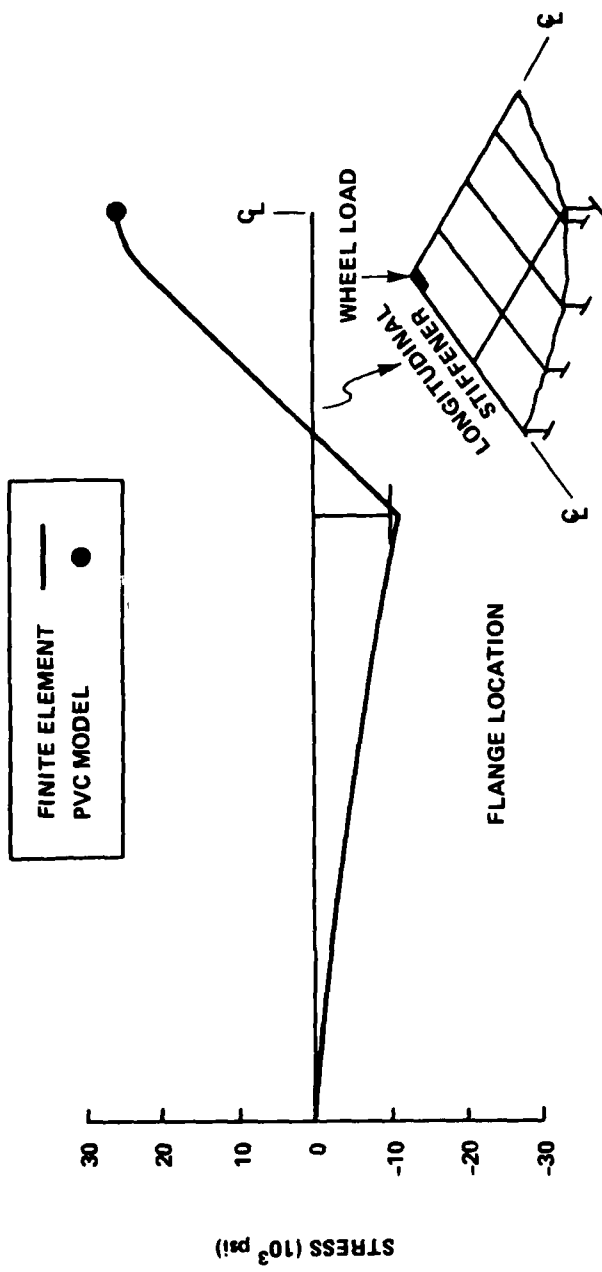


Figure 30 - Flange Stress Profile for Center-Line Longitudinals in 270, Configuration I (for Load Case 1, Table 2)

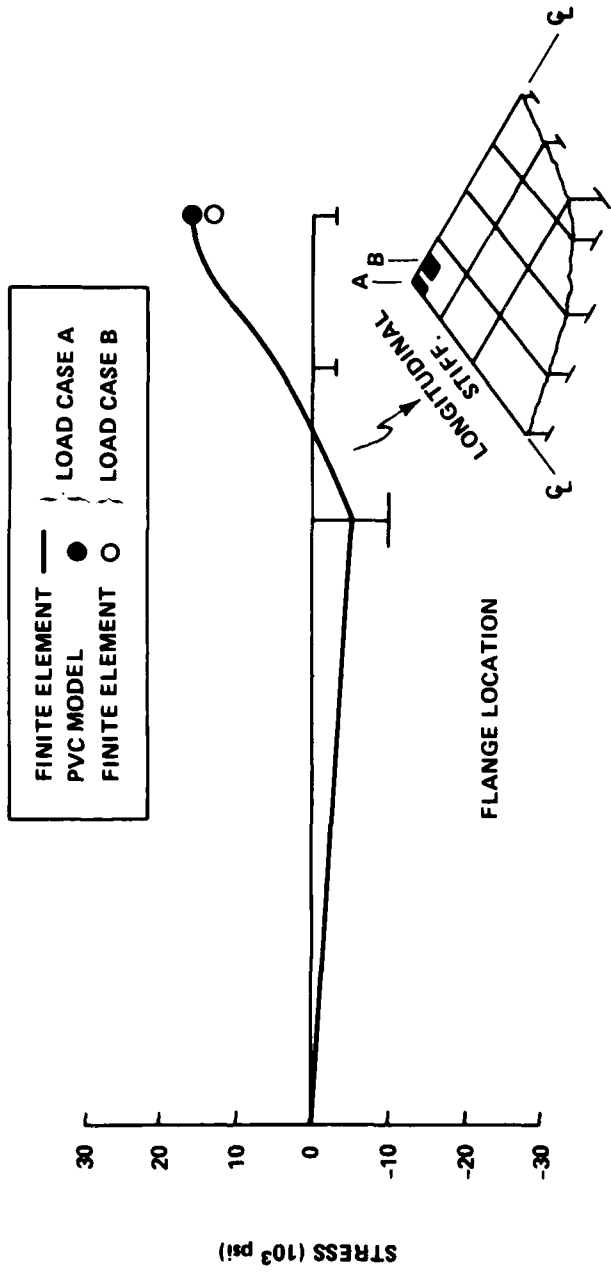


Figure 31 - Flange Stress Profile for Center-Line Longitudinals in 270, Configuration II (for Load Case 1, Table 2)

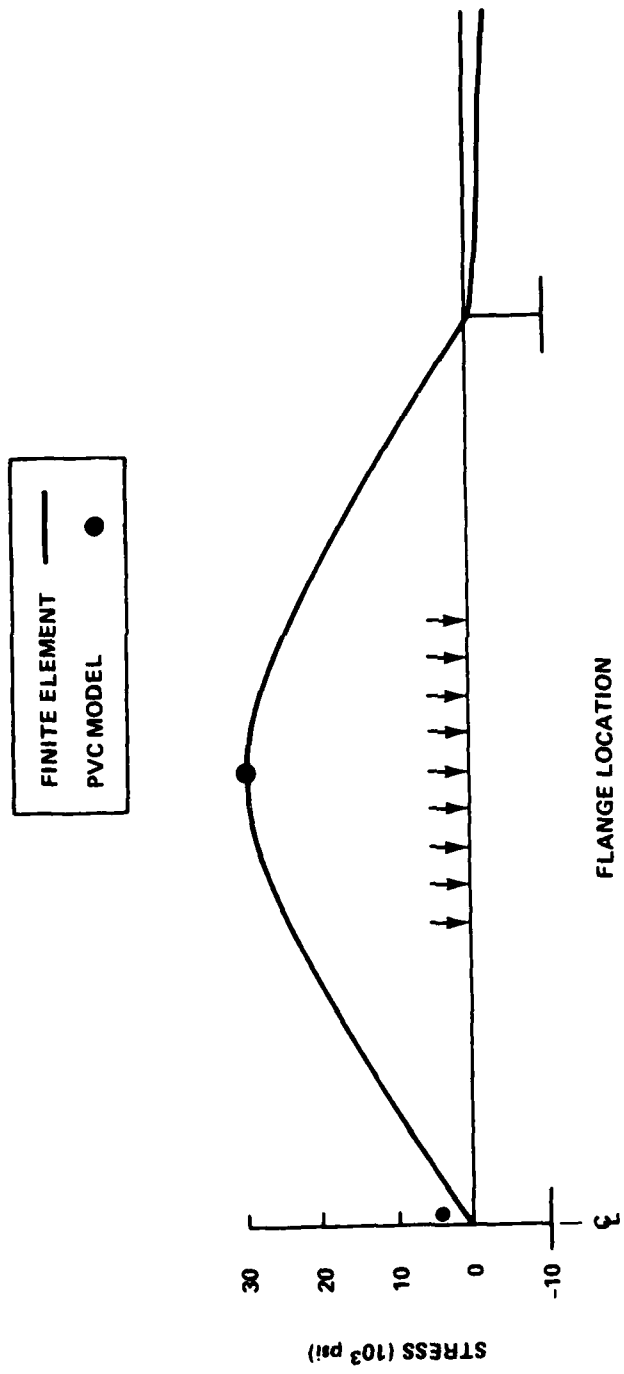


Figure 32 - Flange Stress Profile for Headers in 270, Configuration II
(for Load Case 1, Table 2)

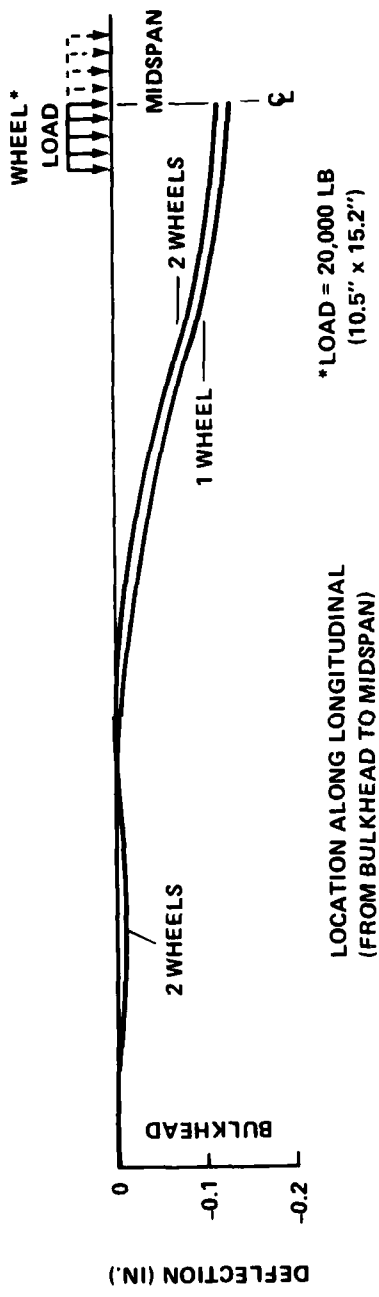


Figure 33 - Deflection Profile for Center-Line Longitudinal in 270, Configuration I
(One and Two Wheels for Load Case 1, Table 2)

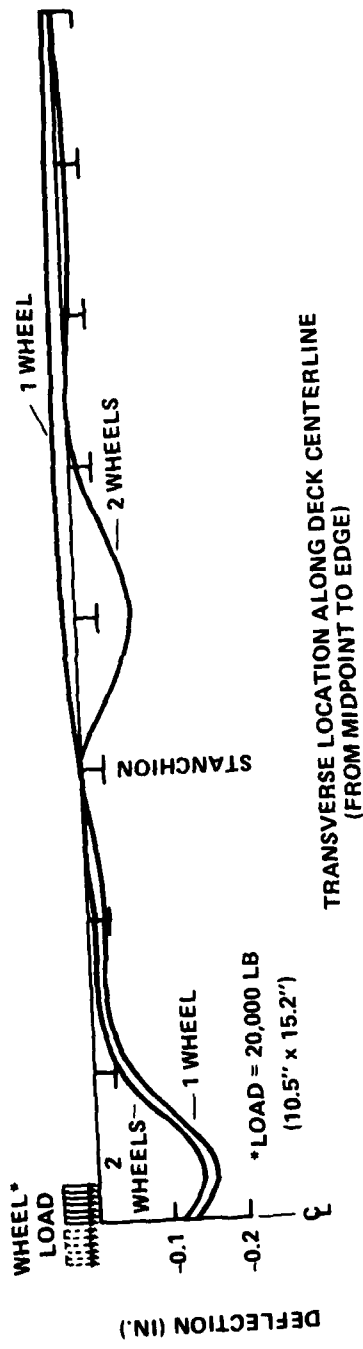


Figure 34 - Deflection Profile along Transverse Center-Line of 270, Configuration I
(One and Two Wheels for Load Case 1, Table 2)

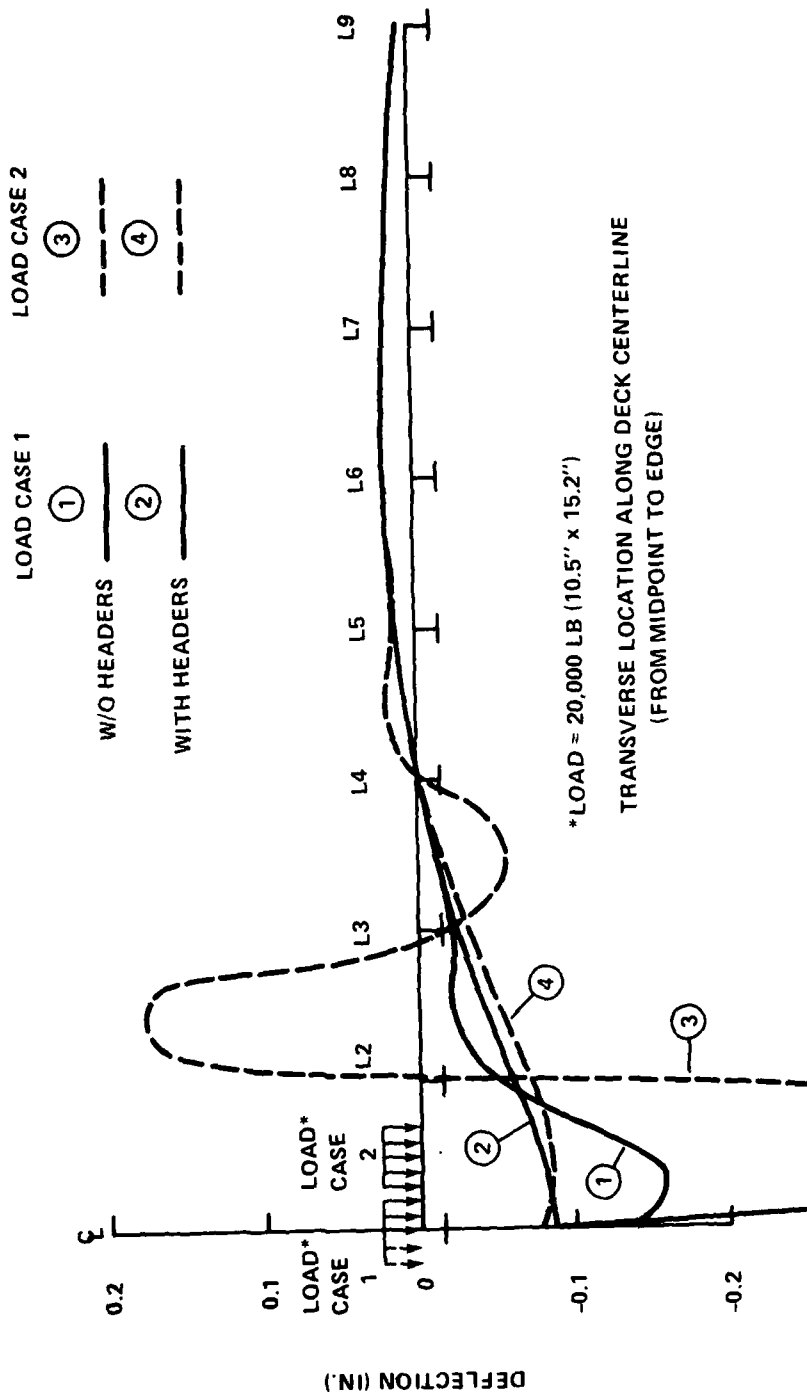


Figure 35 – Deflection Profiles Along Transverse Center-Line for 270,
Configurations I and II (Wheel Load On and Between Stiffeners)

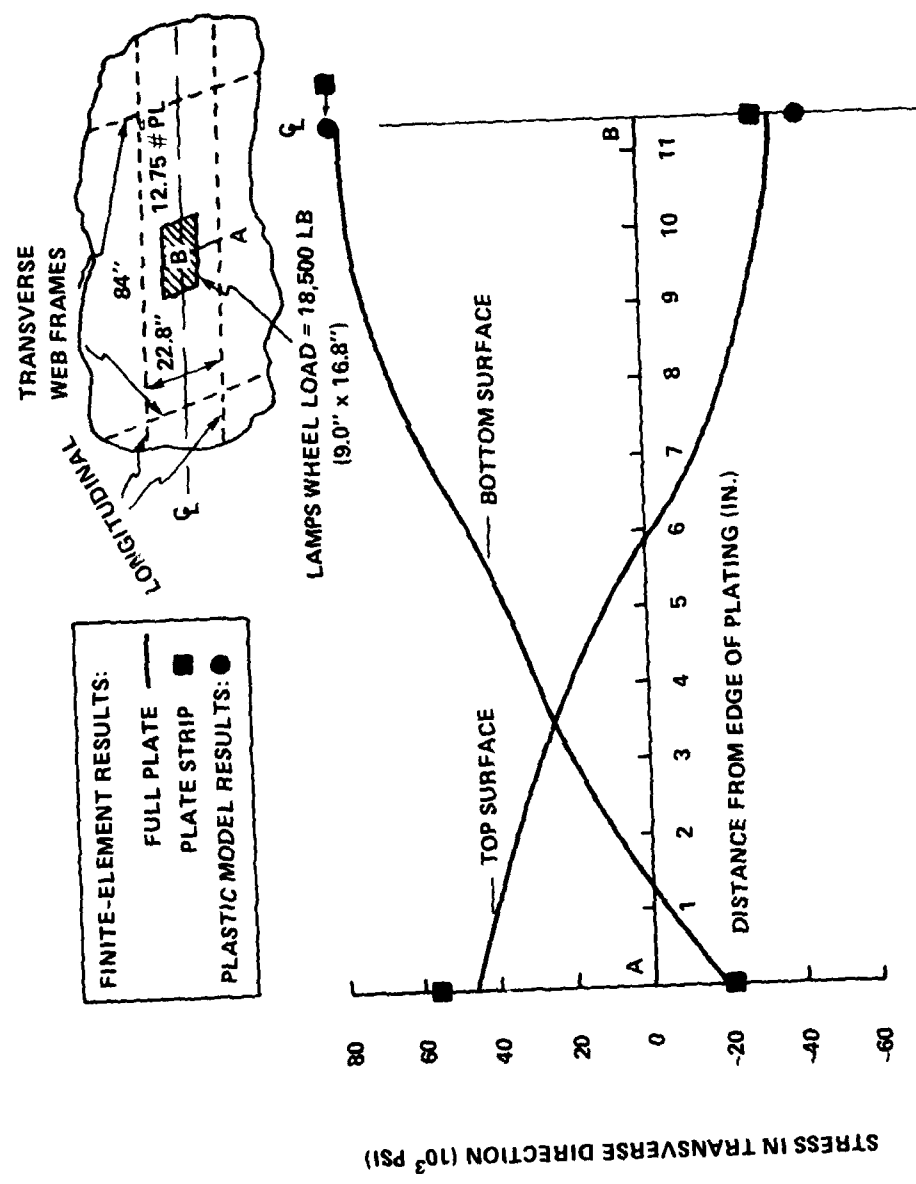


Figure 36 - Plating Stress Profiles in Transverse Direction for 270, Configuration I
Stresses Plotted Include Bending Membrane Components

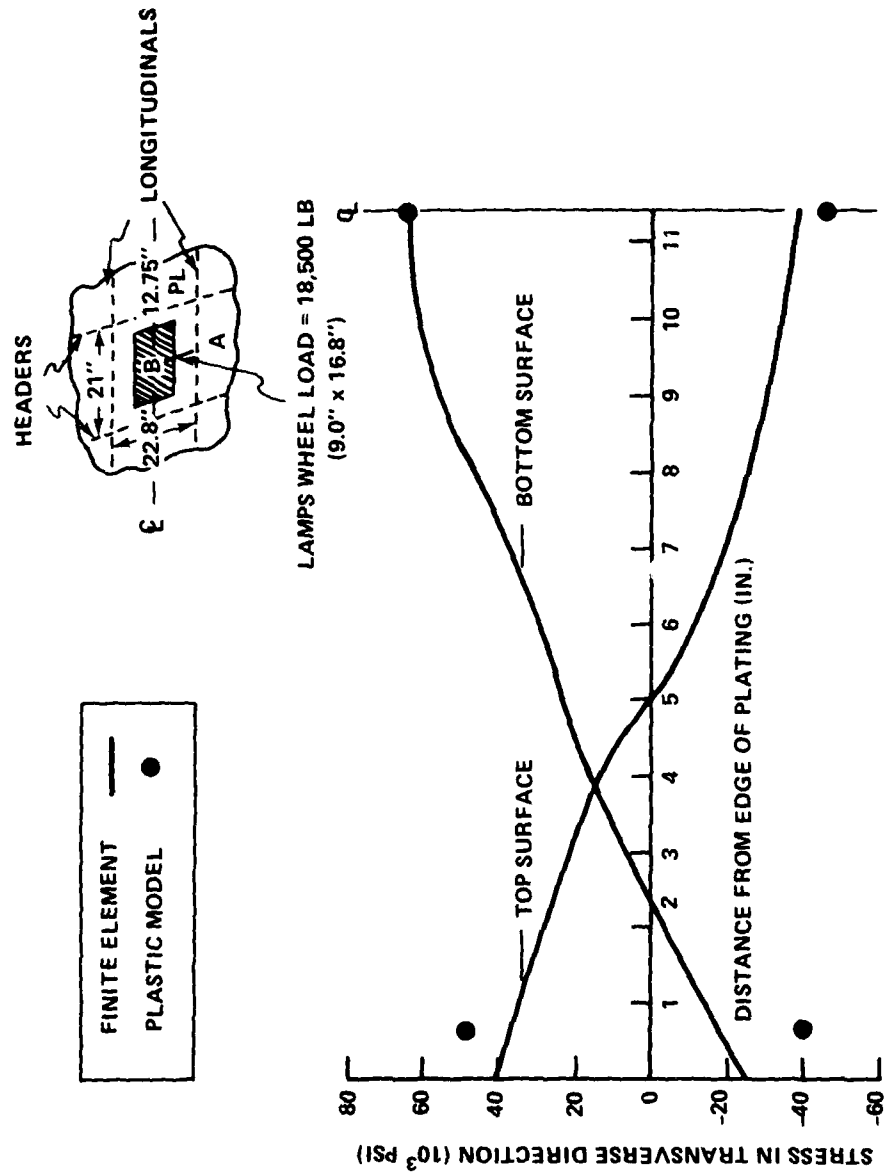


Figure 37 - Plating Stress Profiles in Transverse Direction for 270, Configuration II
Stresses Plotted Include Bending and Membrane Components

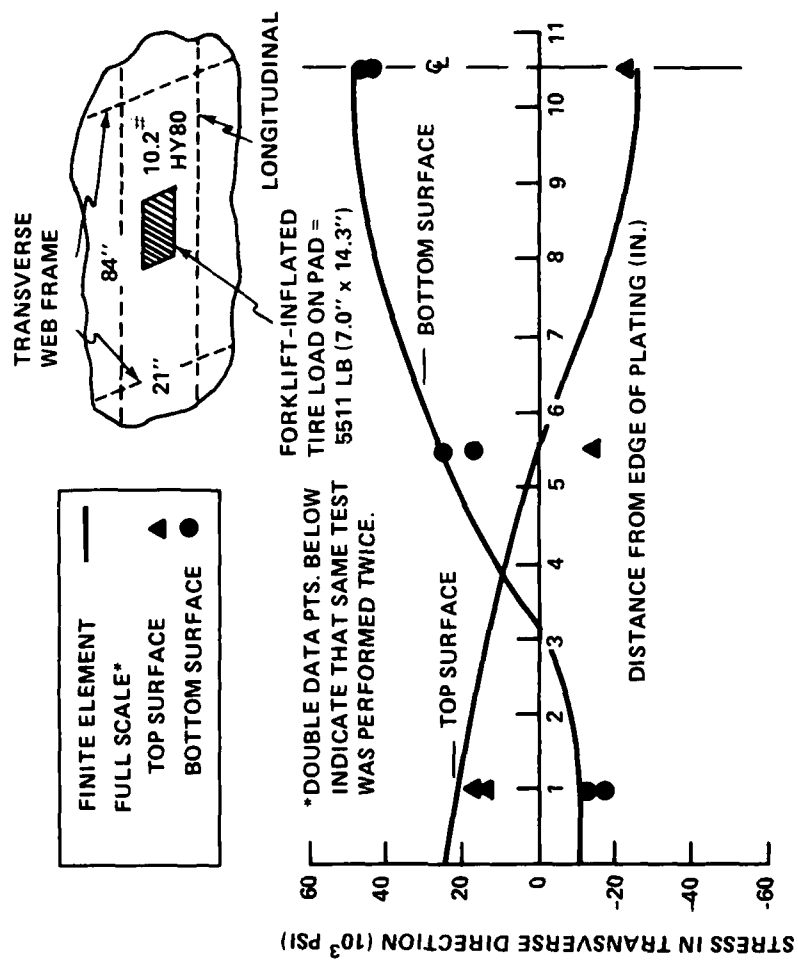


Figure 38 - Plating Stress Profiles in Transverse Direction for 210 Cutter STEADFAST

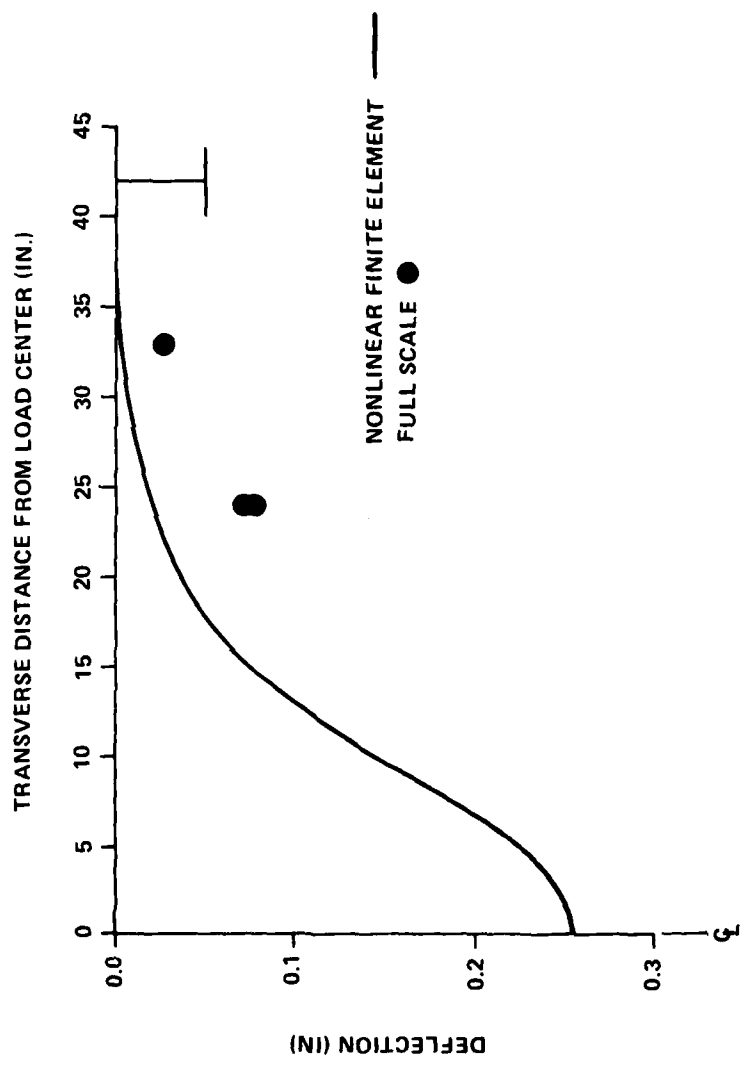


Figure 39 - Plating Deflection Profile in Transverse Direction for 210 Cutter STEADFAST

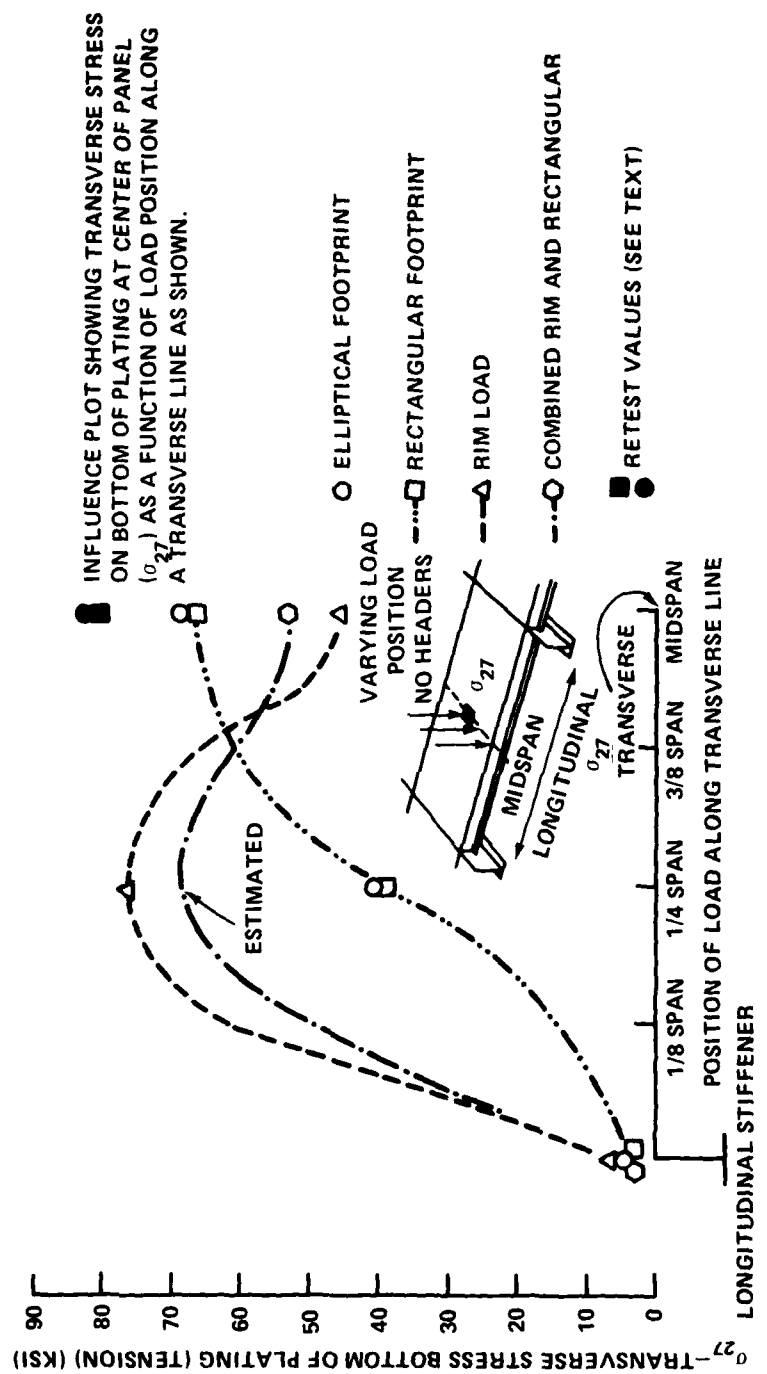


Figure 40 - Transverse Plating Stress at Center of Panel for Varying Load Type and Position on Configuration I

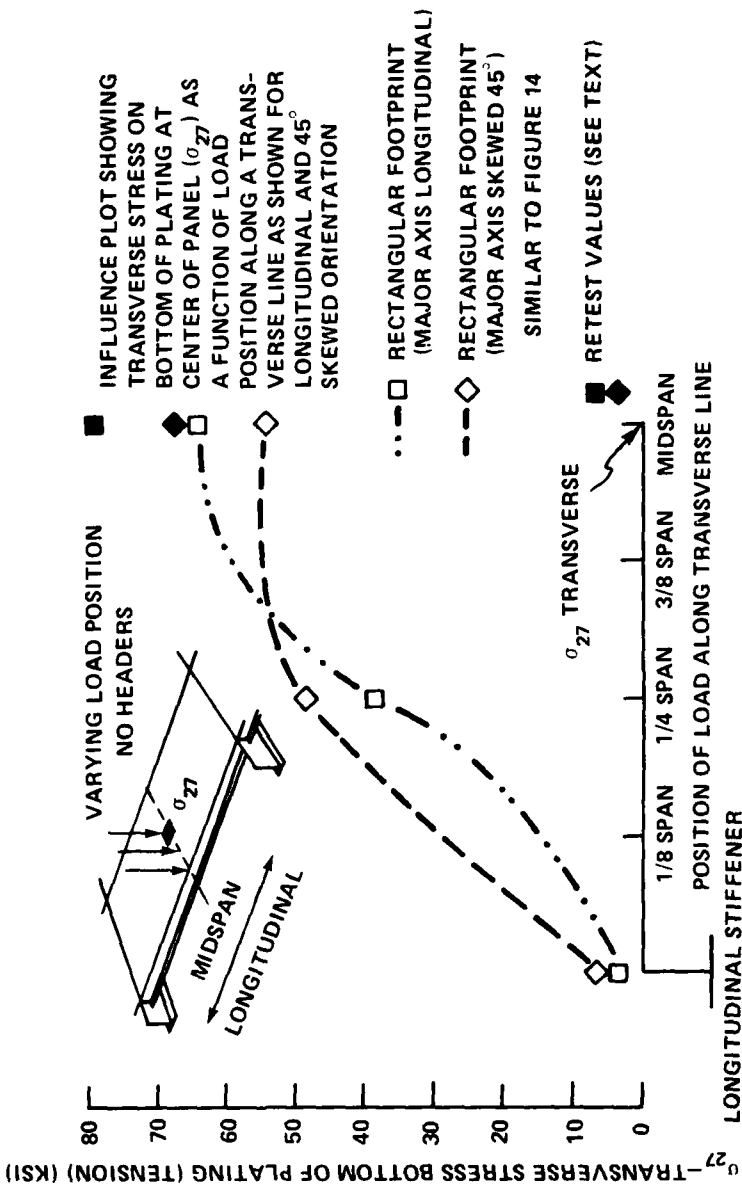


Figure 41 - Transverse Plating Stress at Center of Panel for Varying Load Position on Configuration I Using 45 Degree Skew Load

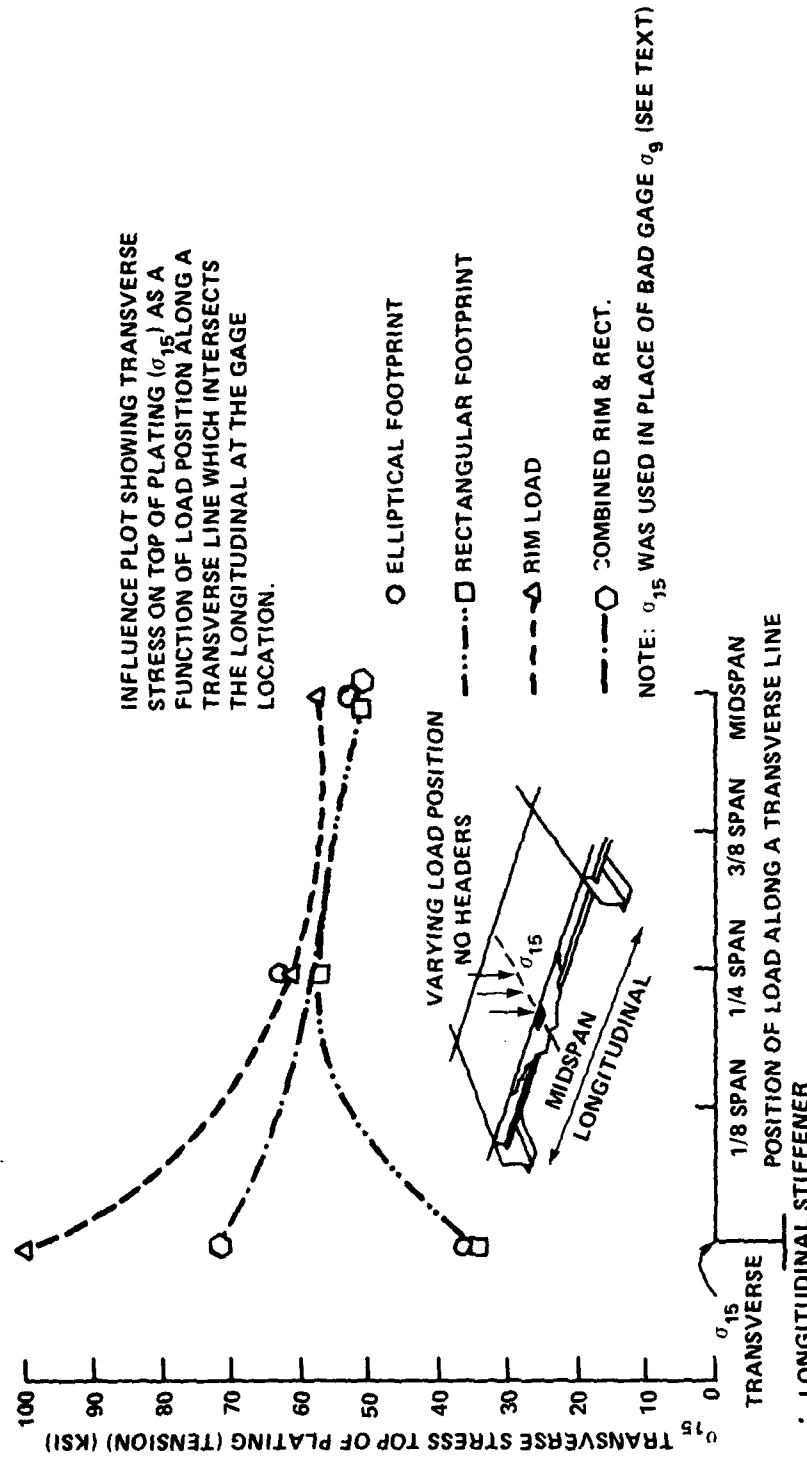


Figure 42 - Transverse Plating Stress at Edge of Panel for Varying Load Type and Position on Configuration 1

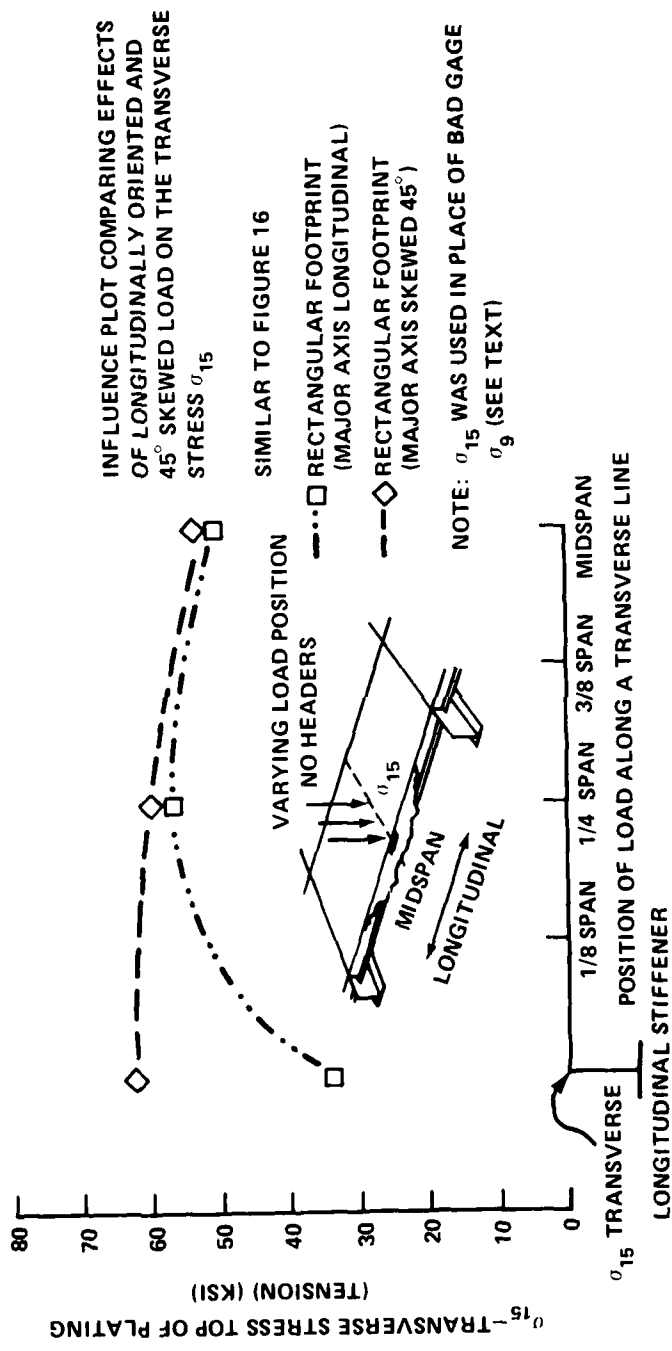


Figure 43 - Transverse Plating Stress at Edge of Panel for Varying Load Position on Configuration I Using 45 Degre Skew Load

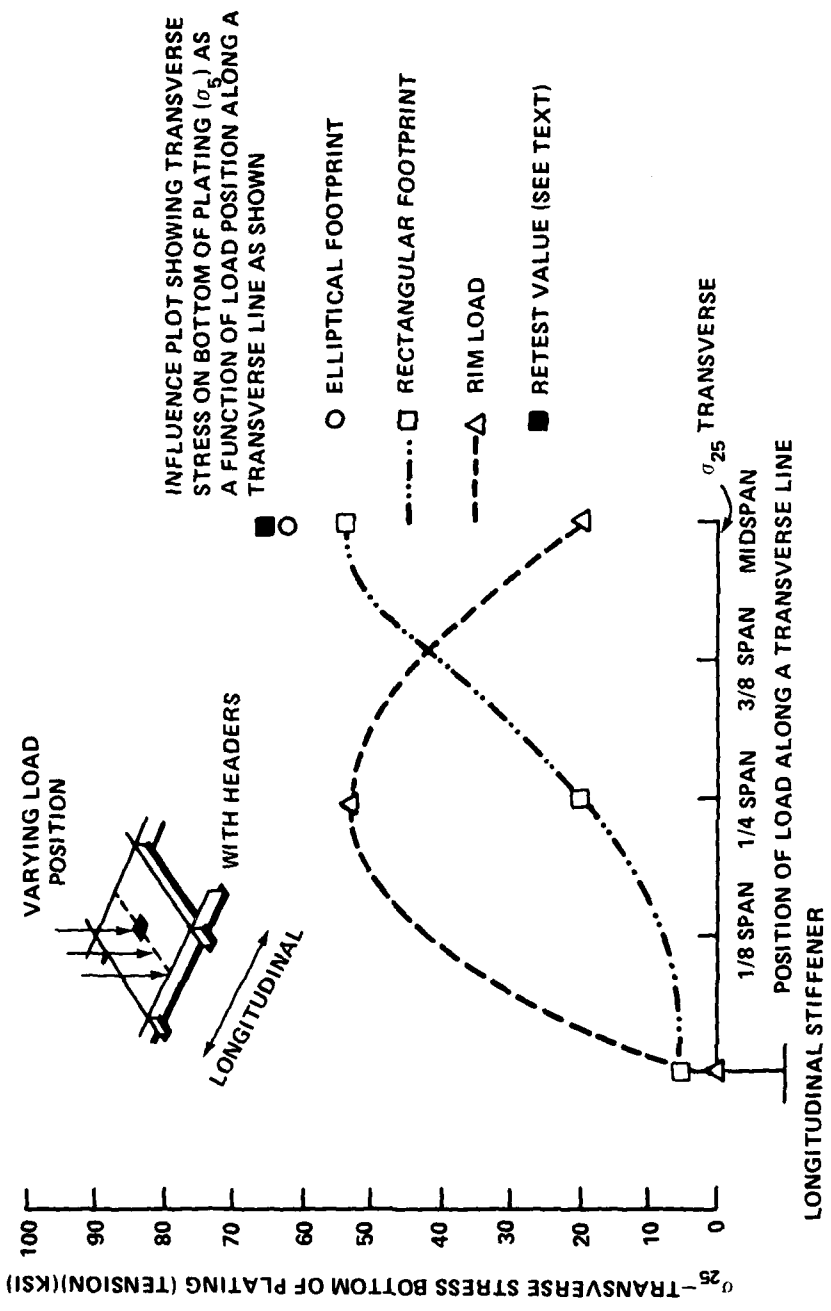


Figure 44 - Transverse Plating Stress at Center of Panel for Varying Load Type and Position for Configuration II

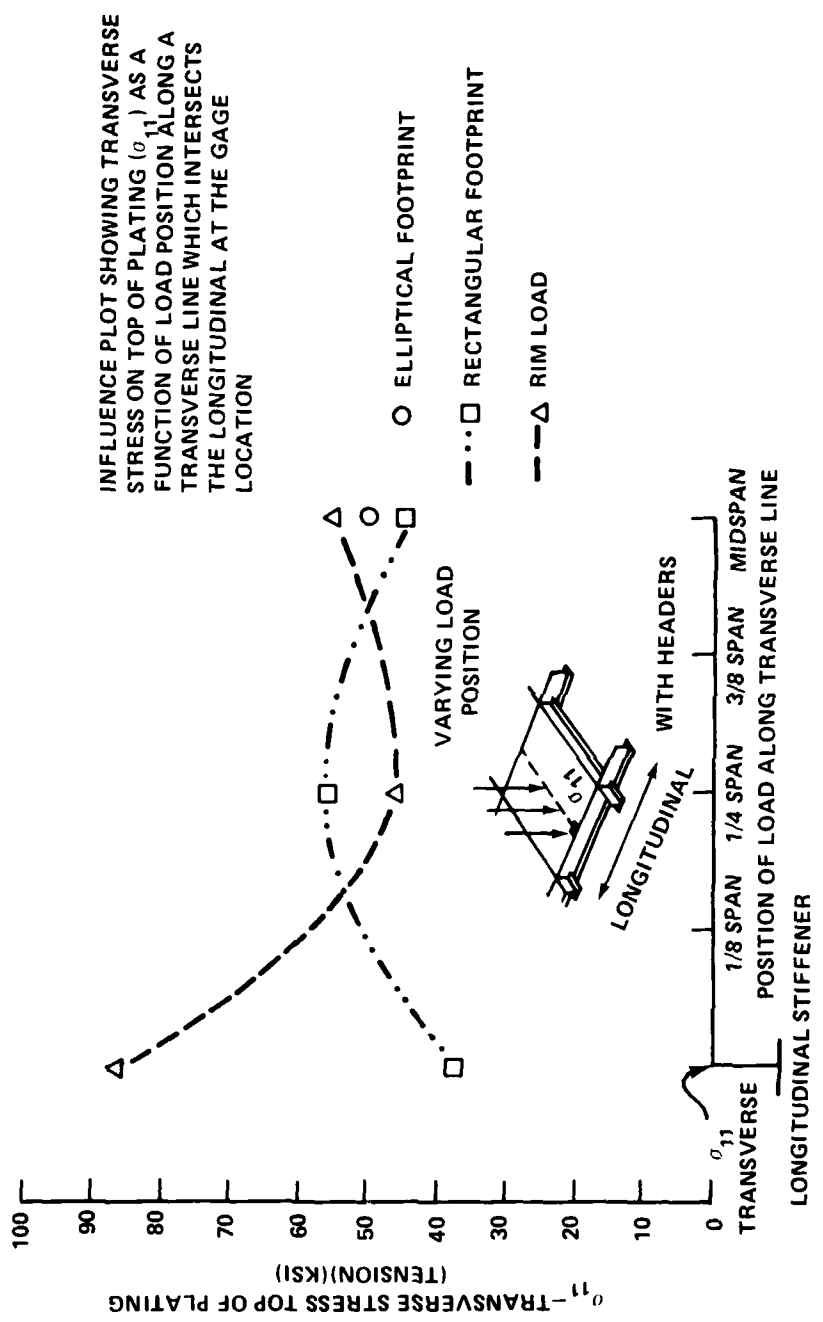


Figure 45 - Transverse Plating Stress at Edge of Panel for Varying Load Type and Position for Configuration II

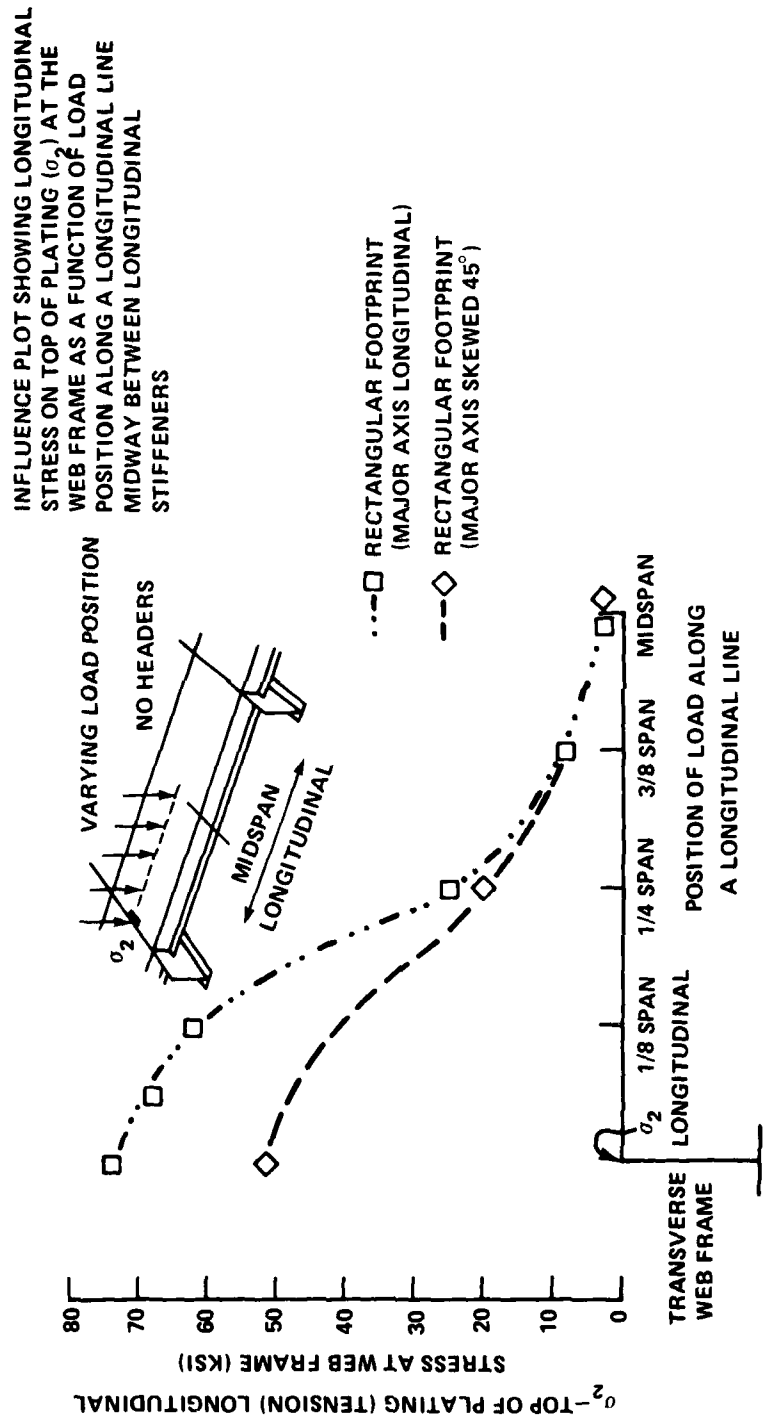


Figure 46 - Longitudinal Plating Stress at Web Frame for Configuration I
as a Function of Load Position Longitudinally

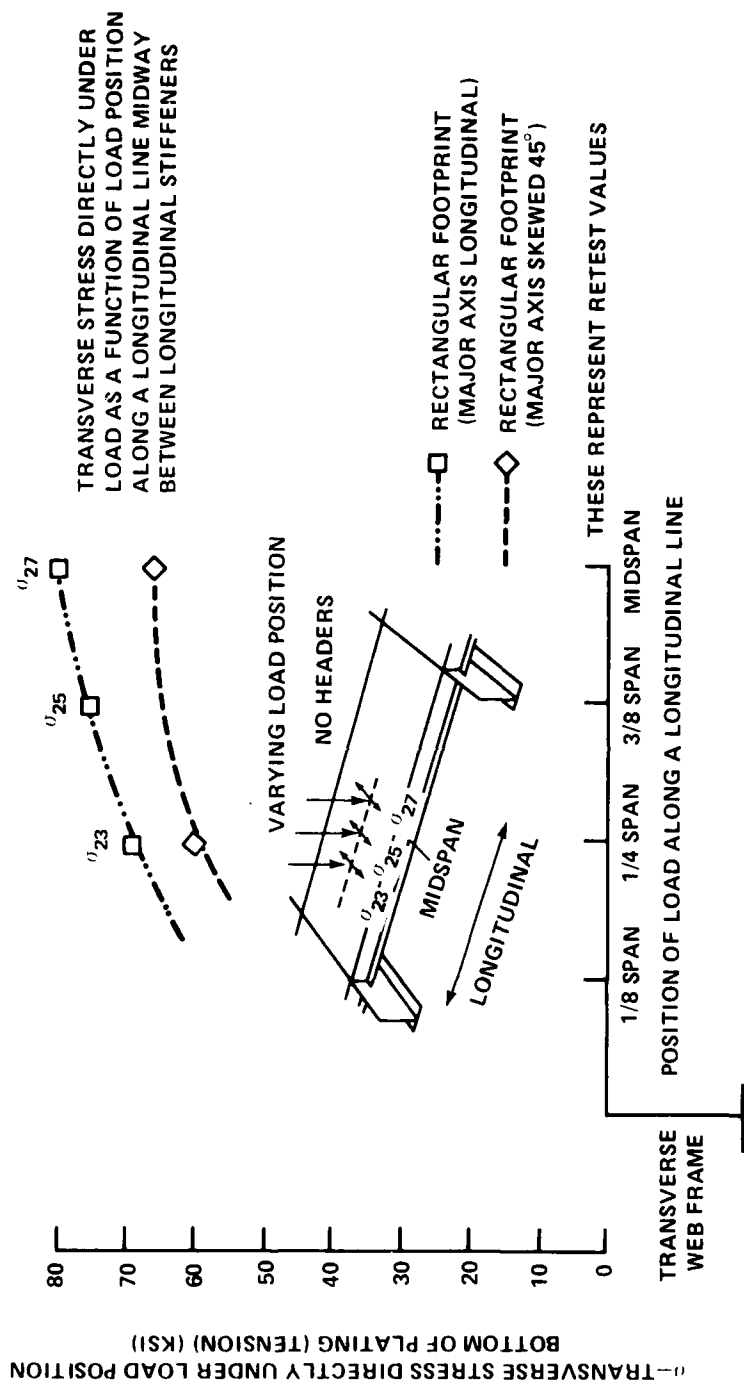


Figure 47 - Transverse Stress Directly Under Load for Configuration I

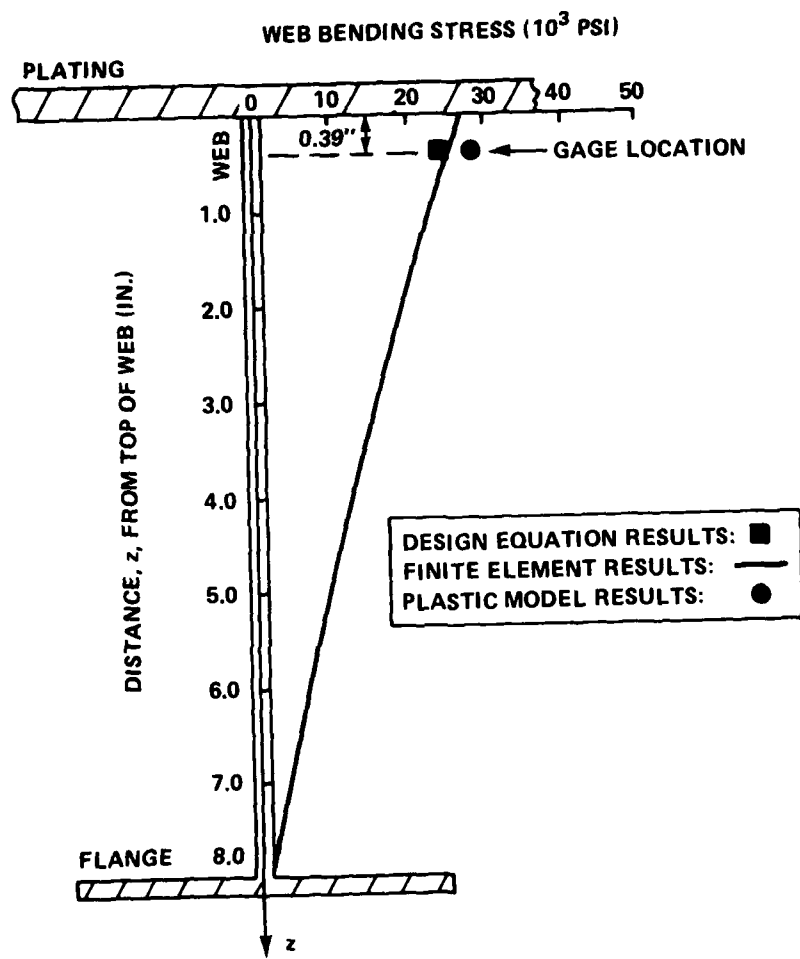


Figure 48 - Variation of Web Bending Stress with Web Depth for Longitudinal in 270, Configuration I

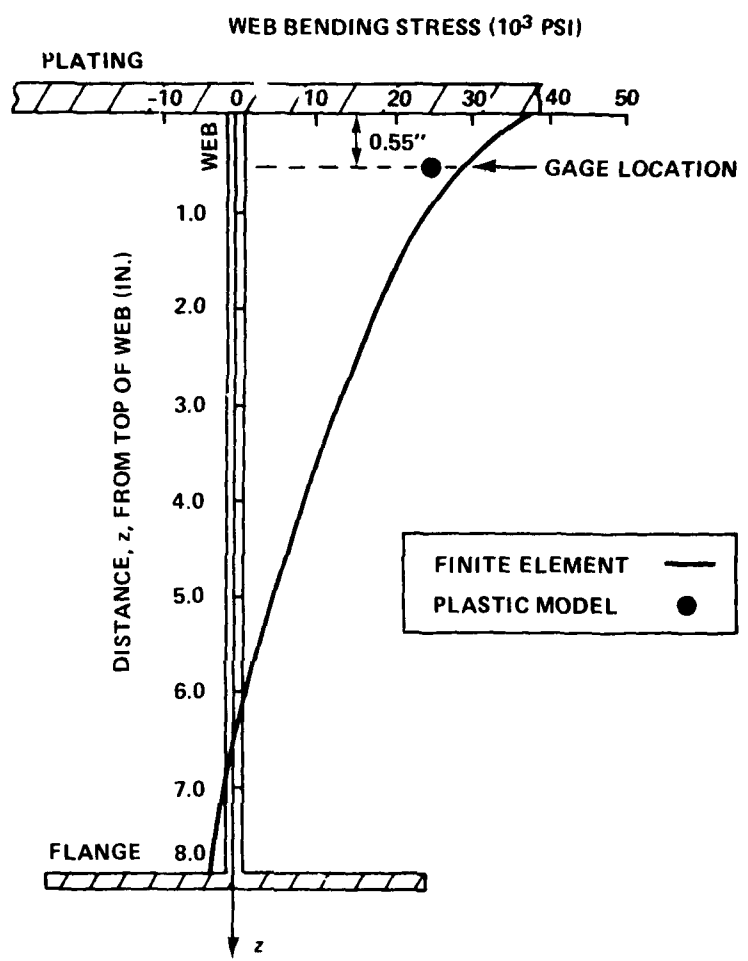


Figure 49 - Variation of Web Bending Stress with Web Depth for Longitudinal in 270, Configuration II

AD-A102 420 DAVID W TAYLOR NAVAL SHIP RESEARCH AND DEVELOPMENT CE--ETC F/G 13/10
STRUCTURAL RESPONSE METHODS AND EVALUATION RESULTS FOR HELICOPT--ETC(U)
JUL 81 M O CRITCHFIELD, J L RODD, W H HAY MIPR-Z-70099-6-65439
UNCLASSIFIED DTNSRDC-81/009 NL

REF ID:
A102-420

END
DATE
19 81
DTIC

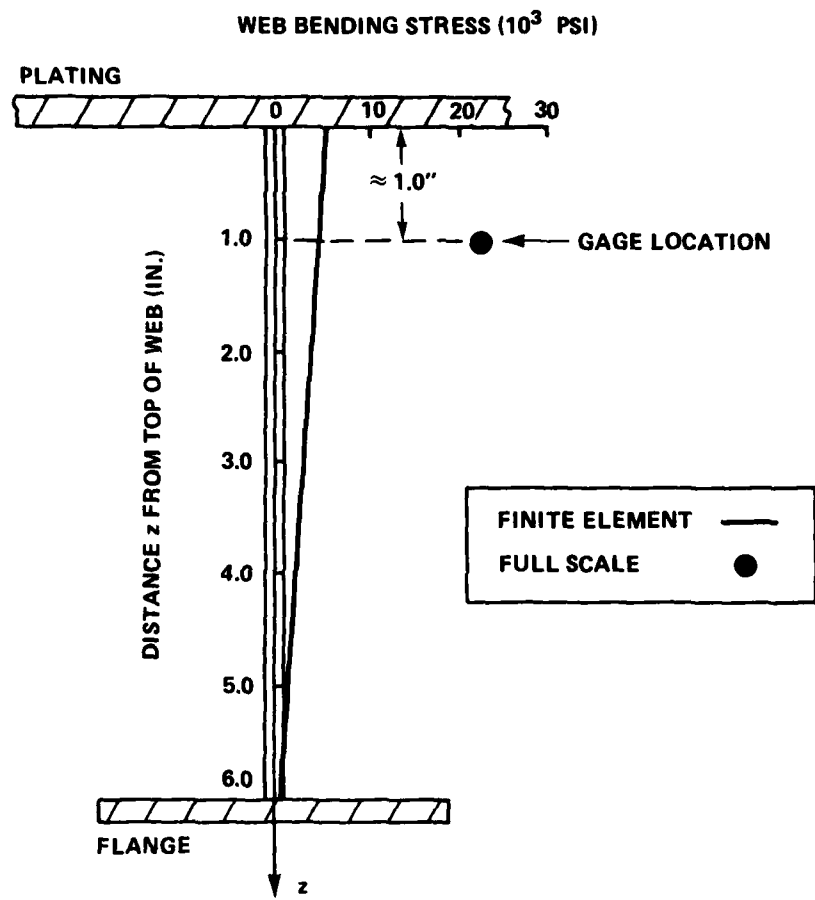


Figure 50 - Variation of Web Bending Stress with Web Depth for Longitudinal in 210 Helo Deck (Unmodified)

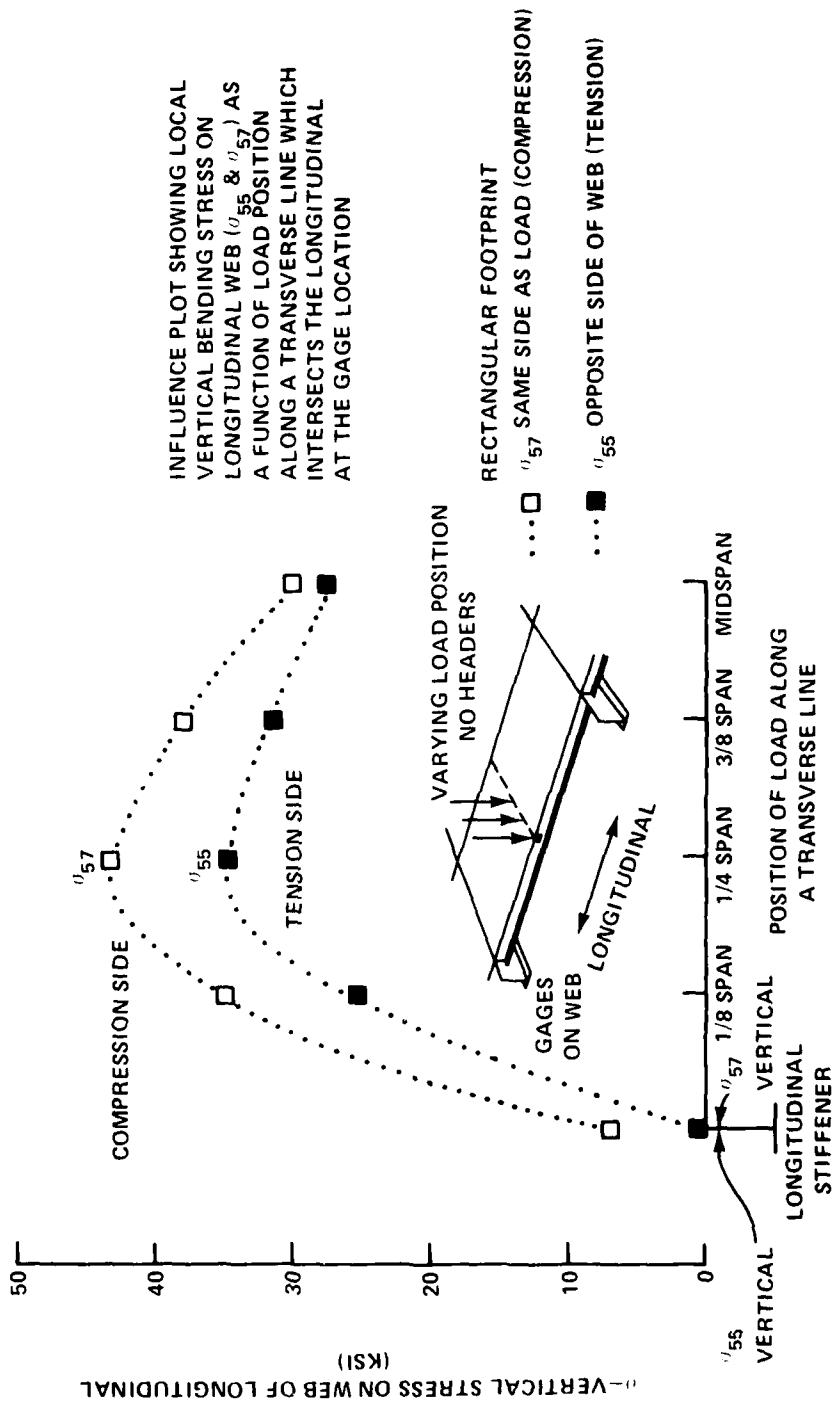


Figure 51 - Local Vertical Bending Stress on Longitudinal Web--for No-Header Case

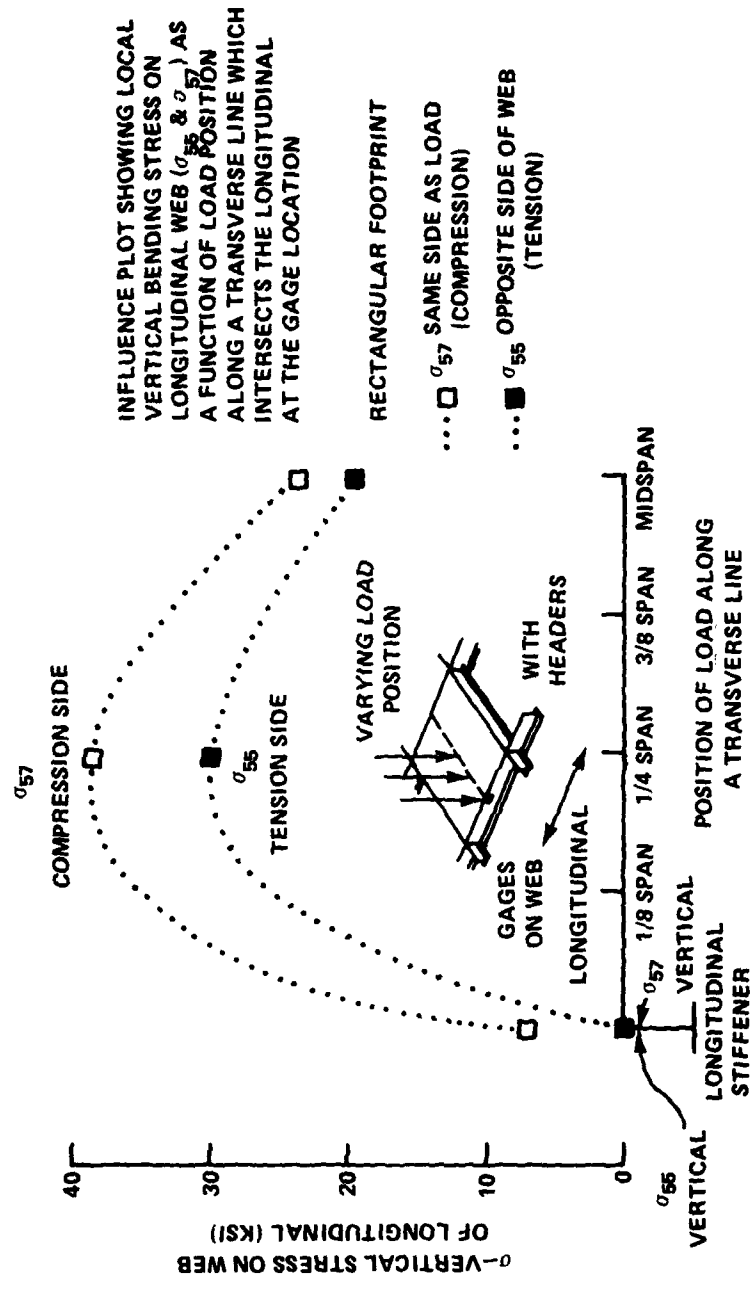


Figure 52 - Local Vertical Bending Stress on Longitudinal Web--for Header Case

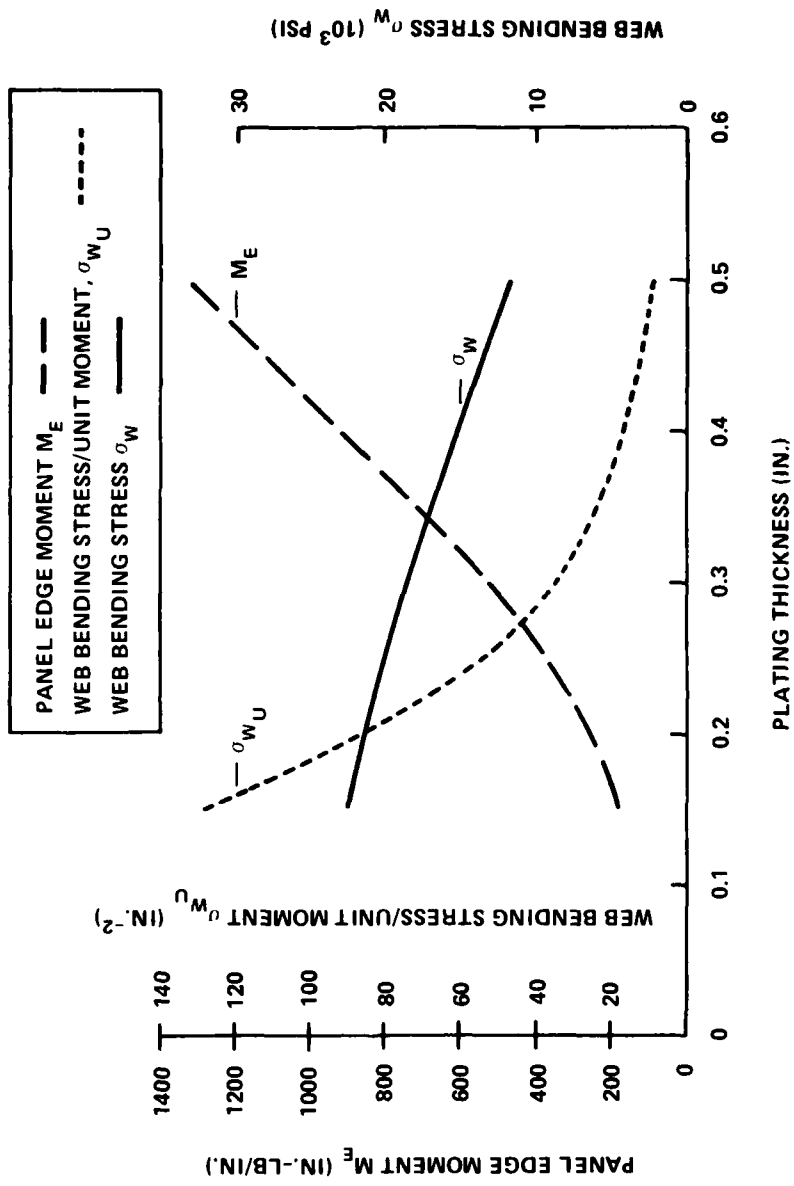


Figure 53 - Variation of Panel Edge Moment and Web Bending Stress with Plating Thickness for Constant Longitudinal Stiffener Properties and Spacing from Configuration I

TABLE 1 - EVALUATIONS PERFORMED ON HELICOPTER LANDING DECKS OF 210- AND 270-FOOT LONG USCG CUTTERS

Evaluation Type	Helicopter Landing Decks Evaluated					
	I	II	III	IV	(Existing) 210	(Modified) 210
Finite Element and Other Analytical	*	*	*	*	*	*
Rigid Vinyl Model	*	*				
Full-Scale					*	

TABLE 2 - HELICOPTER LANDING GEAR LOAD DATA FOR 210- AND 270-CLASS EVALUATIONS

Ref.	Wheel Load Conditions	Load (lb)	Pressure (psi)	Footprint Dimensions Width x Length (in. x in.)	Area ² (in. ²)	Applied to Configuration
1	Lamps Helo Main Gear (Initial)	20,000	E	162.9	8.8x18.2	122.8
			R	162.9	7.7x16.0	123.2
			F	125.3	10.5x15.2	159.6
2	Lamps Helo Main Gear (Revised)	18,500	E	123.3	10.0x19.0	150.0
			R	122.4	9.0x16.8	151.2
			P,M	122.4	9.0x16.8	151.2
			F	144.9	7.6x16.8	127.7
3a	Lamps Helo Main Gear (Final) (Symmetrical Landings)	18,800	R,	98.9	8.6x22.2	190.0
			F			270 (IV)
3b	Main Gear (Rolled Landings)	19,430	R, P	98.6	8.7x22.6	197.0
3c	Dual Tail Wheel	20,000	R, P	153.8	5.1x12.7 (Each Wheel)	130.0
4	Forklift Tire	5,510	R, P	55.0	7.0x14.3	100.1
5	SRR Helo- Sikorsky	7,700	R, F	226.0	5.3x8.6	34.0
						210 (Modified Deck)

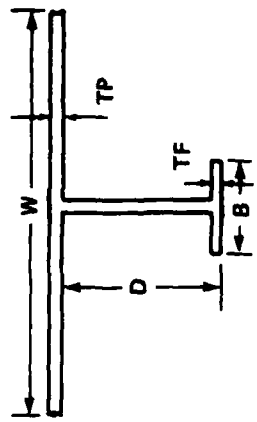
*E - Elliptical Tire Print Data Furnished by the USCG.

R - Rectangular Tire Print Data Computed Based on E Data.

F,P - Footprint Data for Framing (F) and Plating (P) Analyses.

M - Data Used in Rigid Vinyl Model Evaluation.

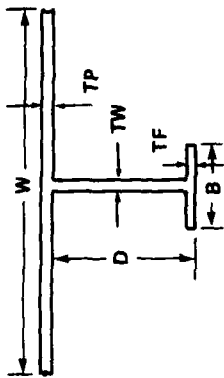
TABLE 3 - SECTIONAL PROPERTIES OF LONGITUDINALS AND HEADERS FOR
210- AND 270-CLASS EVALUATIONS



Sectional Properties (See Sketch)	270 Configurations I, II, AND III		270 Conf. IV	210 (Existing)	210 (Modified)
	Longitudinal Headers 8x4x10#I-T	Header 4x2 1/4x3.25#T	Longitudinals & Headers 6x4x7#T	Longitudinal Headers 6x3x5.9#T	Longitudinal Headers 6x3x5.9#T
W^*	12.5	12.5-II 10.0-III	8.5	10.0	10.0
TP	0.3125 (HY80)	0.3125-II 0.25-III (HY80)	0.25 (HY100-) (Tempered Up)	0.25 (HY80)	0.25 (HY80)
D	7.9	4.0	5.96	6.00	6.00
TW	0.17	0.14	0.20	0.18	0.18
B	3.94	2.28	3.97	3.06	3.06
TF	0.20	0.19	0.22	0.23	0.23

* $W = 2\sqrt{E/\sigma_y}$ (TP); E = Modulus of elasticity and σ_y = yield strength.

TABLE 4 - COMPARISON OF SECTIONAL PROPERTIES FOR FULL-SCALE
LONGITUDINALS AND HEADERS BASED ON RIGID VINYL MODEL



Sectional Properties (See Sketch)	Longitudinal-270 (8x4x10#I-T)		Header-270 (4x2 1/4x3.25#T)		Longitudinal-210 (6x3x5.9 #T)		Header-210 (4x2 1/4x3.25#T)	
	Full Scale	Scaled-up PVC	Full Scale	Scaled-up PVC	Full Scale	Scaled-up PVC	Full Scale	Scaled-up PVC
W* (40TP)	12.5	12.512	12.5	12.512	10.0	10.0	10.0	10.0
TP	0.3125	0.3126	0.3125	0.3128	0.25	0.25	0.25	0.25
D	7.9 (7.7**)	7.8706 (7.682**)	4.0 (3.81**)	4.0066 (3.818**)	6.0 (5.77**)	6.0 (5.77**)	4.0 (3.81**)	4.0 (3.81**)
TW	0.17	0.1886	0.14	0.138	0.18	0.18	0.14	0.14
B	3.94	4.1722	2.28	2.3	3.06	3.06	2.28	2.28
TF	0.20	0.1886	0.19	0.1886	0.23	0.23	0.19	0.19

*W = $2\sqrt{E/\gamma_y}$ (TP); E = Modulus of elasticity and σ_y = yield strength.

**For web bending analysis.

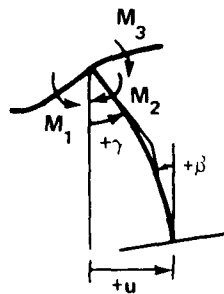
TABLE 5 - ELASTIC BOUNDARY RESTRAINT CONSTANTS FOR PLATING AND WEB BENDING ANALYSES

Panel Boundary	a (in.)	b (in.)	t (in.)	k_p (Plating)	k_s (Stiffener)	$k_T = k_p + k_s$	From NASTRAN Solution
				Continuous Beam	Finite Element	Design Equation	
Longitudinal (without Headers) Case	84.0	22.8	0.3125	12045	12050	2175	14225
Longitudinal (with Headers) Case	21.0	22.8	0.3125	12045	25460	*	30000 20000
Transverse (with Headers) Case	22.8	21.0	0.3125	13080	23800	4930	28730
Longitudinal (without Headers) Case	78.0	21.0	0.25	6695	6690	**	**
Longitudinal (with Headers) Case	19.5	21.0	0.25	6695	14040	*	**
Transverse (with Headers) Case	21.0	19.5	0.25	7210	13220	*	**

*= Not applicable

**= Not available.

TABLE 6 - COMPARISON OF WEB BENDING PREDICTIONS USING DESIGN EQUATIONS
AND FINITE ELEMENT



$$\begin{aligned}
 A &= 84.0 \text{ in.}, S = 7.7 \text{ in.}, t = 0.17 \text{ in.} \\
 I &= 1.02254 \text{ in.}^4, J = 0.02312 \text{ in.}^4 \\
 l &= 0.06570 \text{ in.}^6, C = 12046 \frac{\text{in. - lb/in.}}{\text{rad.}} \\
 E &= 30 \times 10^6 \text{ psi}, v = 0.3, M_1 = 100.0 \text{ in.-lb/in.}
 \end{aligned}$$

Variable	Basis			
	Test	Equations	FINEL*	Using Ref. 6
u (in.)	-	0.0311	0.0310	0.0309
β (rad)	-	0.0024	0.0026	0.0025
γ (rad)	-	0.0070	0.0070	0.0070
M_2 ($\frac{\text{in.-lb}}{\text{in.}}$)	-	15.28	15.66	16.06
M_3 ($\frac{\text{in.-lb}}{\text{in.}}$)	-	84.72	84.34	83.94
σ_w (psi) (Web Bending Stress)	-	3173	3249	3334

*Adamchak, John C., "User's Manual for the Modified Finite Element Program FINEL", NSRDC Rept. 3609, Nov. 1970.

TABLE 7 - SCALING LAWS FOR 270-CLASS HELO DECK MODEL

Quantity	Scaling Law*
Length	$L_p = \lambda L_m$
Deflection	$\delta_p = \lambda \delta_m$
Strain	$\epsilon_p = \epsilon_m$
Stress	$\sigma_p = e \sigma_m$
Force	$F_p = e \lambda^2 F_m$
Moment	$M_p = e \lambda^3 M_m$
Moment of Inertia	$I_p = \lambda^4 I_m$
Section modulus	$S_p = \lambda^3 S_m$
where	
$\lambda = L_p/L_m = 4.6$	
$e = E_p/E_m = 66.67$	
$E_p = 30 \times 10^6 \text{ psi}$	
$E_m = 0.45 \times 10^6 \text{ psi}$	
$*p = \text{prototype}, m = \text{model}$	

TABLE 8 - MAXIMUM FRAMING STRESSES FOR 210- AND 270-FOOT HELO
DECK CONFIGURATIONS

Helo Deck Structure	Stress (psi)		
	Finite Element	AISC Equations	Plastic Model
270' Cutter - Configuration I			
Longitudinal	26000	26500	26000
270' Cutter - Configuration II*			
Longitudinal	16100	16500	16000
Header	28900	29200	29000
270' Cutter - Configuration IV			
Longitudinal	19890	20300	*
Header	19850	20650	*
210' Cutter - Class B			
Longitudinal	*	12350	12480**
210' Cutter - Class B (Modified)			
Longitudinal	9280	9210	*
Header	14500	15500	*
*Results are applicable to Configuration III also. **Full-Scale. * = Data not available			

TABLE 9 - PLATING STRESSES FOR 270-CLASS HELO DECK DESIGNS DUE TO CENTRAL PANEL LOADS

Helo Deck Configurations	Load Case (Table 2)	Stress (psi)				$\left(\frac{F-M}{M}\right) \times 100\%$
		Finite Element (F)		Rigid Vinyl Model (M)		
Center	Edge	Center	Edge	Center	Edge	Center
I	2	77800	46200	80000	* *	-2.8
II	2	63000	40800	65000	48000	-3.1
III	2	68800	46800	*	*	*
IV	3b	72700	59000	*	*	*

* = Not modelled.

** = Not available (faulty gage).

TABLE 10 - PLATING STRESSES FOR 270-CLASS HELO DECK DESIGNS DUE TO
WHEEL LOADS STRADDLING LONGITUDINAL AND TRANSVERSE
STIFFENERS (WEB FRAMES AND HEADERS)

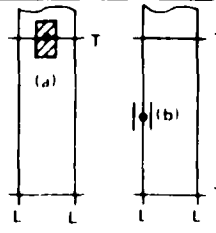
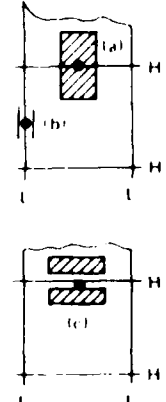
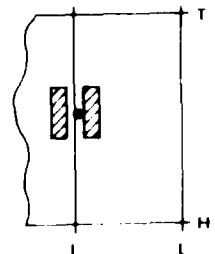
Load Condition (1b)	Load Case (Table 2)	Plating Stress (psi)		Load Placement and Stress Locations (•)
		Finite Element	Rigid Vinyl Model	
Configuration I				
(a) 18500	2	*	73500	
(b) 18500	RIM	*	100000	
Configuration II				
(a) 18500	2	91700 ¹	76000	
(b) 18500	RIM	*	86500	
Configuration III				
(a) 18500	2	125700 ¹	*	
(a) 19430	3b	120250 ¹	*	
(c) 20000 Dual tail wheel	3c	168700 ¹	*	
Configuration IV				
20000 Dual tail	4c	141500 ² (rigid long.)	*	
20000 Dual tail	4c	136000 ² (flexible long.)	*	
*				
¹ Simply supported boundaries (except for loaded side).				
² Elastically restrained boundaries.				

TABLE 11 - WEB BENDING STRESSES FOR 210-AND 270-CLASS HELO
DECK DESIGNS*

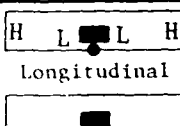
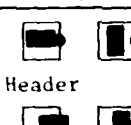
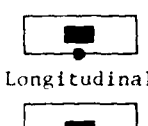
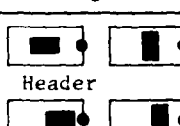
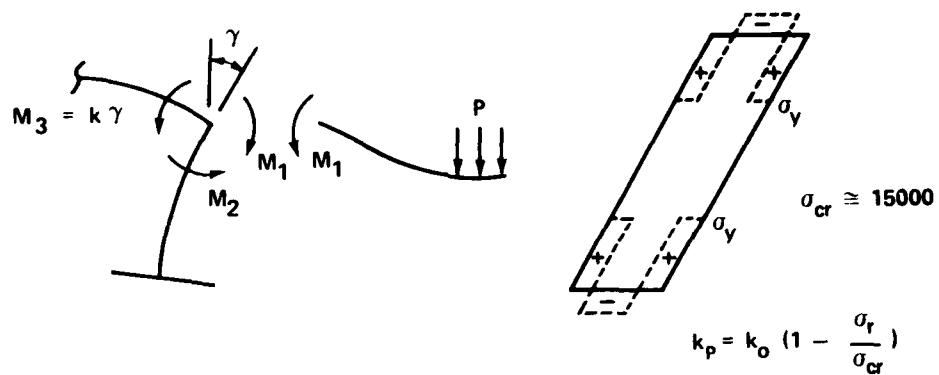
Helo Deck Structure	Wheel Load Condition (1b)	Web Bending Stress (psi)		
		Test Results	Finite Element	Design Equation
270' Cutter-Configuration I				
 Longitudinal	18500 (midspan)	28800 ** (30000)	25600	24400
	18500 (1/4 span)	38900 ** (43000)	34600	33000
270' Cutter-Configuration II				
 Longitudinal	18500 (midspan)	24500 ** (27000)	28800	*
	18500 (1/4 span)	37000 ** (41000)	43500	*
 Header	18500 (midspan)	42900 36500 *** (40000) **,***	*	44630
	18500 (1/4 span)	30000 54000 *** (60000) **,***	*	*
270' Cutter-Configuration IV				
 Longitudinal	19430 (midspan)	*	*	41300
	19430 (1/4 span)	*	*	59000
 Header	19430 (midspan)	*	*	21000 21000 ***
	19430 (1/4 span)	*	*	yield yield ***
210' Cutter-Class B				
Longitudinal	3260 (midspan)	22800	4500	4000
<small>*Results are for longitudinally oriented tire prints, except where noted in table by ***.</small>				
<small>**Web surface stress (bending and compression).</small>				
<small>***Transversely oriented footprint.</small>				
<small>* = Results not available.</small>				

TABLE 1.2 - WEB BENDING STRESS CALCULATIONS FOR LONGITUDINALS IN
EXISTING 210-FOOT DECKS

Results	Stresses (psi)			Bending Moments (in.-lb/in.)		
	σ_1	σ_2	σ_3	M_1	M_2	M_3
Test	17000	22750	5150	177.1	122.9	53.6
Finite Element	17000	5550	14325	177.1	30.0	149.2
Design Equation	17000	4980	14430	177.1	26.9	150.3
						177.2

TABLE 13 - RESIDUAL STRESS EXPLANATION FOR WEB BENDING IN HELO
DECK LONGITUDINALS OF 210-FOOT CUTTER STEADFAST



Residual Stress σ_r	Plating Stiffness k_p	Vertical Web Bending Stress σ_w (psi)
0	6700	4000
14940	200	22700

APPENDIX A

DERIVATION OF WEB BENDING EQUATIONS

Using an energy technique, design equations are derived in this section for computing web bending stresses in holo deck stiffeners. As illustrated in Figures 18 and 54, the bending moment M_1 at the edge of a loaded panel produces local vertical bending in the stiffener web in addition to lateral bending, torsion, and longitudinal warping of the stiffener as a whole. The web bending response is a function of this moment, but also of the slenderness of the web (depth/thickness), the lateral rigidity of the flange, and the flexural rigidity of the plating. For example, the web bending stress is found to increase with increasing flange rigidity if the web slenderness is held constant.

Figure 54 shows the cross-sectional profile of a stiffener, before and after web bending deformation, at a typical location along the stiffener length. Note the presence, in the deflected configuration of the stiffener cross section, of the various deformation modes mentioned above. The principal variables for describing the deformation of the stiffener cross section are u , the lateral displacement of the stiffener flange, along with γ and β , the rotation angle of the top and bottom points in the stiffener web respectively. The distributions of displacements u , γ , and β with location along the stiffener axis, as well as the bending moments M_1 , M_2 , and M_3 , were found to be approximately sinusoidal based on previous finite-element analyses. Therefore, in the derivation of the design equations, the sinusoidal approximation is used.

The first step in deriving the web bending equations involves developing a mathematical expression for the total potential energy of the structural system in Figure 54 as discussed, in part, in Reference 10. This expression is then minimized using the procedure described on page 344 of Reference 11 to arrive at the equilibrium configuration of the deformed stiffener under the applied loading. Contributions to the total energy include the potential energy of the applied moment M_1 and the energies associated with the various modes of stiffener deformation (web bending, lateral bending, torsion, and longitudinal warping of the stiffener) and flexure of the plating. The potential energy expression for the web bending

contribution, unlike the other contributions, may not be written down in a straightforward manner. Therefore, an expression for the web bending energy is developed first.

The potential energy of web bending V_{WB} is expressed by

$$V_{WB} = \int_0^a U_{WB} dz \quad (1)$$

where U_{WB} is the web bending strain energy per unit length (for a vertical strip of web of unit width) along the stiffener. The unit strain energy U_{WB} is given by

$$U_{WB} = \int_0^S \frac{M_w^2(\eta) d\eta}{2EI} \quad (2)$$

where $M_w(\eta)$ is the moment in the web strip as a function of the distance η from the top end (line of attachment between the stiffener web and the plating).

It is clear from Equations (1) and (2) that the potential energy V_{WB} of web bending may be obtained once an expression for the moment $M_w(\eta)$ in the web has been determined. This is accomplished by relating the displacement δ and rotation θ of the uppermost point of the web (see Figure 55) to the P and moment M_2 associated with these displacements as follows:

$$\delta = \delta_P + \delta_{M_2} = \frac{1}{3} \frac{PS^3}{EI} + \frac{1}{2} \frac{M_2 S^2}{EI} \quad (3)$$

$$\theta = \theta_P + \theta_{M_2} = \frac{1}{2} \frac{PS^2}{EI} + \frac{M_2 S}{EI} \quad (4)$$

where S is the depth of the web and EI is the flexural rigidity of a vertical strip of web of unit width ($EI = Et^3/12$; t is the web thickness). From Equation (3),

$$P = \frac{3EI\delta}{S^3} - \frac{3}{2} \frac{M_2}{S} \quad (5)$$

Next, substituting Equation (4) into $\gamma = \theta + \beta$ (from Figure 54) and introducing $M_2 = M_1 - M_3 = M_1 - c\gamma$, it may be shown that

$$\gamma = \left(\frac{M_1 S}{4EI} + \beta + \frac{3}{2} \frac{\delta}{S} \right) / \left(1 + \frac{cS}{4EI} \right) \quad (6)$$

Equations (5) and (6) are needed below. The moment $M_w(\eta)$ in the web is given by

$$M_w(\eta) = M_2 + P\eta \quad (7)$$

where η is the distance from the upper edge of the web to the point where the moment is desired. Substituting P from Equation (5) into Equation (7) along with $M_2 = M_1 - c\gamma$ and Equation (6) for γ , it may be shown that

$$M_w(\eta) = M_1 \left(1 - \frac{3}{2} \frac{\eta}{S} \right) + A \left(\frac{M_1 S}{4EI} + \beta + \frac{3}{2} \frac{\delta}{S} \right) \left(\frac{3}{2} \frac{c\eta}{S} - c \right) + \frac{3EI}{S^3} \delta \eta \quad (8)$$

$$\text{where } A = 1 / \left(1 + \frac{cS}{4EI} \right)$$

Substituting Equation (8) for $M_w(\eta)$ into Equation (2) for U_{WB} , then, in turn, U_{WB} into Equation (1) and setting $EI = Et^3/12$, one obtains the potential energy V_{WB} for the entire web

$$V_{WB} = \int_0^a \left[\frac{3}{2} \frac{M_1^2 S}{E t^3} + \frac{3}{2} \frac{A^2 c^2 S}{E t^3} \left(\frac{3M_1 S}{E t^3} + \beta + \frac{3\delta}{2S} \right)^2 - \frac{3M_1 A c S}{E t^3} \left(\frac{3M_1 S}{E t^3} + \beta + \frac{3\delta}{2S} \right) + \frac{E t^3 \delta^2}{8S^3} \right] dz \quad (9)$$

The total potential energy of the structural system in Figure 54 is then expressed by

$$V = V_{LB} + V_W + V_T + V_{WB} + V_{M_1} + V_P \quad (10)$$

where

$$V_{LB} = \int_0^a EI_{yy} u_{zz}^2 dz \quad (\text{lateral bending}) \quad (11)$$

$$V_W = \int_0^a E\Gamma \beta_{zz}^2 dz \quad (\text{longitudinal warping}) \quad (12)$$

$$V_T = \int_0^a GJ \beta_z^2 dz \quad (\text{torsion}) \quad (13)$$

where

V_{WB} is given by Equation (9)

$$V_{M_1} = - \int_0^a M_1 \gamma dz \quad (\text{due to applied moment } M_1) \quad (14)$$

$$V_P = \frac{1}{2} \int_0^a c \gamma^2 dz \quad (\text{plate flexure}) \quad (15)$$

In the above I_{yy} is the moment of inertia for lateral bending,
 Γ is the longitudinal warping constant,
 J is the torsional constant, and
 c is an equivalent elastic rotational spring constant for the plating.
Therefore, substituting Equations (9), (11)–(15), Equation (6) for γ (with $EI = Et^3/12$), and $\delta = u - S\beta$ into Equation (10), the total potential energy of the system becomes

$$\begin{aligned}
V = & \frac{1}{2} \int_0^a [EI_{yy} u_{zz}^2 + E\Gamma \beta_{zz}^2 + GJ \beta_z^2] dz \\
& + \int_0^a \left[\frac{3}{2} \frac{M_1^2 S}{Et^3} + \frac{3}{2} \frac{A^2 c^2 S}{Et^3} \left(\frac{3M_1 S}{Et^3} + \beta + \frac{3(u-S\beta)}{2S} \right)^2 \right. \\
& \left. - \frac{3M_1 A c S}{Et^3} \left(\frac{3M_1 S}{Et^3} + \beta + \frac{3(u-S\beta)}{2S} \right) + \frac{Et^3 (u-S\beta)^2}{8S^3} \right] dz \\
& - \int_0^a M_1 A \left(\frac{3M_1 S}{Et^3} + \beta + \frac{3(u-S\beta)}{2S} \right) dz \\
& + \frac{1}{2} \int_0^a c A^2 \left(\frac{3M_1 S}{Et^3} + \beta + \frac{3(u-S\beta)}{2S} \right)^2 dz \quad (16)
\end{aligned}$$

Recall that u , β , and M_1 may be approximated by sinusoidal distributions along the length of the stiffener as follows:

$$\begin{aligned}
u &= u_o \sin \frac{\pi z}{a} \\
\beta &= \beta_o \sin \frac{\pi z}{a} \\
M_1 &= M_o \sin \frac{\pi z}{a} \quad (17)
\end{aligned}$$

Substituting into Equation (16) and carrying out the indicated differentiations and integrations, the following expression for V in terms of the variables u_o and β_o results:

$$\begin{aligned}
 V = & \frac{\pi^4}{4a^3} \left(EI_{yy} u_o^2 + EI\beta_o^2 \right) + \frac{\pi^2}{4a} GJ\beta_o^2 \\
 & + K_1 + K_3 \left(K_2 + \beta_o + \frac{3}{2S} (u_o - S\beta_o) \right)^2 \\
 & + K_4 \left(K_2 + \beta_o + \frac{3}{2S} (u_o - S\beta_o) \right) + K_5 (u_o - S\beta_o)^2
 \end{aligned} \tag{18}$$

$$\text{where } K_1 = \frac{3}{4} \frac{M_o^2 Sa}{Et^3} (1-\nu^2)$$

$$K_2 = \frac{3M_o S (1-\nu^2)}{Et^3}$$

$$K_3 = \frac{3}{4} \frac{A^2 c^2 Sa (1-\nu^2)}{Et^3} + \frac{caA^2}{4}$$

$$K_4 = -\frac{3}{2} \frac{M_o AcSa}{Et^3} (1-\nu^2) - \frac{M_o Aa}{2}$$

$$K_5 = \frac{Et^3 a}{16S^3 (1-\nu^2)}$$

At structural equilibrium, the total potential energy of the system must be a minimum. This is expressed by

$$\frac{\partial V}{\partial u_o} = 0 \text{ and } \frac{\partial V}{\partial \beta_o} = 0 \tag{19}$$

Substitution of Expression 18 into 19 produces two simultaneous equations in u_o and β_o whose solution is given by

$$u_o = \frac{c_2 c_6 - c_5 c_4}{c_3 c_2 - c_1 c_4} \text{ and } \beta_o = \frac{c_5 c_3 - c_1 c_6}{c_3 c_2 - c_1 c_4} \quad (20)$$

$$\text{where } c_1 = \frac{\frac{\pi^4}{2a^3} EI_{yy}}{} + \frac{4.5K_3}{S^2} + 2K_5$$

$$c_2 = -\frac{1.5K_3}{S} - 2K_5 S$$

$$c_3 = -\frac{1.5K_3}{S} - 2K_5 S = c_2$$

$$c_4 = \frac{\frac{\pi^4}{2a^3} E\Gamma}{\cdot} + \frac{\pi^2 GJ}{2a} + \frac{K_3}{2} + 2K_5 S^2$$

$$c_5 = -\frac{3K_2 K_3}{S} - \frac{1.5K_4}{S}$$

$$c_6 = K_2 K_3 + \frac{K_4}{2}$$

Knowing u_o and β_o , the maximum web rotation angle γ_o is found by inserting u_o and β_o from Equation (20) above into

$$\gamma_o = \left(\frac{3M_o S (1-\nu^2)}{Et^3} + \beta_o + \frac{3}{2} \frac{(u_o - S\beta_o)}{S} \right) A \quad (21)$$

which follows from Equation (6).

Recalling that u_o , β_o , and M_o (see Equation (17)) as well as γ_o represent the maximum values of these parameters which occurs at stiffener midspan or $z = a/2$, it is now straightforward to compute the corresponding maximum value of web bending moment as follows,

$$M_{2(\max)} = M_o - c\gamma_o \quad (22)$$

Finally, the web bending stress is given by

$$\sigma_w = \frac{6M_{2(\max)}}{t^2} \quad (23)$$

Web bending stresses σ_w are computed by successively solving Equations (20) (with K_1 through K_5 defined in Equation (18)) through Equation (23). A program which implements this solution procedure has been written for the 4051 Tektronix mini-computer and has been validated against finite-element results, as was discussed earlier in the report. The necessary input data for this program is defined at the beginning of the program listing in Appendix B.

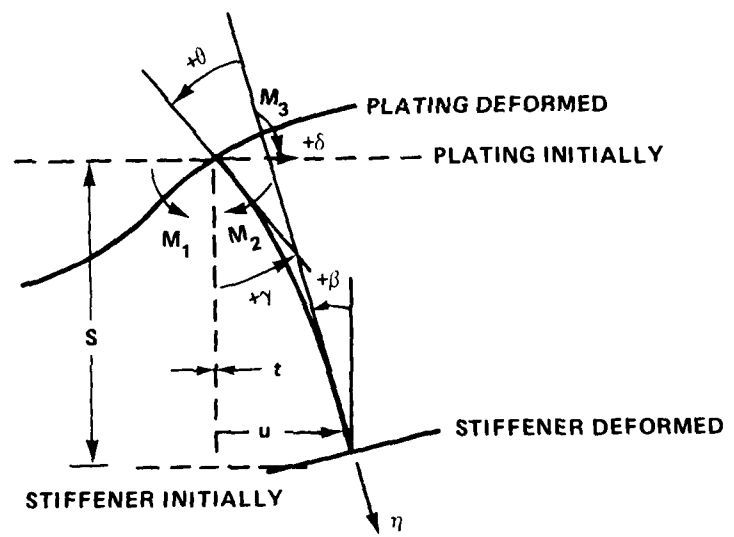


Figure 54 - Typical Cross-Sectional Profile of Stiffener and Plating during Web bending

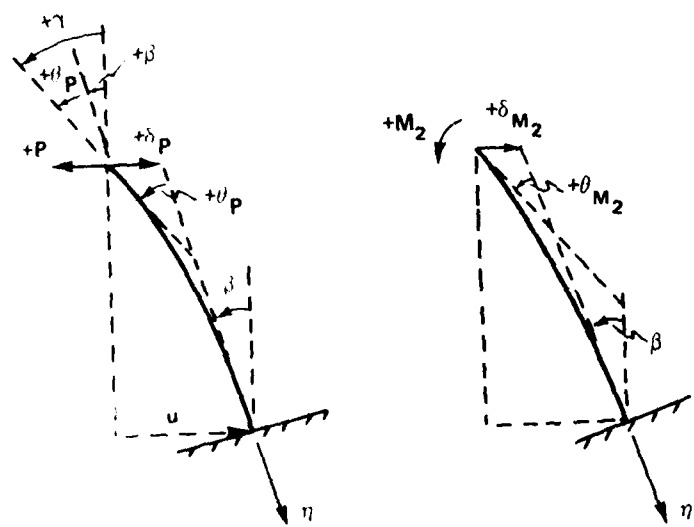


Figure 112 - Decomposition of Web Bending Deflection into
Force- and Moment-Induced Components

APPENDIX B

LISTING AND TYPICAL OUTPUT FOR TEKTRONIX 4051 COMPUTER PROGRAM
"COMPUTATION OF VERTICAL WEB BENDING STRESS"

LISTING

```
LIST
90 REMARK **PROGRAM 6**
100 PRINT "COMPUTATION OF VERTICAL WEB BENDING STRESS"
110 PRINT "INPUT"
120 PRINT "LENGTH OF STIFFENER,A=";
130 INPUT A
140 PRINT "DEPTH OF STIFFENER WEB,S=";
150 INPUT S
160 PRINT "WEB THICKNESS,T=";
170 INPUT T
180 PRINT "HORIZONTAL (LATERAL) MOMENT OF INERTIA,I=";
190 INPUT I
200 PRINT "TORSIONAL CONSTANT,J=";
210 INPUT J
220 PRINT "LONGITUDINAL WARPING CONSTANT,G1=";
230 INPUT G1
240 PRINT "PLATING ROTATIONAL RESTRAINT CONSTANT,C=";
250 INPUT C
260 PRINT "MODULUS OF ELASTICITY,E=";
270 INPUT E
280 PRINT "POISSONS RATIO,V=";
290 INPUT V
300 PRINT "APPLIED MOMENT,M=";
310 INPUT M
320 PRINT "OUTPUT"
330 C=E/(2*(1+V))
340 E1=E*T^3/(1-V*V)
350 A1=1/(1+3*C*S/E1)
360 K1=0.75*(M*M*S*A)/E1
370 K2=3*M*S/E1
380 K3=0.75*(A1*A1*C*C*S*A)/E1+C*A*A1*A1/4
390 K4=-1.5*(M*A1*C*S*A)/E1-M*A1*A/2
400 K5=E1*A/(16*S^3)
410 C1=PI^4*E*I/(2*A^3)+4.5*K3/S^2+2*K5
420 C2=-1.5*K3/S-2*K5*S
430 C3=-1.5*K3/S-2*K5*S
440 C4=PI^4*E*C1/(2*A^3)+PI^2*C*J/(2*A)+0.5*K3+2*K5*S*S
450 C5=-3*K2*K3/S-1.5*K4/S
460 C6=K2*K3+K4/2
470 U=(C2*C6-C5*C4)/(C3*C2-C1*C4)
```

```

480 B=(C5*C3-C1*C6)/(C3*C2-C1*C4)
490 D=U-S*B
500 G5=(3*M*S/E1+B+1.5*D/S)*A1
510 M1=M-G5*C
520 S1=6*M1/T^2
530 P=0.25*E1*D/S^3+1.5*M1/S
540 PRINT "U= ";U
550 PRINT "B= ";B
560 PRINT "D= ";D
570 PRINT "G= ";G5
580 PRINT "M= ";M1
590 PRINT "P= ";P
600 PRINT "STRESS= ";S1
610 END

```

TYPICAL OUTPUT

RUN
COMPUTATION OF VERTICAL WEB BENDING STRESS
INPUT
 LENGTH OF STIFFENER, A=84.0
 DEPTH OF STIFFENER WEB, S=7.7
 WEB THICKNESS, T=0.17
 HORIZONTAL (LATERAL) MOMENT OF INERTIA, I=1.02254
 TORSIONAL CONSTANT, J=0.02312
 LONGITUDINAL WARPING CONSTANT, C1=0.06570
 PLATING ROTATIONAL RESTRAINT CONSTANT, C=12046
 MODULUS OF ELASTICITY, E=30.0E+06
 POISSONS RATIO, V=0.3
 APPLIED MOMENT, M=100.0
OUTPUT
 U= 0.0311048352545
 B= 0.00241329680457
 D= 0.0125224498593
 G= 0.00703265494249
 M= 15.2846385627
 P= 4.08810371847
 STRESS= 3173.28136251

REFERENCES

1. Austin, S.L., "Design History of the Rigid Vinyl Model of the Hydrofoil Plainview (AGEH-1)," NSRDC, Structures Department Report 3883 (Oct 1972).
2. Rodd, J.L., "Verification of the Rigid Vinyl Modeling Technique: The SL-7 Structure," Ship Structure Committee Report SSC-259, U.S. Coast Guard Headquarters, Washington, D.C. (1976).
3. "The NASTRAN User's Manual (Level 15)," NASA Washington, D.C. (June 1972).
4. Bergan, P.G., "Non-linear Analysis of Plates Considering Geometric and Material Effects," U. of California, Dept. of Civil Engineering Report No. USCESM 71-7 (Apr 1971).
5. "Design Manual for Orthotropic Steel Plate Deck Bridges," American Institute of Steel Construction, New York, N.Y. (1963).
6. Kavlie, D. and P.W. Clough, "A Computer Program for Analysis of Stiffened Plates Under Combined Inplane and Lateral Loads," U. of California, Dept. of Civil Engineering Report No. USCESM 71-4 (Mar 1971).
7. Critchfield, M.O., "Plate-Strip Equations for Large Deflection Response of Ship Plating Under Patch Loads and Elastic End Restraint," DTNSRDC Formal Report (to be published).
8. Faulkner, D., "Ship Structural Design Concepts," Chapters 21 of "Compression Strength of Welded Grillage," Ship Structure Committee Final Report on Project SR-200, "Structural Design Criteria," (1974).
9. Jackson, R.I. and P.A. Frieze, "Design of Deck Structures under Wheel Loads," Royal Institution of Naval Architects, Paper No. 12, Spring Meeting (1980).
10. Adamchak, J.C., "Design Equations for Tripping of Stiffeners Under In-plane and Lateral Loads," DTNSRDC Report 79/064 (Oct 1979).
11. Timoshenko, S. and S. Woinowsky-Krieger, "Theory of Plates and Shells," McGraw-Hill (1959).

INITIAL DISTRIBUTION

Copies	Copies
1 DDR&E/Library	1 NAVSHIPYD CHARLESTON SC
1 CNO/OP 098T	1 NAVSHIPYD LONG BEACH CA
1 CNR/Code 474	1 NAVSHIPYD PEARL HABOR HI
2 CHNAVMAT 1 MAT 08T23 1 Lib	1 NAVSHIPYD PHILADELPHIA PA
1 USNA	1 NAVSHIPYD PORTSMOUTH NH
1 NAVPGSCOL	1 NAVSHIPYD PORTSMOUTH VA
1 USNROTCU & NAVADMINU MIT	12 DDC
1 DNL	1 Wright-Patterson AFB Structures Div.
1 NRL Tech Lib	3 U.S. COGARD 1 Naval Eng Div 1 Merchant Marine Tech Div. 1 Ship Structures Comm
16 NAVSEA 1 SEA 03R 1 SEA 312 1 SEA 312 (Aronne) 1 SEA 32 1 SEA 32R (Pohler) 1 SEA 321 1 SEA 322 1 SEA 323 1 SEA 323 (O'Brien) 1 SEA 323 (Arntson) 1 SEA 323 (Dye) 1 SEA 323 (Gallagher) 1 SEA 323 (Swann) 1 SEA 05R 1 SEA 05R (Vanderveldt) 1 SEA 996 (Tech Lib)	1 Lib of Congress 2 MARAD 1 Div. of Ship Design 1 Off of Res and Dev 1 NSF Engr Div Lib 1 Univ of California, Berkeley Dept of Naval Arch 1 Catholic Univ Dept Mech Engr
1 NAVAIRSYSCOM Str Br (Code 5302)	1 George Washington Univ School of Engr & Applied Sci
1 NAVOCEANSYSCEN	1 Lehigh Univ/Dept Civil Engr
1 NAVSHIPYD BREMERTON WA	

Copies		Copies	Code	Name
1	Mass Inst of Tech Dept Ocean Engr	1	1770	
1	Univ of Michigan Dept NAME	1	1770.7	M. Wright (m)
1		1	185	
1	Southwest Res Inst	1	281	
1	Stevens Inst Tech Davidson Lab	10	5211.1	Reports Distribution
1	Virginia Poly Inst & State Univ/Dept	1	522.1	Unclassified Lib (C)
1	Webb Inst	1	522.2	Unclassified Lib (A)
2	National Academy of Sci 1 National Res Council 1 Ship Hull Res Comm			
1	SNAME			
1	American Bureau of Shipping			

CENTER DISTRIBUTION

Copies	Code	Name
1	11	
1	1605	
1	17	
1	1706	C. Eynon (m)
1	1720	
1	1730	
1	1730.1	
1	1730.2	
1	1730.3	
1	1730.4	
20	1730.5	
1	1730.6	
1	1740	
1	1750	